

Curriculum Vitae

Name: Ryan Mayers

E-Mail: mayersrp@gmail.com

EDUCATION AND TRAINING

University of Maryland School of Medicine Jul 2020 – Dec 2025
Ph.D. in Neuroscience
Dissertation Advisor: Brian Polster
GPA: 3.76

Northwestern University Sep 2018 – Jun 2020
M.S. in Biotechnology
Graduate Minor in Entrepreneurship & Innovation
Project Advisor: Evangelos Kiskinis
GPA: 3.75

University of Pennsylvania Aug 2013 – May 2017
B.A. in Biology, Concentration in Neurobiology
Minor in Philosophy

RESEARCH EXPERIENCE

Graduate Research Assistant, Polster Lab Aug 2021 – Oct 2025
University of Maryland School of Medicine, Department of Anesthesiology
Principal Investigator: Dr. Brian Polster
Dissertation: Investigating the Role of *TPCNI* and Pro-Inflammatory Microglial
Activation in Mitochondrial Bioenergetics and Dynamics

*Rotating Graduate Student, University of Maryland School of Medicine Program in
Neuroscience* Jan 2021 – Aug 2021
University of Maryland School of Medicine

- Lipinski Lab, Department of Anesthesiology
- Longden Lab, Department of Physiology
- Monteiro Lab, Department of Anatomy and Neurobiology
- Polster Lab, Department of Anesthesiology

Graduate Research Assistant, Kiskinis Lab Dec 2018 – Aug 2020
Northwestern University, Department of Neurology
Principal Investigator: Dr. Evangelos Kiskinis
Project: ALS-related *NEK1* loss-of-function disrupts nucleocytoplasmic transport via the
microtubule cytoskeleton

Post-Baccalaureate IRTA Fellow, Laboratory of Neurogenetics, Cell Biology Section
National Institutes of Health, National Institute on Aging Jun 2017 – Sep 2018
Principal Investigator: Dr. Mark Cookson
Project: Cloning candidate risk factor genes for Parkinson's Disease

Undergraduate Research Assistant, Betley Lab
University of Pennsylvania, Department of Biology
Principal Investigator: Dr. J. Nicholas Betley
Project: Identifying molecular and behavioral subpopulations of AgRP neurons in mice

Feb 2016 – May 2017

Undergraduate Research Assistant, Linksvayer Lab
University of Pennsylvania, Department of Biology
Principal Investigator: Dr. Timothy Linksvayer
Project: Developing a novel assay to identify “pathfinder” phenotypes among
Monomorium pharaonis

Sep 2014 – Dec 2015

PEER-REVIEWED PUBLICATIONS

S Zhang, X Ding, K Ding, J Zhang, K Galinsky, M Wang, **RP Mayers**, Z Wang, H Kharrazi. ProtoBERT-LoRA: Parameter-Efficient Prototypical Finetuning for Immunotherapy Study Identification. *AMIA annual symposium 2025*, Atlanta, GA. *Accepted*.

JR Mann, ED McKenna, D Mawrie, V Pappakis, F Alessandrini, EN Anderson, **R Mayers**, HE Ball, E Kaspi, K Lubinski, DM Baron, L Tellez, JE Landers, UB Pandey, and E Kiskinis. Loss of function of the ALS-associated *NEK1* kinase disrupts microtubule homeostasis and nuclear import. *Sci Adv.* 2023 Aug 18;9(33):eadi5548. PubMed Central PMCID: PMC10431718.

Berg, A.*, **Mayers, R***. & Richards, S*. ‘Biogen’s Aduhelm controversy as a case study for accelerated approval biomarkers in Alzheimer’s and related diseases.’ *MIT Science Policy Review* 3, 128-135 (2022). <https://doi.org/10.38105/spr.y9p3sxuqg1>. *co-first authors

SELECTED ABSTRACTS AND PRESENTATIONS (>30 TOTAL)

RP Mayers, BM Polster. “Mitochondrial deficits in HAP1 *TPCNI* knockout cells are unlikely due to Alzheimer’s disease-linked *TPCNI* gene ablation.” Invited seminar at the National Institute on Drug Abuse as part of the Baltimore Brain Series. March 2025. *Presenter*

BM Polster, DD Freeman, **RP Mayers**, M Karbowski. “Mdivi-1 Inhibits Late Phase NF- κ B Activation in Pro-inflammatory Microglia in Association with Suppressed Mitochondrial Donut Formation.” Abstract at the International Anesthesia Research Society annual meeting. Honolulu, Hawaii, US. March 2025.

RP Mayers, BM Polster. “The Alzheimer’s disease-linked gene *TPCNI* is required for mitochondrial homeostasis in human HAP1 cells.” Poster sessions at the Gordon Research Seminar & Gordon Research Conference on Neurobiology of Brain Disorders. Castedellfels, Spain. August 2024. *Presenter*

RP Mayers, BM Polster. “The Alzheimer’s disease-linked gene *TPCN1* is required for mitochondrial homeostasis in human HAP1 cells.” Invited seminar at the Einstein Dialogues in Graduate Education symposium. New York City, NY, US. May 2024.

Presenter

N Zhang, S Vongdeuane, N Yadava, **RP Mayers**, H Hwang, BM Polster. “Decoding the mechanisms of mitochondrial electron transport chain component loss upon pro-inflammatory microglial activation.” Poster session at the Society for Neuroscience’s 2023 annual conference. Washington, DC, US. November 2023.

E Daley, **R Mayers**, L Tellez, J Landers, and E Kiskinis. ‘*NEK1* Haploinsufficiency Disrupts Nucleocytoplasmic Transport’ Poster session at the 9th Annual Les Turner Symposium on ALS and NeuroRepair. Chicago, IL, USA. November 2019. *Presenter*

R Mayers, E Daley, L Tellez, J Landers, and E Kiskinis. ‘*NEK1* loss-of-function in iPSC-derived motor neurons causes ALS-related phenotypes’ Poster session at the Society for Neuroscience’s 2019 annual conference. Chicago, IL, USA. October 2019. *Presenter*

R Mayers, E Daley, L Tellez, J Landers, and E Kiskinis. ‘ALS-Related *NEK1* Loss of Function Disrupts Nucleocytoplasmic Transport via the Microtubule Cytoskeleton’ Oral & Poster presentations at Northwestern University’s Annual Master of Biotechnology Industrial Advisory Board Meeting, Evanston, IL, USA. June 2019. *Presenter. Selected as top poster presentation*

R Mayers. ‘Evaluating Candidate Genes and Establishing New Isogenic iPSC Lines for Parkinson’s Disease’ Oral presentation as part of the IRTA Post-Baccalaureate Seminar Series at National the Institutes of Health, Bethesda MD, USA. March 2018. *Presenter*

S Kim, Z Zhu, **R Mayers**, and E Lin Shiao. ‘Global Health and Science Policy Learning Initiative: Epidemiological Analysis of Disease Burden on the Korean Peninsula.’ Poster presentation at the AAAS Science & Diplomacy Conference, Washington DC, USA. March 2017

E Lin Shiao, L Vaccari, **R Mayers**. ‘Introducing science diplomacy at the university level: challenges and lessons learned’ Poster presentation at the AAAS Science & Diplomacy Conference, Washington DC, USA. March 2017. *Presenter*

S Reeder, P Joquino, E Lin Shiao, **R Mayers**, L Vaccari, S Kim, M Iwanicki, and A Cember. ‘USA-Philippines: Exposing underserved youth to science and technology.’ Poster presentation at the AAAS Science & Diplomacy Conference, Washington DC, USA. March 2017

AWARDS AND HONORS

10/2024 – 05/2025 President’s Entrepreneurial Fellow, UM Ventures
03/2025 Invited Speaker, Baltimore Brain Series

11/2024	First Place, Global Biotech Revolution “Voices of Tomorrow” Life Sciences Consulting Case Competition
06/2024	Travel Fellowship, University of Maryland Graduate Student Association
05/2024	Global Travel Fellowship, University of Maryland Center for Global Engagement
05/2024	Invited Speaker, Einstein Dialogues in Graduate Education Symposium (one of 7)
11/2022 – 11/2023	Ambassador, Global Biotech Revolution (among 35 selected)
10/2022 – 10/2023	Appointed to NIGMS T32 Predoctoral Fellowship – Training Program in Integrative Membrane Biology
09/2022	Finalist Team, Global Biotech Revolution “Voices of Tomorrow” Bioinnovation Pitch Competition
05/2022	Global Biotech Revolution “Leader of Tomorrow” (1 of 100)
09/2018 – 06/2020	Northwestern Master of Biotechnology Program Merit Scholarship
06/2019	Best Poster Presentation at Northwestern University MBP Industrial Advisory Board Meeting
06/2017 – 09/2018	NIH Post-Baccalaureate Intramural Research Training Award
08/2015 – 05/2017	Charles H. Schmidt UPenn Named Scholarship
08/2013 – 05/2017	Gordon-Greenblatt Family UPenn Named Scholarship
04/2017	Harrison College House Outstanding Motivational Inspirational Engagement Award

TEACHING EXPERIENCE

08/2023 – 12/2023	Graduate Teaching Assistant, GPLS 737 (Proseminar in Experimental Design)
09/2019 – 12/2019	Graduate Teaching Assistant, MBIOTECH 410-0 (Technology Commercialization Fundamentals)

MENTORSHIP EXPERIENCE

2024	Yugantar Gera, Rotating Neuroscience PhD student
2024	Daniel Freeman, Rotating Neuroscience PhD student
2023	Jessica Gore; Rotating Molecular Medicine PhD student
2023	Jean Jouffroy; Rotating Neuroscience PhD student
2023	Elizabeth Pattie; Rotating Neuroscience PhD student
2023	Aidan Pham; Rotating Neuroscience PhD student
2019	Katherine Lubinski; Undergraduate Neuroscience student

PROFESSIONAL SOCIETY MEMBERSHIPS

2024 – Present	International Society to Advance Alzheimer’s Research and Treatment
2023 – Present	International Society for Molecular Neurodegeneration
2023	American Society for Cell Biology
2022	Society for Redox Biology and Medicine
2019 – 2022	Society for Neuroscience

VOLUNTEERING AND LEADERSHIP EXPERIENCES

05/2025 – Present Entrepreneurship Director for the US & Canada, Global Biotech Revolution

01/2023 – Present Alumni Ambassador, Northwestern University Master of Biotechnology Program

2025 Ad hoc reviewer, Neurotoxicity Research

01/2025 – 10/2025 Student Representative, UM-MIND Seminar Committee

05/2023 – 10/2025 Student Representative, University of Maryland, Baltimore Graduate Assistant Advisory Committee

07/2019 – 02/2024 Alumni Mentor, Various Programs at the University of Pennsylvania

06/2023 – 05/2024 Primary Senator for the Graduate School, UMB University Student Government Association

05/2022 – 05/2024 Program Representative and Vice President, University of Maryland, Baltimore Graduate Student Association

11/2022 – 11/2023 Ambassador, Global Biotech Revolution

10/2018 – 08/2020 Science Diplomacy and Medical Campus Chair, Northwestern University Science Policy Outreach Taskforce

01/2019 – 12/2019 Founder and Organizer, Neuroscience Journal Club

12/2018 – 12/2019 President, Association of Biotechnology Students

04/2016 – 05/2017 Conference Delegate, Ivy Council (3 conferences)

08/2015 – 05/2017 Member and Head of Operations, Penn Science Diplomacy Group

09/2014 – 05/2017 Member and Chair of Several Committees, Phi Gamma Nu Professional Business Fraternity

ABSTRACT

Title of Dissertation: Investigating the Role of *TPCNI* and Pro-Inflammatory Microglial Activation in Mitochondrial Bioenergetics and Dynamics

Ryan Patrick Mayers, Doctor of Philosophy, 2025

Dissertation Directed by: Brian M. Polster, Professor, Department of Anesthesiology

Defects in the capability of the mitochondrial electron transport chain to participate in oxidative phosphorylation and in mitochondrial fission-fusion dynamics are hallmark characteristics of neurodegenerative diseases, including Alzheimer's Disease and Lewy Body Dementia. This mitochondrial dysfunction is bidirectionally influenced by chronic pro-inflammatory microglial activation and is believed to be a key contributor to the onset and progression of neurodegenerative conditions. This dissertation tested two hypotheses related to immunometabolism in neurodegeneration. First, we tested if genetic ablation of the endolysosomal cation channel TPC1 – mimicking loss of expression seen in the microglia of dementia patients – would result in mitochondrial bioenergetic dysfunction. We found that commercially available *TPCNI* knockout HAP1 cells exhibit deficits in mitochondrial oxygen consumption and electron transport chain protein subunit expression. Despite prior implication of TPC1 in mitophagy, these protein-level decreases were not attributable to autophagy or proteasomal activity, conventional mechanisms for post-translational regulation of mitochondrial homeostasis. Furthermore, we were unable to rescue these deficits by TPC1 protein overexpression and identified many de novo mutations that might alternatively contribute to the phenotype, leaving the requirement of TPC1 for mitochondrial homeostasis unresolved. These findings highlight

the need for increased rigor in haploid model knockout studies. Second, we tested if inhibiting mitochondrial fission is required for suppression of nitric oxide release from pro-inflammatory microglia by the DRP1 inhibitor mdivi-1. We found mdivi-1 suppressed NO release but failed to block acquisition of rounded mitochondrial morphology following stimulation of HAPI microglial cells with lipopolysaccharide and interferon-gamma. We also found that a structurally distant, more potent DRP1 inhibitor, Drpitor1a, failed to recapitulate protective effects of mdivi-1, while mdivi-1's protective effects on NO secretion were mimicked by the FGFR inhibitor infigratinib. These results provide indirect support for an alternative mechanism of mdivi-1 protective action. In addition to these hypothesis-driven studies, this dissertation also addresses limitations of existing in vitro model systems for the study of microglial immunometabolism, by recharacterizing HAPI cells as a mouse microglia-like cell line exhibiting suppression of mitochondrial oxygen consumption in response to classical pro-inflammatory stimuli and by conducting the first bioenergetic studies of human monocyte-derived microglia and induced pluripotent stem cell-derived iTF-Microglia.

Investigating the Role of *TPCNI* and Pro-Inflammatory Microglial Activation in Mitochondrial Bioenergetics and Dynamics

by
Ryan Patrick Mayers

Dissertation submitted to the Faculty of the School of Graduate Studies
of the University of Maryland, Baltimore in partial fulfillment
of the requirements for the degree of
Doctor of Philosophy
2025

©Copyright 2025 by Ryan Patrick Mayers

All rights Reserved

Acknowledgements

There are many people to thank for making this dissertation possible. Immediately, I would like to thank my advisor, Dr. Brian Polster, for his unwavering support of my projects throughout their many complications and all the antibodies that still appeared in knockout cell lines. Prior to coming to the University of Maryland, I had never worked with mitochondria or microglia. Dr. Polster's patience, expertise, and mentorship in both immunometabolism and the art of doing rigorous research has shaped my development enormously. I am especially grateful for his willingness to allow me to pursue my own interests within and beyond the lab, from introducing stem cell-derived models, to hosting seminar speakers, to attending international conferences. In the same vein, I would like to thank the other members of Dr. Polster's lab, past and present, who assisted in my training, troubleshooting, and scientific development as a mitochondrial biologist. These lessons have had, and will continue to have, an enormous impact on how I do science.

I would also like to thank the other members of my dissertation committee – Dr. Ivy Dick, Dr. Shengyun Fang, Dr. Mariusz Karbowski, Dr. Marta Lipinski, and Dr. Yvette Wong. Their generosity with their time and scientific expertise was instrumental in refining my research direction and ensuring the highest standard of rigor. I would like to extend additional thanks to Dr. Karbowski for his active collaboration on the super-resolution AiryScan imaging that appears in Chapter 4 of this dissertation, and to Drs. Lipinski and Wong for agreeing to serve as my dissertation readers.

I would like to thank my other collaborators, especially Dr. Ola Awad, who provided enormous assistance and laboratory space in establishing the human stem cell-derived microglial system described in Chapter 5.

I would like to thank the other members of the neuroscience community at the University of Maryland, Baltimore, who helped shape my scientific and professional development. Among this group, I would particularly like to thank Dr. Joseph Mauban, Dr. Shilpa Kumar, and Dr. Thomas Blanpied, whose expertise supported my training in advanced microscopy techniques and analyses both within and the confocal core. I would also like to thank Dr. Thomas Longden, who extended his support and mentorship many times as I pursued external training and funding opportunities.

Outside the University of Maryland, I would like to thank my past mentors and the many other scientists who have taken their time to share their expertise and research with me over the years. In regard to this dissertation, I would especially like to thank Dr. Amanda McQuade, who patiently answered many, many emails on best practices and troubleshooting of the iTF-Microglia system employed in Chapter 5.

Finally, I would like to thank my family and loved ones, especially my parents Shawn and Terry, my sister Megan, and my girlfriend Xiyu for their support in pursuing a career in science. My parents, especially, have always made sure that I could pursue any opportunity that presented itself – without you, I wouldn't have been able to thank everyone else on this list.

Table of Contents

Contents	viii
List of Tables	viii
List of Figures	ix
List of Abbreviations	xi
Chapter 1: Introduction	1
1.1 Immunometabolism in Neurodegenerative Disease	1
<i>1.1.1 Chronic microglial pro-inflammatory activation in neurodegeneration</i>	1
<i>1.1.2 Mitochondrial bioenergetic deficits in neurodegenerative diseases</i>	3
<i>1.1.3 Immunometabolism</i>	5
1.2 Two-Pore Channel 1 (TPC1)	7
<i>1.2.1 TPC1 in immunity and metabolism</i>	9
<i>1.2.2 TPC1 in neurodegeneration</i>	10
1.3 In Vitro Microglial Models	11
<i>1.3.1 HAPI cells</i>	14
1.4 Mitochondrial Fission in Neurodegeneration	16
<i>1.4.1 DRP1 ≠ Mitochondrial Fission</i>	19
<i>1.4.2 DRP1-Dependent Mitochondrial Fission in Neurodegenerative Disease</i>	22
<i>1.4.3 Mdivi-1 Poorly Inhibits DRP1 GTPase Activity</i>	29
<i>1.4.4 Mdivi-1 is Not a Specific DRP1 Inhibitor</i>	31
<i>1.4.5 Mdivi-1 Treatment and DRP1 Knockout Each Impair Mitophagy and Induce Stress Response Pathways</i>	33
<i>1.4.6 A Fragmentated Mitochondrial Network Appearance Does Not Always Indicate Fission</i>	35
<i>1.4.7 Conclusions</i>	36
Chapter 2: HAPI TPCN1 Knockout Cells Exhibit Impaired Mitochondrial Bioenergetics	39
2.1 Introduction	39
2.2 Materials and Methods	40
<i>2.2.1 HAPI cell culture</i>	40
<i>2.2.2 Quantitative real-time polymerase chain reaction (PCR)</i>	41
<i>2.2.3 HAPI cell culture</i>	41
<i>2.2.4 HT1080 cell culture</i>	42

2.2.5 TPCN1 overexpression.....	42
2.2.6 Western blotting.....	42
2.2.7 Immunocytochemistry.....	44
2.2.8 Seahorse microplate-based respirometry.....	44
2.2.9 Whole-Genome Sequencing.....	45
2.3. Results	47
2.3.1 HAPI microglia-like cells exhibit lower levels of Tpcn1 mRNA following pro-inflammatory activation.....	47
2.3.2 TPCN1 KO HAPI cells exhibit decreased mitochondrial bioenergetic function.....	47
2.3.3 The ETC subunit loss in TPCN1 KO HAPI cells is not rescued by an autophagy or proteasome inhibitor.....	51
2.3.4 Genetic manipulations of TPC1 levels or activity fail to rescue or recreate the mitochondrial phenotypes seen in TPCN1 KO HAPI cells.....	54
2.3.5 HAPI cells exhibit many de novo mutations that could alter the functional interpretations of KO studies.....	57
2.4 Discussion	60
Chapter 3: Recharacterization of HAPI Cells as Mouse Microglia-like Cells Useful for Immunometabolism Studies	63
3.1 Introduction	63
3.2 Materials and Methods	64
3.2.1 Materials.....	64
3.2.2 Cell Culture.....	65
3.2.3 Cortex Tissue Isolation.....	65
3.2.4 Short Tandem Repeat (STR) Profiling.....	65
3.2.5 mRNA Expression.....	66
3.2.6 Immunocytochemistry.....	67
3.2.7 Quantification of Nitric Oxide.....	67
3.2.8 Morphology.....	68
3.2.9 XF24 microplate-based respirometry.....	68
3.3 Results	68
3.3.1 HAPI cells are mouse cells expressing microglia selective markers.....	68
3.3.2 LPS, IFN γ , and IFN α induce activation-associated morphological changes in HAPI cells.....	73

3.3.3 <i>IFNγ and IFNα each synergize with LPS to suppress mitochondrial oxygen consumption in HAPI cells</i>	75
3.4 Discussion	76
Chapter 4: Mdivi-1 Inhibits Pro-Inflammatory Microglial Activation Without Preventing Mitochondrial Fission	78
4.1. Introduction	78
4.2. Materials and Methods	80
4.2.1 <i>HAPI Cell Culture</i>	80
4.2.2 <i>Immunocytochemistry</i>	80
4.2.3 <i>Quantification of Mitochondrial Morphology</i>	81
4.2.4 <i>Phase-Contrast Imaging</i>	81
4.2.5 <i>Proteomics</i>	81
4.2.6 <i>Quantification of Nitric Oxide</i>	82
4.2.7 <i>Western Blotting</i>	83
4.3 Results	84
4.3.1 <i>Mdivi-1 fails to rescue the mitochondrial length shortening induced by LPS/IFNγ treatment</i>	84
4.3.2 <i>The structurally distinct DRP1 inhibitor, Drpitor1a, does not mimic mdivi-1's protective effect against microglial pro-inflammatory activation</i>	85
4.3.3 <i>The FGFR inhibitor infigratinib blocks iNOS induction but not ETC deficits in LPS/IFNγ-activated HAPI cells</i>	89
4.4. Discussion	91
Chapter 5: Assessment of Human Induced Microglia Models for Bioenergetic Studies	94
5.1. Introduction	94
5.2. Materials and Methods	95
5.2.1 <i>Differentiation of MDMis from PBMCs</i>	95
5.2.2 <i>Differentiation of microglia from iPSCs</i>	95
5.2.3 <i>Immunocytochemistry</i>	96
5.2.4 <i>Seahorse microplate-based respirometry</i>	97
5.3. Results	97
5.3.1 <i>Differentiation and bioenergetic assessment of MDMis</i>	97
5.3.2 <i>Differentiation and bioenergetic assessment of iTF-Microglia</i>	100
5.4. Discussion	102

Chapter 6: Discussion	104
References	111

List of Tables

Table 1.1. Biological Effects of Mdivi-1.....	37
Table 2.1. qPCR Primers to detect Tpcn1 and Tpcn2 expression levels.....	41
Table 2.2. TPCN1 knockout HAP1 cells exhibit impaired oxidative phosphorylation....	53
Table 2.3. Prevalence of genetic variants from the human reference genome in protein-encoding genes of HAP1 cell lines.....	59
Table 2.4. MitoCarta3.0 variants found in TPCN1 KO HAP1 cells.....	59
Table 3.1. Primers against transcripts preferentially expressed by microglia and macrophages.....	66
Table 3.2. HAPI cells are mouse cells closely related to SIM-A9 cells.....	71

List of Figures

Figure 1.1. HMGB1-induced pro-inflammatory activation.....	8
Figure 1.2. <i>TPCN1</i> expression profiles in the brain in AD and LBD patients from public datasets.....	12
Figure 1.3. DRP1- and non-DRP1-mediated effects of mdivi-1.....	19
Figure 1.4. Functional roles of DRP1.....	21
Figure 2.1. LPS/IFN γ suppresses mRNA expression of <i>Tpcn1</i> in HAPI cells.....	48
Figure 2.2. Next generation sequencing validation of <i>TPCN1</i> KO.....	50
Figure 2.3. <i>TPCN1</i> knockout HAPI cells exhibit impaired respiration.....	52
Figure 2.4. <i>TPCN1</i> knockout cells exhibit decreased levels of several mitochondrial electron transport chain proteins but overexpressed TPC1-HA does not predominantly localize to mitochondria.....	55
Figure 2.5. Inhibition of autophagy or proteasomal activity does not recapitulate the mitochondrial ETC protein loss observed in <i>TPCN1</i> KO HAPI cells.....	56
Figure 2.6. Other genetic manipulations of TPC1 levels or activity fail to rescue or recreate the mitochondrial phenotypes seen in <i>TPCN1</i> KO HAPI cells.....	57
Figure 2.7. NGS validation of <i>MTFMT</i> sequencing.....	60
Figure 3.1. HAPI cell STR profiling results.....	70
Figure 3.2. HAPI cells exhibit microglia-specific markers.....	72
Figure 3.3. HAPI cells exhibit similar sensitivity and magnitude of response to mouse- and rat-origin IFN γ in their release of nitric oxide.....	74
Figure 3.4. LPS, IFN α , and IFN γ induce synergistic morphological changes in HAPI cells.....	75
Figure 3.5. LPS, IFN α , and IFN γ suppress mitochondrial oxygen consumption in HAPI cells.....	76
Figure 4.1. Mdivi-1 slightly suppresses LPS/IFN γ -induced rounding of mitochondria in activated HAPI cells, but does not restore long tubular mitochondrial morphology.....	86
Figure 4.2. Drp1 synergizes with LPS/IFN γ to induce HAPI cell death.....	87
Figure 4.3. Mdivi-1, but not Drp1, suppresses LPS/IFN γ -induced NO secretion.....	88
Figure 4.4. Proteomics reveals mdivi-1 as a possible inhibitor of FGFR3 signaling.....	90
Figure 4.5. The FGFR inhibitor infigratinib confers dose-dependent protection against NO secretion in HAPI cells following LPS/IFN γ treatment.....	91
Figure 5.1. Differentiation of MDMs.....	98

Figure 5.2. MDMis express microglia-selective markers.....99

Figure 5.3. MDMi oxygen consumption rates following HMGB1 or IL-1 β treatment....99

Figure 5.4. iTF-Microglia differentiation yields morphologically homogeneous cells
expressing the microglia-specific marker P2RY12.....101

Figure 5.5. Oxygen consumption rate of iTF-Microglia following treatment with various
pro-inflammatory stimuli.....101

List of Abbreviations

AA, Antimycin A

AD, Alzheimer's Disease

ADOA, Autosomal dominant optic atrophy

ALS, Amyotrophic lateral sclerosis

APP/PS1, Amyloid precursor protein/presenilin 1

Asc, Sodium ascorbate

ATF4, Activating transcription factor 4

ATP, Adenosine triphosphate

ATP5A, ATP synthase F1 subunit alpha

BMDMs, Bone-marrow derived macrophages

BSA, Bovine serum albumin

BWA, Burrow-Wheeler Aligner

Ccdc127, Coiled-coil domain containing 127

cDNA, Complementary DNA

cGAS, Cyclic GMP-AMP synthase

CMT, Charcot-Marie-Tooth disease

CNS, Central nervous system

CPTIO, 2-(4-Carboxyphenyl)-4,4,5,5-tetramethylimidazole-1-oxyl-3-oxide

CRISPR, Clustered regulary interspaced short palindromic repeats

Cx3cr1, CX3C motif chemokine receptor 1

DAMP, Damage-associated molecular pattern

DAPI, 4',6-diamidino-2-phenylindole, dihydrochloride

DMEM, Dulbecco's Modified Eagle Medium

DMT1, Divalent metal transporter 1

DN, Dominant negative

DNA, Deoxyribonucleic acid

DNM1, Dynamin 1

DRP1, Dynamin-related protein 1

ECAR, Extracellular acidification rate

eIF2 α , Eukaryotic initiation factor 2 alpha
ER, Endoplasmic reticulum
ESC, Embryonic stem cell
ETC, Electron transport chain
EV, Empty vector
FBS, Fetal bovine serum
FCCP, Carbonyl cyanide p-trifluoromethoxyphenylhydrazone
FDX1, Ferredoxin 1
FGFR3, Fibroblast growth factor receptor 3
FRS2, Fibroblast growth factor receptor substrate 2
FIS1, Mitochondrial fission 1 protein
GAPDH, Glyceraldehyde-3-Phosphate Dehydrogenase
GATK, Genome Analysis Toolkit
GDAP1, Ganglioside-induced differentiation-associated protein 1
GFAP, Glial fibrillary acidic protein
GSK-3 β , Glycogen synthase kinase 3 beta
GTP, Guanosine triphosphate
GWAS, Genome-wide association study
HA, Hemagglutinin
HAPI, Highly aggressive proliferating immortalized
HEPES, 4-(2-hydroxyethyl)-1-piperazineethanesulfonic acid
HMGB1, High mobility group box 1
HRI, Heme-regulated inhibitor
ICC, Immunocytochemistry
IFN α , Interferon-alpha
IFN γ , Interferon-gamma
IL-1 β , Interleukin-1 beta
iNOS, Inducible nitric oxide synthase
iPSC, Induced pluripotent stem cell
iTF-Microglia, Induced-transcription factor microglia-like cells

JPT2, Jupiter microtubule associated homolog 2
KO, Knockout
LBD, Lewy Body Dementia
LC3, Microtubule-associated proteins 1A/1B light chain 3A
LPS, Lipopolysaccharide
LRRK2, Leucine-rich repeat kinase 2
MCL1, MCL1 Apoptosis Regulator, BCL2 Family Member
MCOLN1, Muclopin-1
Mdivi-1, Mitochondrial division inhibitor 1
MFF, Mitochondrial fission factor
MFN1, Mitofusin 1
MiD49, Mitochondrial dynamics protein of 49 kilodaltons
MiD51, Mitochondrial dynamics protein of 51 kilodaltons
MPTP, N-methyl-4-phenyl-1,2,3,6-tetrahydropyridine
mRNA, Messenger RNA
MT-CO2, Mitochondrially Encoded Cytochrome C Oxidase II
mtDNA, Mitochondrial DNA
MTFMT, Mitochondrial methionyl-tRNA formyltransferase
NAADP, Nicotinic acid adenine dinucleotide phosphate
NDUFB8, NADH:ubiquinone oxidoreductase subunit B8
NF κ B, Nuclear factor kappa B
NLRP3, NLR family pyrin domain containing 3
NMDA, N-methyl D-aspartate
NO, Nitric oxide
NRF2, Nuclear factor erythroid 2-related factor 2
NUPBL, Nucleotide-binding protein-like
OCR, Oxygen consumption rate
OPA1, OPA1 Mitochondrial Dynamin-like GTPase
PAMP, Pathogen-associated molecular pattern
PBS, Phosphate-buffered saline

PCR, Polymerase chain reaction
PD, Parkinson's Disease
PI(3,5)P2, Phosphatidylinositol 3,5-bisphosphate
PINK1, PTEN-induced Kinase 1
POLG, DNA Polymerase Gamma, Catalytic Subunit
PSEN1, Presenilin 1
Pyr, Sodium pyruvate
RAGE, Receptor for advanced glycation endproducts
RNA, Ribonucleic acid
ROS, Reactive oxygen species
SCI, Spinal cord injury
SDHB, Succinate Dehydrogenase Complex Iron Sulfur Subunit B
SDS, Sodium dodecyl sulfate
SIM-A9, Spontaneously immortalized microglia clone A9
siRNA, Small interfering RNA
SNP, single-nucleotide polymorphism
STING, Stimulator of interferon genes
STR, Short tandem repeat
TBE, Tris/Borate/EDTA
TBI, Traumatic brain injury
TBS-T, Tris-buffered saline containing 0.1% v/v Tween-20
TDP-43, Transactive response DNA binding protein 43 kDa
TLR4, Toll-like receptor 4
Tmem119, Transmembrane protein 119
TMPD, N,N,N',N'-Tetramethyl-p-phenylenediamine
TNF- α , Tumor necrosis factor alpha
TPC, Two-pore channel
TRAP1, TNF Receptor-associated Protein 1
T_{reg}, Regulatory T-cells
TREM2, Triggering receptor expressed on myeloid cells 2

TRPML, Transient receptor potential cation channel, mucolipin subfamily

UQCR2, Ubiquinol-cytochrome c reductase core protein 2

WGS, Whole-genome sequencing

WT, Wild-type

Ø, Untreated

Chapter 1: Introduction

1.1 Immunometabolism in Neurodegenerative Disease

Neurodegenerative diseases are a wide range of disorders associated with neuronal cell death and hallmark pathologies characterized by aggregated protein deposits of one or more signature protein species. The most common of these conditions – which include Alzheimer’s Disease (AD), Parkinson’s Disease (PD), amyotrophic lateral sclerosis (ALS), and Lewy Body Dementia (LBD), among many others – are fatal, age-associated diseases which lack effective disease-modifying therapies. Many factors contribute to the pathogenesis and progression of these diseases, including neuronal cell death; pathological protein aggregation; synaptic and neuronal network defects; aberrant proteostasis; cytoskeletal abnormalities; altered energy homeostasis; DNA and RNA defects; and inflammation. Additionally, these hallmarks are also applicable to neurodegenerative injuries such as traumatic brain injury (TBI), stroke, and spinal cord injury (SCI), which result in a subset of similar symptoms as, and are often risk factors for, neurodegenerative diseases¹. This dissertation focuses specifically on two of these disease hallmarks – microglial pro-inflammatory activation and altered mitochondrial bioenergetics – both as separate and interconnected processes.

1.1.1 Chronic microglial pro-inflammatory activation in neurodegeneration

Chronic, proinflammatory activation and proliferation of microglia (“microgliosis”) is a key component of the “inflammation” hallmark of neurodegenerative diseases across most major conditions, including AD and LBD¹⁻⁵. Proinflammatory activation is itself a broad term, referring to a set of microglial states induced by signaling pathways initiated in response to markers of infection or injury, so-called “damage-associated molecular

patterns” (DAMPs) or “pathogen-associated molecular patterns” (PAMPs)⁶. These DAMPs and PAMPs bind to cell surface signaling receptors, including toll-like receptor 4 (TLR4), which then initiate downstream signaling cascades⁶. Many of these downstream signaling pathways converge on translocation and activation of the transcription factor nuclear factor kappa b (NFkB), which promotes the induction of the NLRP3 inflammasome and, subsequently, the maturation and secretion of pro-inflammatory factors. These include reactive oxygen species (ROS), nitric oxide (NO), and the cytokines IL-1 β and TNF- α ⁶. Increased microglial proliferation and phagocytosis also occur⁶. While an acute pro-inflammatory response is a homeostatic component of the microglial injury response, chronic inflammation – as seen in neurodegenerative disorders – can contribute to further neuronal death and continued microglial activation, as many of the secreted factors are neurotoxic or act as DAMPs themselves^{1,6}. Accordingly, depletion of microglia *in vivo* was shown to be therapeutically beneficial in multiple rodent neurodegenerative disease models^{7–11}. DAMPs in the context of neurodegenerative diseases include pathological protein aggregates such as amyloid-beta, factors released from dying neurons like HMGB1, and cytokines and ROS released from already-activated microglia⁶. *In vitro*, a common approach to inducing a pro-inflammatory microglial activation state that is considered to have broad overlap with the states seen in neurodegenerative disease and injury is co-treatment of cultured cells with lipopolysaccharide (LPS) and interferon- γ (IFN γ)^{12,13}. Of note, many genetic risk variants for neurodegenerative diseases reside in genes that regulate microglial pro-inflammatory response, such as *TREM2* variants that are major risk factors AD^{14,15}.

1.1.2 Mitochondrial bioenergetic deficits in neurodegenerative diseases

Deficits in mitochondrial oxidative phosphorylation activity are seen across neurodegenerative diseases and are well-established as early changes in disease onset and progression, across both patient studies and experimental model systems.

In AD, these changes include decreases in the expression of genes and proteins corresponding to components of the mitochondrial electron transport chain (ETC)¹⁶⁻²². These reductions in ETC gene and protein expression are distinct from those seen in normal aging, and appear to preferentially affect brain regions where early metabolic changes are detected in imaging studies of AD patients^{16,21,22}. Unsurprisingly, AD patient samples show deficits in mitochondrial oxidative phosphorylation activity, especially in Complex IV (cytochrome *c* oxidase)^{23,24}. In some animal models of AD, these deficits have been observed to precede the development of the classical amyloid plaque pathology considered the characteristic marker of AD histopathology²⁵.

ETC Complex I deficiency is particularly closely associated with PD. A substantial advancement towards identifying this association was the discovery of environmentally induced parkinsonism resulting from 1-methyl-4-phenyl-1,2,3,6-tetrahydropyridine (MPTP) exposure. MPTP is metabolized to the blood-brain barrier permeable compound 1-methyl-4-phenylpyridinium (MPP⁺), which is preferentially taken up by dopaminergic neurons, where it acts as an inhibitor of Complex I²⁶⁻³¹. Similar environmentally-induced parkinsonism has since been reported due to exposure to pesticides containing Complex I-inhibiting compounds, such as rotenone³¹. Both MPTP/MPP⁺ exposure and rotenone exposure result in clinical and pathological presentations with striking similarities to genetic forms of PD and have since become common model systems for the study of PD

pathogenesis and progression in the lab. The Complex I deficits in environmental parkinsonism are also reflective of bioenergetic shifts in idiopathic PD patients, and mice with genetic ablation of Complex I subunits have been reported in some studies to develop motor dysfunction and dopaminergic neuron loss consistent with clinical presentations of PD^{32,33}. LBD pathology and pathogenesis overlaps strongly with PD, and postmortem immunohistology supports Complex I deficiency in LBD patients as in PD³⁴.

Similar to AD patients, both motor neurons and muscle fibers from ALS patients display deficiencies in Complex IV activity, and these deficiencies have been reported to increase in severity alongside disease progression^{35,36}. In a rat model, genetic ablation of mitochondrial DNA (mtDNA)-encoded Complex IV subunits resulted in the selective loss of motor neurons, paralysis, and cytosolic accumulation of Transactive response DNA binding protein 43 kDa (TDP-43), all pathological hallmarks of clinical presentations of ALS³⁶. Particular recent attention has been paid to the role of RNA trafficking via lysosomal hitchhiking in motor neuron axons of ALS models, which is thought to be a source of selective vulnerability in disease³⁷. This long-distance RNA transport is a mechanism to enable the synthesis of local proteins at sites of distal metabolic activity and appears to be particularly important for the trafficking and translation of nuclear-encoded mitochondrial ribosomes and ETC subunits^{38,39}. In an ALS mouse model, ablation of mitochondrial mRNA trafficking or pre-synaptic mitochondria resulted in decreased neuromuscular junction activity and axonal degeneration, and rescue of local translation of ETC subunit proteins via the clearance of RNA binding protein condensates was sufficient to restore neuromuscular junction innervation³⁹.

This overview is far from comprehensive, and it should be noted that neurodegenerative diseases display a wide range of deficits in both mitochondrial biology beyond oxidative phosphorylation (e.g. in mtDNA stability, mitophagy, or fission/fusion dynamics, the latter of which is covered in section 1.4. of this dissertation) and in non-mitochondrial bioenergetics (e.g. glycolysis deficits in AD, which are well-characterized as among the earliest changes seen in neuroimaging studies of patients and can be used to identify young adults at risk of developing AD and to predict progression from mild cognitive impairment to AD diagnosis)^{40,41}. Still, this introduction highlights the importance of deficits in the expression and function of multiple components of the mitochondrial ETC to pathogenesis and progression across the spectrum of neurodegenerative disorders.

1.1.3 Immunometabolism

Further, pro-inflammatory signaling and mitochondrial bioenergetic dysfunction influence each other in a bidirectional manner. Pro-inflammatory signaling pathways induced by DAMP signaling can decrease the expression of mitochondrial subunits or alter degradation processes that clear defective mitochondria, while defective mitochondria or their components like oxidized mitochondrial DNA (mtDNA) can serve as further DAMPs propagating microglial activation. These DAMPs may act either at the cell surface via TLR-mediated signaling or within the cytosol as part of the cyclic GMP-AMP synthase (cGAS) - stimulator of interferon genes (STING) DNA-sensing pathway^{1,6,42-46}. Figure 1.1 illustrates this bidirectional interaction as mediated by the DAMP HMGB1; other DAMPs and PAMPs initiate overlapping signaling pathways. This intersection of mitochondrial and immune function is referred to as immunometabolism. In both *ex vivo* and *in vitro* primary

microglia treated with the PAMP lipopolysaccharide (LPS), alone or in combination with IFN γ , a suppression of mitochondrial oxygen consumption and spare respiratory capacity is observed concomitant to an increase in glycolysis⁴⁷⁻⁴⁹. This metabolic shift is thought to be primarily toll-like receptor 4 (TLR4)-mediated and to contribute to the pro-inflammatory reprogramming of microglia in a range of neurodegenerative diseases and brain or spinal cord injury^{47,50,51}.

Following pro-inflammatory activation, altered glutamine metabolism contributes to increased production of succinate, the substrate for Complex II⁵²⁻⁵⁴. This imbalance in the relative contribution of Complex II activity causes a “reverse” electron transport from ubiquinol back to Complex I, a process which results in the generation of ROS^{52,55}. Mitochondrial ROS contributes to pro-inflammatory activation through stabilization of the transcription factor HIF-1 α ^{52,53,55,56}. While increased production of itaconate, a Complex II inhibitor, is also reported following pro-inflammatory activation, it is suggested that parallel accumulation of NO following iNOS induction inhibits the activity of aconitase 2, an enzyme upstream of itaconate production^{53,54,56-59}. This inhibition moderates itaconate levels, preventing the reversion of the pro-inflammatory state^{56,60}. Discrepancies in the reported regulation of itaconate may be a factor of time since itaconate levels are initially elevated with pro-inflammatory stimulation but later become suppressed as NO accumulates. Studies differ on whether mitochondrial bioenergetic changes are strictly required to sustain pro-inflammatory activation of microglia and related cell types; this remains an area of ongoing research⁵⁷.

1.2 Two-Pore Channel 1 (TPC1)

Two-pore channels (TPCs) are a family of evolutionarily related cation channels characterized by their structure. They consist of homologous Shaker-like pore-forming domains, and functional pores are formed by dimerization. TPCs are found in the membrane of acidic storage organelles, including endosomes and lysosomes in animals and vacuoles in plants; however the regulation of channel permeability in animal and plant TPCs is evolutionarily divergent. Most mammalian species express three TPCs, the endolysosomal cation channels TPC1-3, though both primates and rodents, through evolutionarily separate processes, lack TPC3^{61,62}. The number of TPC homologs present in animal species appears to be inversely correlated with the number of homologs for TRPML channels, another endolysosomal cation channel family with overlapping ion selectivity and functional roles.

TPC1, encoded by the gene *TPCNI* in humans, is expressed in both endosomes and lysosomes, with some studies suggesting preferential or isoform-dependent expression in endosomes⁶³⁻⁶⁵. TPC1 ion permeability has historically been controversial, but the current consensus is that both human TPCs exhibit two ligand-dependent selectivity paradigms. The first of these is a nonselective permeability to species including Ca^{2+} , H^+ , and Fe^{2+} mediated by NAADP, while a second, Na^+ -selective modality is evoked by $\text{PI}(3,5)\text{P}_2$ ⁶⁶⁻⁶⁸.

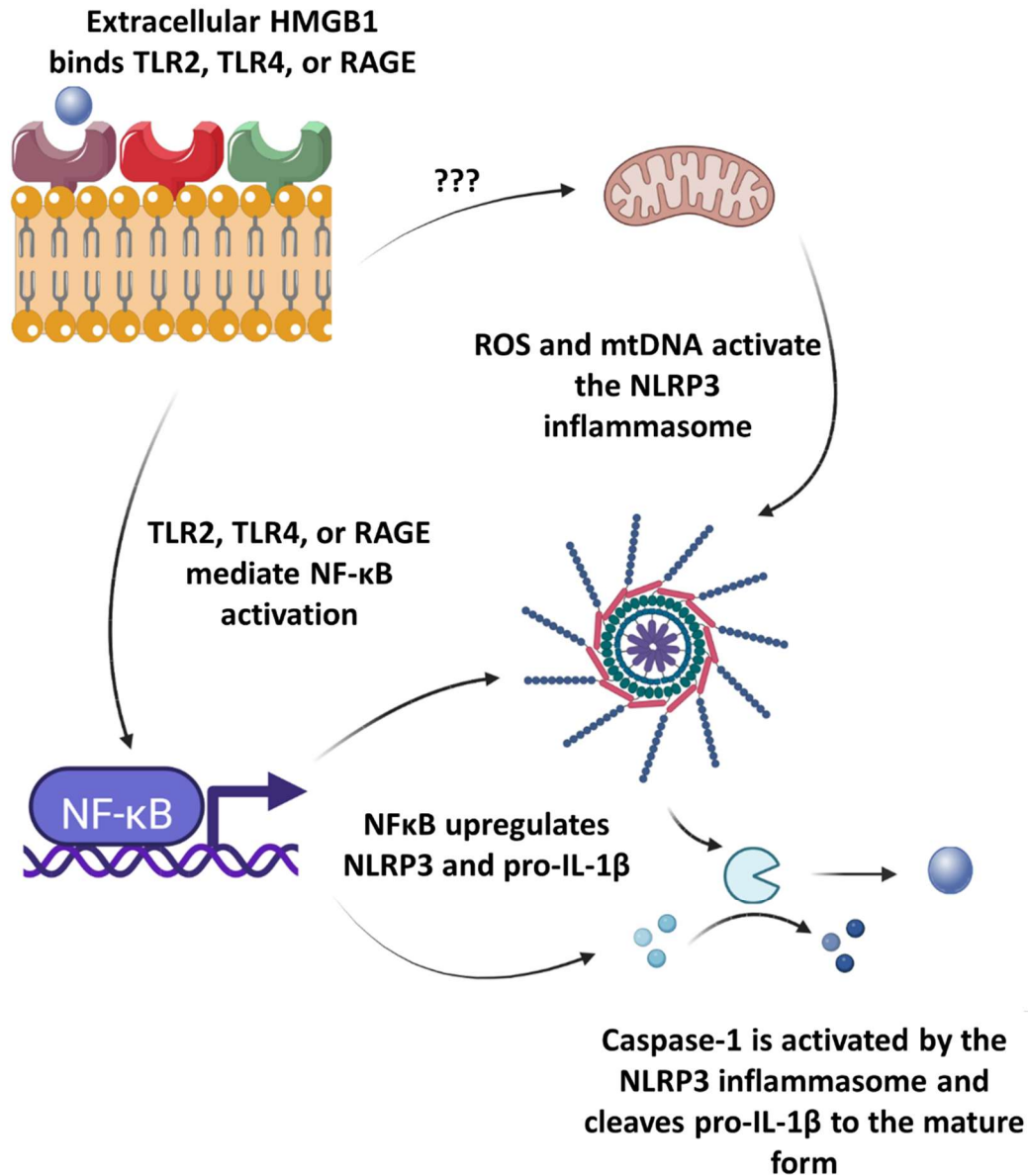


Figure 1.1. HMGB1-induced pro-inflammatory activation

Model of how HMGB1-induced signaling pathways contribute to upregulation of the NLRP3 inflammasome and secretion of further DAMPs, including the role of mitochondrial deficits both downstream of HMGB1 signaling and upstream of NLRP3 inflammasome activation.

1.2.1 TPC1 in immunity and metabolism

TPC1 plays complex roles in immune responsiveness, which is thought to be tied to its roles in regulating intracellular calcium stores, endocytosis, phagocytosis, and macropinocytosis^{69,70}. Inhibition of TPC1 has been viewed as a potential therapeutic approach for its ability to block Ebola infection (via TPC1's role in micropinocytosis) and the accumulation of cholera toxin in the Golgi (via TPC1's role in endosomal trafficking)^{63,71}. On the other hand, some pro-inflammatory shifts are induced specifically by the loss of TPC1 expression. For example, genetic or pharmacological inhibition of TPC1 promotes increased expression of cell-surface TNF in dendritic cells and macrophages, contributing to downstream proliferation of T_{reg} cells⁷². Similarly, knockout or inhibition of TPC1 in mast cells elevates the exocytosis of histamine in allergic and anaphylactic responses⁷³.

Studies of the role TPC1 may play in regulating mitochondria – either broadly or as part of its role in immune responses – are limited; those which do exist suggest that TPC1's role in regulating endolysosomal calcium and iron stores may promote the toxic accumulation of mitochondrial ROS via the Fenton reaction (an H₂O₂-dependent and Fe³⁺-catalyzed generation of ROS) and the opening of the mitochondrial permeability transition pore (a calcium-dependent channel of unknown molecular identity which spans the inner and outer mitochondrial membranes)⁷⁴⁻⁷⁷. In a human glioblastoma cell study, loss of lysosomal acidification induced by treatment with HIV-1 coat protein gp120 promoted efflux of Fe²⁺ from endolysosomes to the cytosol, where the iron was subsequently taken up by mitochondria via the mitochondrial permeability transition pore and divalent metal transporter 1 (DMT1)⁷⁵. The increased mitochondrial iron level

contributed to the accumulation of mitochondrial ROS via the Fenton reaction. Implicating TPC1 in this process, endolysosomal iron efflux was suppressed by treatment with Ned-19, an inhibitor of both TPC1 and TPC2⁷⁵. TPC1 channel activity was further linked to mitochondrial permeability transition pore opening in a mouse study of cardiac reperfusion injury. In that model, pharmacological inhibition of TPCs decreased the reoxygenation-induced Ca²⁺ oscillation frequency. Specifically implicating TPC1, genetic knockout of *Tpcn1* delayed opening of the transition pore and decreased infarct size following reoxygenation, mimicking the effects of pharmacological TPC inhibition⁷⁴. Thus, while evidence linking TPC1 to mitochondrial function is sparse, these studies suggest that TPC1 may play an important role in influencing the severity of mitochondrial dyshomeostasis in pathological states.

1.2.2 *TPC1 in neurodegeneration*

The most direct evidence for a role of TPC1 in neurodegenerative diseases comes from genome-wide association studies (GWAS). The first, in 2022, identified a single-nucleotide polymorphism (SNP) in an intronic region of *Tpcn1* as associated with an increased risk of developing clinically-diagnosed AD⁷⁸. Subsequent GWAS showed that this SNP is associated with a 309-base pair deletion, that AD patients with this variant are more prone to exhibiting TDP-43 pathology and decreased cognitive resilience, and that the variant is also associated with an increased risk of LBD⁷⁹⁻⁸². The association of *TPCNI* risk variants with TDP-43 is particularly notable, as TDP-43 is traditionally considered a hallmark pathology of ALS and FTD, the latter of which is the second-most common dementia and shares overlapping diagnostic criteria with AD, especially in early-onset cases^{83,84}. While we were unable to identify any studies directly implicating

TPC1 function in a neurodegenerative disease model, we note a 2015 study by Lee et al which found that *PSENI* knockout cells exhibit elevated lysosomal pH and NAADP-dependent but TPC2-independent calcium efflux⁸⁵. The authors considered this evidence for TRPML1 as a target of NAADP in this AD model. However, the more recent discovery of NAADP-binding proteins JPT2 and LSM12 and their role as TPC adaptors mean that TRPML channels are no longer thought of as NAADP-activated channels, suggesting that this phenotype may instead have been mediated by TPC1^{67,86–88}. Of note, the other two-pore channel expressed by rodents and humans, TPC2, has been shown to exhibit overactive Ca²⁺ release in *LRRK2*-linked PD models^{89,90}. Within the brain, TPC1 is preferentially expressed by astrocytes and microglia (Figure 1.2.A)^{69,91–93}. Our own exploration of public datasets suggests that *TPCNI* mRNA expression decreases in microglia and astrocytes in both AD and LBD, in line with a possible role in the pro-inflammatory response (Figure 1.2.B-C)^{91,92,94,95}.

1.3 *In Vitro* Microglial Models

Robust *in vitro* microglial cell models facilitate the interrogation of signaling pathways and functional alterations induced by isolated pro-inflammatory stimuli. However, available systems cannot fully capture *in vivo* microglial biology. When selecting a model, both the cellular model and the pro-inflammatory insult should be carefully chosen based on physiological relevance and experimental tractability.

From a cellular perspective, three broad categories of monoculture systems are available to researchers; primary isolated microglia, immortalized cell lines, and induced microglia (iMGs) derived from either monocytes (so-called monocyte-derived microglia,

or MDMIs) or stem cells (both embryonic stem cells, ESCs, and induced pluripotent stem cells, iPSCs).

A *TPCN1* - Homo sapiens

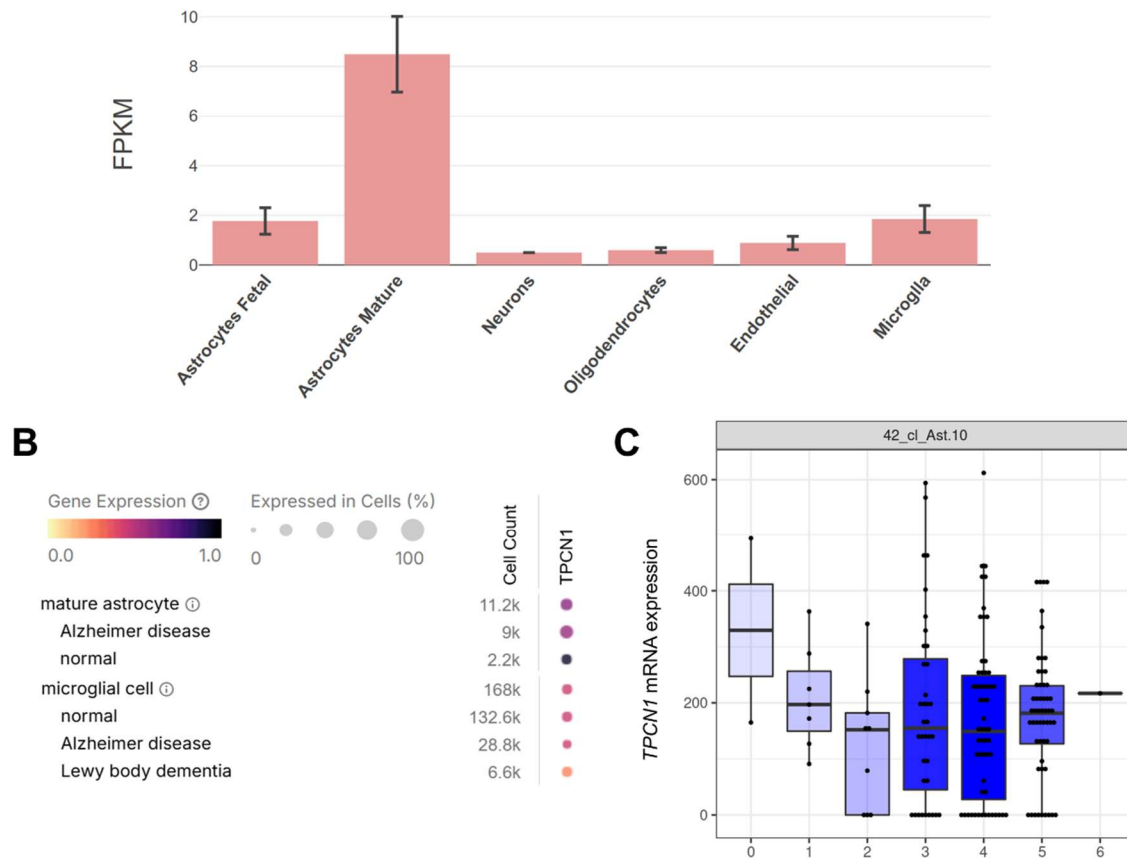


Figure 1.2. *TPCN1* expression profiles in the brain in AD and LBD patients from public datasets

(A) *TPCN1* mRNA is most expressed in astrocytes and microglia in human brains (Zhang et al., 2016, analysis via Brain RNA-Seq platform)⁹¹. (B) *TPCN1* mRNA expression decreases, either as a function of expression level in LBD or of percentage of cells in AD, in both microglia and astrocytes (Abdulla et al., 2025, analysis via CZ CELLxGENE Discover platform)⁹⁴. (C) *TPCN1* mRNA expression decreases correlate with Braak staging in an astrocyte subpopulation implicated in AD disease progression (Green et al., 2023, analysis via application portal hosted by the lab of Vilas Menon)⁹⁵.

Primary microglia were first isolated as a monoculture in 1986, and are traditionally thought of as the closest to *in vitro* systems^{96,97}. However, the process of isolating and preparing primary microglia has been shown to induce transcriptional and metabolic changes more akin to those in pro-inflammatory microglial states⁹⁷⁻⁹⁹. An additional key limitation is the availability and yield of primary cells; many isolation protocols result in few viable cells from a single preparation, which is especially limiting when working with precious human samples.

Immortalized systems were first developed starting with BV2 cells in 1990, and originate from primary microglial cultures which were either oncogenically transformed – such as the mouse BV2 and human HMC3 lines – or purportedly spontaneously immortalized, as in the mouse HAPI and SIM-A9 cell lines¹⁰⁰⁻¹⁰³. The primary benefit of immortalized microglial cultures is their ability to be expanded through repeated passage, circumventing the yield-based limitation of primary cells. However, immortalized microglia only partially recreate primary cell phenotypes¹⁰⁴. Additionally, the two major human microglial cell lines, HMC3 and HMO6, each come with major limitations. HMC3 cells exhibit limited response to pro-inflammatory stimuli such as LPS, low phagocytic capacity, and their microglial identity been called into question, while HMO6 cells are patented and require licensing for experimental use¹⁰⁵⁻¹⁰⁸. For both immortalized and primary microglia, an additional concern for molecular studies is that it is more difficult to transfect or transduce terminally differentiated microglia relative to other cell types, and successfully doing so can induce pro-inflammatory activation¹⁰⁹⁻¹¹¹.

Finally, iMGs were first differentiated from embryonic stem cells in 2005, from isolated monocytes in 2006, and from iPSCs in 2016¹¹²⁻¹¹⁴. All of these approaches more

faithfully produce cells resembling primary microglia than immortalized cells do, though stem cell-derived models do so more closely than MDMis, and both models (stem cell and monocyte-derived) are considered more reflective of fetal microglia than of adult cells^{113,115–118}. Between the two iMG paradigms, a main strength of MDMis is their relative ease of differentiation – microglia-like cells can be isolated from monocytes within peripheral blood mononuclear cell (PBMC) preparations without a need for fibroblast reprogramming¹¹⁸. Stem cell-derived protocols, by contrast, are lengthier and more complex, although on the plus side, there is more standardization and the protocols have been routinely adapted for applications requiring gene editing^{117,118}. In both cases, a strong advantage over primary microglial cultures is the ability to generate comparatively large yields of human microglia for functional studies.

Beyond the cell model, the choice of pro-inflammatory activation stimulus is another point to consider for neurodegenerative disease modeling. A commonly used stimulus thought to induce phenotypes broadly reflective of states seen in neurodegenerative diseases is the PAMP LPS, in large part due to its ability to induce TLR4-mediated signaling^{12,13}. However, it is important to consider that microglial activation *in vivo* during neurodegenerative diseases is often the result of complex combinations of DAMPs that include HMGB1, which induce transcriptional states that only partially overlap with LPS¹¹⁹.

1.3.1 HAPI cells

Highly aggressive proliferating immortalized (HAPI) cells were first reported in 2001, when they were putatively isolated from a mixed glial preparation from a 3-day old rat brain¹⁰³. HAPI cells were initially identified as spontaneously immortalized rat

microglia based on this purported origin and three characteristics shared with in vivo microglia. First, via immunocytochemistry (ICC), HAPI cells were reported to express markers consistent with microglial or macrophage identity (e.g., GLUT5) but not those associated with astrocytes (e.g., GFAP). Second, HAPI cells were capable of phagocytosis. Third, HAPI cells responded to lipopolysaccharide (LPS) stimulation with increased expression of mRNAs encoding inducible nitric oxide synthase (iNOS) and tumor necrosis factor-alpha (TNF- α), as well as nitric oxide (NO) and TNF- α secretion¹⁰³. The findings that HAPI cells are capable of phagocytosis and produce NO and other pro-inflammatory molecules in response to LPS and the type II interferon, interferon-gamma (IFN- γ), have been independently replicated many times^{104,120-135}. These findings, as well as direct comparisons of HAPI cells to primary microglia and another immortalized microglial cell line, BV-2, supported the use of HAPI cells for studying microglial immune responses¹⁰⁴. While employing HAPI cells as a microglial model system, including in experiments described in Chapter 2, we performed next generation sequencing of multiple genes and found results that suggest they are of mouse, not rat, origin. Subsequently, we found that the HAPI cells are listed on the International Cell Line Authentication Committee's Register of Misidentified Cell Lines as mouse, not rat, cells based on personal communication with their former suppliers, MilliporeSigma (Burlington, MA). This discovery was not previously reported in peer-reviewed literature, and most publications continue to explicitly refer to HAPI cells as a rat cell line. Therefore, we recharacterized and revalidated HAPI cells as microglia-like cells of mouse origin, the results of which are presented in Chapter 3.

1.4 Mitochondrial Fission in Neurodegeneration

Mitochondria are highly dynamic organelles that undergo continuous fission-fusion cycles in most cell types. These morphological changes play cell-type specific roles in regulating the subcellular distribution of mitochondria, bioenergetic function, intracellular calcium signaling, proline synthesis, inter-organellar contacts, and cellular gene expression^{136–138}. Mitochondrial fission is thought to regulate the subcellular localization of mitochondria and to facilitate the elimination of defective mitochondria via mitophagy, while mitochondrial fusion instead facilitates functional rescue of individually compromised mitochondria within the network via the transfer of proteins and metabolites necessary for bioenergetic function^{139,140}. The GTPase Dynamin-related protein 1 (DRP1) is essential for most known forms of physiological mitochondrial fission in mammals^{136,141}. Consistent with its importance in shaping mitochondria, DRP1-null mouse embryos do not survive past embryonic day 11.5¹⁴². With regard to the central nervous system (CNS), conditional knockout of *Dnm1l*, which encodes DRP1, leads to cerebellar neuron degeneration, degeneration of midbrain dopaminergic neurons, or hippocampal atrophy within the respective cell-type specific mouse models, indicating that DRP1 expression is required for functional adult neurons^{142–145}.

DRP1 serves multiple roles in neurons, many of which are related to mitochondrial scission, or the act of cutting of mitochondria into two. DRP1-mediated mitochondrial fission is thought to prepare dysfunctional mitochondrial segments for mitophagy — an autophagy quality control program that mediates the turnover of damaged mitochondria^{146,147}. The best-described form of mitophagy is that mediated by PINK1 and Parkin, a kinase and E3 ubiquitin ligase, respectively, which directly and indirectly

promote DRP1-dependent fission¹⁴⁸. However, DRP1 is also essential for a Parkin-independent form of mitophagy^{149,150}. Furthermore, DRP1-dependent mitochondrial scission drives the formation of mitochondrial-derived vesicles as part of a different mitochondrial quality control pathway, highlighting the multifaceted roles of DRP1 in maintaining functional mitochondria¹⁵¹. In the CNS, DRP1-driven mitochondrial fission promotes the distribution of mitochondria into axons¹⁴³. At a functional level, DRP1-dependent mitochondrial fission is required for long-term potentiation, a form of synaptic plasticity believed to be crucial for normal learning and memory¹⁵². DRP1 also has CNS roles that extend beyond the control of mitochondrial dynamics. For example, a brain-specific DRP1 isoform regulates post-synaptic clathrin-mediated endocytosis and neuronal dendrite formation through a mitochondrial fission-independent mechanism¹⁵³. Thus, extensive evidence indicates that DRP1, via both mitochondrial fission-dependent and -independent mechanisms, is crucial for healthy brain function.

Consistent with having evolutionarily conserved essential roles, disease-causing mutations that disrupt DRP1 function have been identified in people. The clinical disease course depends on the site and nature of the specific DRP1 mutation, but most mutations result in severe biological consequences¹⁵⁴. Psychomotor developmental delay, optic degeneration, epileptic encephalopathy, and early postnatal death are among the multiple phenotypic manifestations^{154–159}. There are no cures for DRP1-related disorders at present, but there are several pharmaceutical and non-pharmaceutical interventions to help prevent seizures, alleviate symptoms, and overcome physical and developmental impairments.

While the execution of DRP1-dependent mitochondrial fission is crucial for healthy neuronal function in mice and humans, excessive DRP1-mediated fission has neurobehavioral consequences. Mouse studies implicate disproportionate DRP1-dependent mitochondrial fission in depression, anxiety, and addiction¹⁶⁰⁻¹⁶⁴. Furthermore, abnormal or excessive DRP1-dependent mitochondrial fission is thought to be a major driver of neurodegeneration¹⁶⁵. Whether it is simply the affected brain region(s) or additional factors that dictate the diverse phenotypic manifestations of mitochondrial fission-fusion imbalance is poorly understood. However, excessive mitochondrial fission is present in a variety of diseases, including the two most common neurodegenerative conditions, AD and PD, as well as Charcot-Marie-Tooth disease (CMT) and autosomal dominant optic atrophy (ADOA), rarer disorders thought to stem directly from mitochondrial fission-fusion imbalance^{166,167}.

Mdivi-1, a putative DRP1 inhibitor, was the first identified pharmacological inhibitor of mitochondrial fission¹⁶⁸. It confers neuroprotection in many preclinical neurodegenerative disease models¹⁶⁹. However, since its initial identification, several studies have demonstrated quite a few DRP1-independent effects for mdivi-1 (Figure 1.3, Table 1.1), and the model by which mdivi-1 inhibits DRP1-dependent fission has also been questioned¹⁷⁰. These newer reports complicate the interpretation of how mdivi-1 provides neuroprotection. In this introduction, we discuss the approaches used to implicate mitochondrial fission in neurodegeneration and highlight some potentially confounding factors of DRP1-targeted experimental manipulations, including the induction of endogenous neuroprotective stress response pathways. These “off-target”

biological effects do not necessarily limit the therapeutic potential for mdivi-1 and its analogs but should be considered in the interpretation of experimental results.

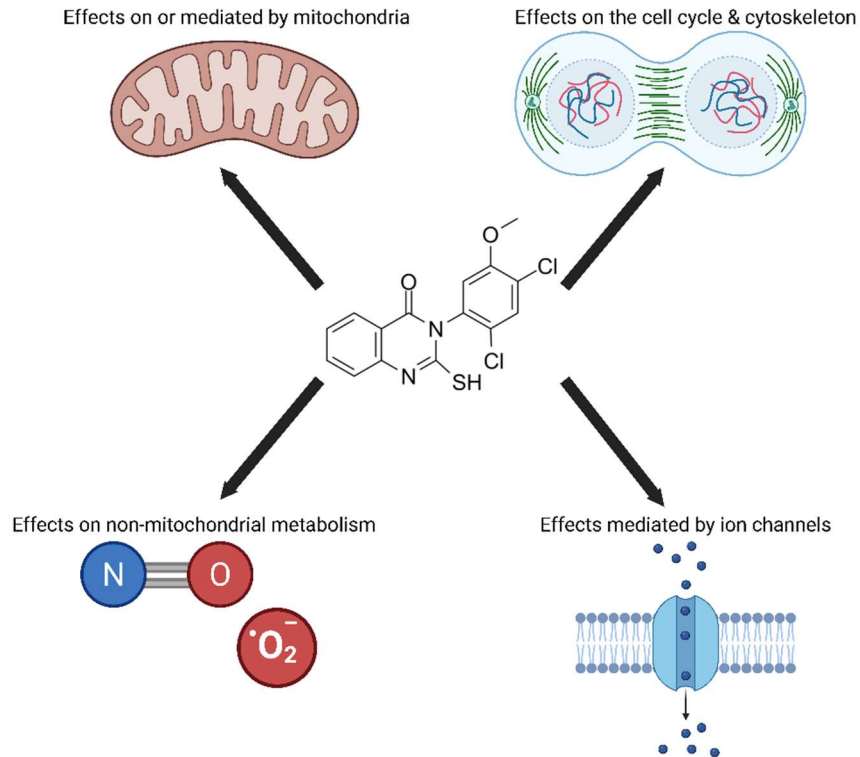


Figure 1.3. DRP1- and non-DRP1-mediated effects of mdivi-1.

Schematic diagram illustrating the biological effects of mdivi-1 treatment.

1.4.1 DRP1 \neq Mitochondrial Fission

DRP1 knockdown is by far the most common genetic method that has been used to antagonize mitochondrial fission. Therefore, inhibiting DRP1 is often equated to inhibiting fission, without adequate recognition that DRP1 is a highly regulated enzyme that carries out multiple fission-independent cellular functions (Figure 1.4).

During mitochondrial fission, a GTP-mediated conformational change allows DRP1 to be recruited to the mitochondrial membrane from the cytosol via adaptor proteins that

include mitochondrial dynamics protein of 49 kilodaltons (MiD49), mitochondrial dynamics protein of 51 kilodaltons (MiD51), and mitochondrial fission factor (MFF), with mitochondrial fission protein 1 (FIS1) also thought to play a regulatory role¹⁷¹⁻¹⁷⁵. These recruitment sites occur specifically where the endoplasmic reticulum (ER) contacts mitochondria^{176,177}. There, DRP1 is assembled into helical oligomers, which begin to constrict the mitochondria^{178,179}. Some found that dynamin 2 (DNM2) may also be recruited to these ER/DRP1 constriction sites and form similar ring-like oligomers, mediating the final severing that results in mitochondrial fission¹⁸⁰. However, others found that DRP1 has both the constriction and severing activities required for mitochondrial fission, suggesting DNM2 involvement is not required¹⁸¹. Regardless, DRP1 recruitment followed by DRP1-dependent constriction appear to be required for most physiological mitochondrial fission.

Nevertheless, there is also evidence for DRP1-independent fission, though it is typically non-canonical, inefficient, or associated with stress responses or disease, including that occurring in neurodegenerative conditions. For example, the PD-associated protein α -synuclein and its mutants localize to mitochondrial membranes and mitochondria-ER contact sites, with α -synuclein overexpression causing mitochondrial fragmentation in both wild-type and DRP1-deficient cells^{182,183}. While the PD-linked E3 ligase Parkin promotes DRP1-mediated mitochondrial fission, it suppresses DRP1-independent mitochondrial division¹⁸⁴. As another example of DRP1-independent fission, the pore-forming protein gasdermin D was reported to mediate mitochondrial fragmentation and remodeling in pro-inflammatory macrophages, innate immune cells that can infiltrate the brain in various diseases¹⁸⁵. Despite DRP1-independent

mitochondrial fragmentation constituting a minority of all mitochondrial fission, it is important to consider both DRP1-dependent and DRP1-independent mechanisms when investigating how mitochondrial fission participates in neurodegenerative processes.

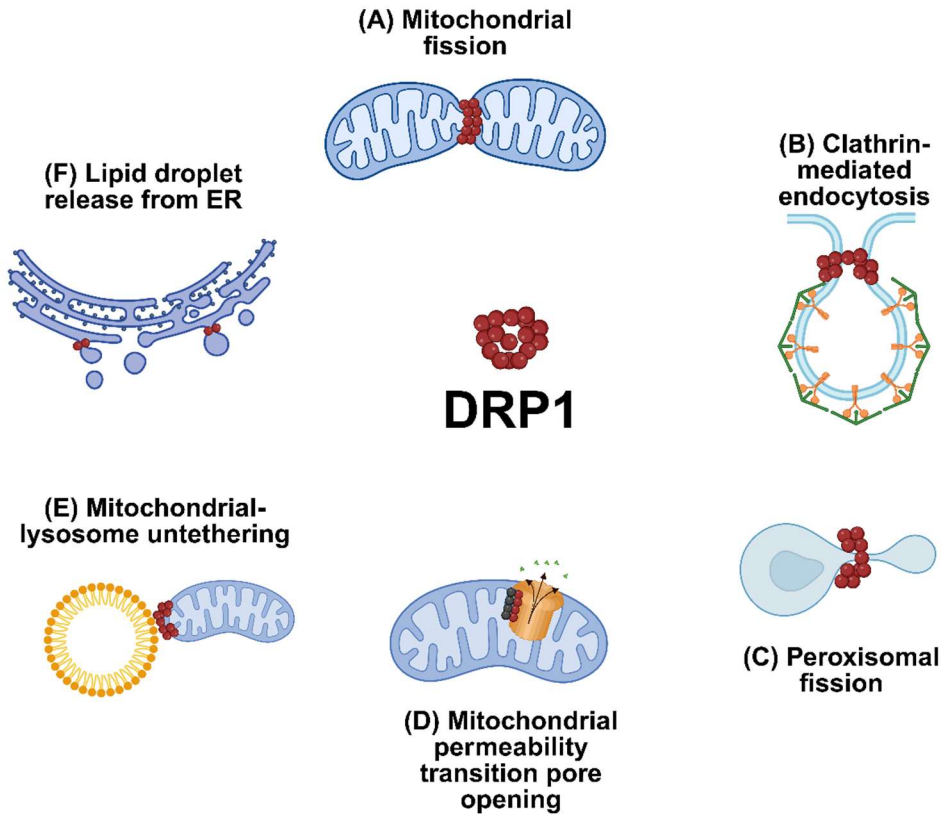


Figure 1.4. Functional roles of DRP1. In addition to its well-characterized role in mitochondrial fission (A), DRP1 also participates in clathrin-mediated endocytosis (B), peroxisomal fission (C), opening of the mitochondrial permeability transition pore (D), mitochondrial-lysosomal untethering dynamics (E), and the release of lipid droplets from the endoplasmic reticulum (ER, F).

Although DRP1 has been most extensively studied in the context of mitochondrial fission, important roles in other biological processes are also described, including the promotion of peroxisomal fission, mitochondrial-lysosomal contact untethering dynamics, the shaping of peripheral ER tubules, lipid droplet maturation, and post-synaptic clathrin-mediated endocytosis^{153,186–190}. DRP1 is also implicated in

mitochondrial permeability transition pore opening through protein-protein interactions¹⁹¹. Several of these DRP1 functions also require its GTPase activity and thus would be inhibited by the K38A dominant negative DRP1 mutant or by DRP1 knockdown—common approaches used to investigate the role of mitochondrial fission in neurodegeneration. Thus, while genetic approaches that interfere with DRP1 function are invaluable to mitochondrial dynamics research, knocking down DRP1 should not be regarded as synonymous with antagonizing mitochondrial fission; unintended consequences may occur and complementary genetic approaches, including modifications to other mitochondrial fission proteins like MFF and FIS1, should be considered. DRP1's emerging roles in many biological processes also warrant the increased implementation of more refined genetic manipulations than knockdown or knockout, e.g., phosphorylation site point mutations more specifically affecting DRP1's fission-promoting mitochondrial translocation.

1.4.2 DRP1-Dependent Mitochondrial Fission in Neurodegenerative Disease

As outlined above, it is well-established that DRP1-dependent fission is required for mitochondrial homeostasis and normal brain function. Therefore, mitochondrial fission is clearly not inherently deleterious. Most studies recognize this by hypothesizing that it is either aberrant or excessive mitochondrial fission that causatively contributes to neurodegeneration, with the former predicting that the mitochondrial fragmentation associated with neuropathology differs mechanistically from the mitochondrial fission observed in healthy cells. To test this first hypothesis of aberrant fission, it is desirable to specifically correct or bypass the fission abnormality — i.e., return fission, or those processes downstream, to the normal state — while to test the second hypothesis of

excessive fission, it is desirable to eliminate only the extra mitochondrial fission or potentially balance it by enhancing fusion— i.e., restore the mitochondrial fission-fusion balance to the physiological, healthy rate.

Unfortunately, neither of these goals are experimentally easy to achieve. Therefore, strategies to inhibit all Drp1-dependent mitochondrial fission, e.g., through either gene ablation or pharmacological inhibition, rather than through specific correction of a fission abnormality, have been most frequently employed. Although neuroprotection yielded by such approaches supports the hypothesis that abnormal or excessive mitochondrial fission promotes neurodegeneration, as will be discussed below, there are alternative explanations for the protective phenotype, e.g., induction of stress-response pathways, that also merit consideration.

Parkinson's Disease

Evidence generally supports a role for a DRP1-dependent, mdivi-1 suppressible fission pathway contributing to PD-related neurodegeneration. The pro-fission proteins DRP1 and MID51 – but also the pro-fusion protein OPA1 – are increased in multiple cell types at both protein and mRNA levels in post-mortem brains of people who had PD¹⁹². Mutations in leucine-rich repeat kinase 2 (*LRRK2*) are the most common cause of autosomal-dominant PD¹⁹³. Overexpression of PD-mutant LRRK2 increases mitochondrial fragmentation through direct interaction with the pro-fission GTPase DRP1¹⁶⁷. In human PD patient cybrid cells, siRNA-mediated *DRP1* knockdown promotes mitochondrial elongation and rescues mitochondrial membrane potential deficits and excess mitochondrial reactive oxygen species (ROS) generation compared to controls¹⁹⁴.

Several studies demonstrate that both genetic manipulation of DRP1 activity and treatment with the DRP1 inhibitor mdivi-1 rescue excess mitochondrial fission and disease phenotypes in PD models. One study found that transgenic rat neurons expressing mutant forms of human *PINK1* exhibit fragmented mitochondria, increased DRP1 and FIS1, and mitochondrial DRP1 translocation¹⁹⁵. Treatment with mdivi-1, siRNA-mediated *DRP1* knockdown, and transduction with the dominant negative *DRP1* K38A mutant were all able to restore normal mitochondrial morphology, as well as downstream deficits in synaptic vesicle release and animal learning and behavioral deficits¹⁹⁵. Similarly, siRNA-mediated *DRP1* knockdown, *DRP1* K38A transduction, or mdivi-1 treatment rescue mitochondrial fragmentation phenotypes and autophagic flux in a mouse model expressing human α -synuclein¹⁹⁶. Furthermore, both *DRP1* K38A and mdivi-1 restore synaptic release of dopamine and ameliorate neurotoxicity in MPTP and *Pink1* knockout mouse models of PD¹⁹⁷. In addition to these multiple approach studies, several studies utilizing mdivi-1 as the sole means of DRP1 inhibition also support a role for mitochondrial fission in PD-related neurodegeneration^{198–202}.

Although mdivi-1 is the predominantly employed DRP1 inhibitor, a few PD studies using MPTP- or *LRRK2*-based models instead employ a small peptide inhibitor of the DRP1-FIS1 interaction, P110. In both patient-derived human cell models and rodent models, P110 treatment blocks DRP1 translocation to the mitochondria, rescues shortened mitochondrial length, inhibits mitochondrial ROS accumulation, and promotes autophagy and neuronal survival^{203–205}.

Despite the convergence of evidence suggesting that DRP1-dependent mitochondrial fission promotes neurodegeneration in PD, not all research favors this interpretation.

Some studies of Pink1-deficient models indicate that the overexpression of wild-type but not dominant negative DRP1 rescue mitochondrial morphology defects, suggesting insufficient rather than excess fission^{206,207}. Results from a *Drosophila* model of α -synucleinopathy suggest that α -synuclein aggregates cause elongated mitochondrial morphology by preventing mitochondrial localization of DRP1, also linking mitochondrial fission and PD in opposite fashion²⁰⁸. Meanwhile, other evidence indicates that α -synuclein can cause DRP1-independent mitochondrial fragmentation^{182,183}. Model system differences may contribute to some of these discrepant results; however, these discordant observations nevertheless support the need for further research.

Alzheimer's Disease

As in PD, disruptions in the mitochondrial fission/fusion balance are linked to the pathogenesis of AD. Extracellular plaques consisting of amyloid- β and intracellular neurofibrillary tangles comprised of tau are cardinal features of AD²⁰⁹. In vitro, treatment of neuronal cultures with either amyloid- β or tau leads to significant fission-mediated mitochondrial shortening²¹⁰⁻²¹⁴. Hyperphosphorylated tau can directly interact with DRP1, which is thought to cause excessive mitochondrial fission²¹⁴. In a human AD patient cybrid model, excess mitochondrial fragmentation could be rescued via siRNA-mediated *DRP1* knockdown, *DRP1* K38A transduction, or mdivi-1 treatment – similar to what is reported in PINK1-deficient models of PD^{195,215}.

Multiple additional studies of AD rodent models support mitochondrial fragmentation contributing to neurodegeneration phenotypes like neuronal apoptosis and amyloid- β pathology that can be rescued by mdivi-1^{212,216,217}. Alterations in the levels of DRP1 and other fission/fusion machinery are also observed and associated with mdivi-1-rescuable

mitochondrial fission in human *in vitro* models of AD^{212,218}. However, these studies do not implement DRP1 genetic manipulations or perform other experiments to help rule out the involvement of alternative mdivi-1 targets.

As in PD, there is limited evidence stemming from the use of the DRP1-FIS1 interaction inhibitor P110 as a different pharmacological approach to understand the pathology of AD. P110 attenuates amyloid- β -induced increases in DRP1 and apoptosis markers while decreasing mitochondrial interconnectivity in SH-SY5Y cells²¹⁹. The same study found that in human fibroblasts from AD patients, P110 reduces DRP1 expression and mitochondrial ROS levels while restoring mitochondrial bioenergetic function and length to wild-type levels²¹⁹. However, the potential for P110 off-target mechanisms of action is entirely unexplored. Furthermore, although P110 showed anti-inflammatory effects in the 5X FAD mouse model of AD, as well as mouse models of Huntington's disease and ALS, P110's ability to disrupt *in vivo* DRP1-FIS1 interactions in the same models was not assessed²²⁰.

Overall, there is less *in vivo* evidence linking mitochondrial fission to AD-related neurodegeneration compared to that from *in vitro* approaches. One study employing an amyloid precursor protein/presenilin 1 (APP/PS1) mouse model identified amyloid- β -induced mitochondrial fission that could be rescued by treatment with either mdivi-1 or lithium chloride, an inhibitor of the DRP1 kinase GSK-3 β ²²¹. However, most of the remaining evidence is either correlative or conflicting. Some studies found increased expression of DRP1 and FIS1, as well as decreased expression of pro-fusion MFN1, MFN2, and OPA1 in postmortem severe AD patient brain tissue or fibroblasts, consistent with a possible role for excessive DRP1-dependent mitochondrial fission^{166,222}. In

contrast, other reports identified reduced DRP1 expression and mitochondrial localization in AD patient fibroblasts, including cells which exhibited slower rates of both mitochondrial fission and fusion^{223–225}. At odds with the excessive fission hypothesis, electron microscopy studies of AD patient tissue as well as mouse, rat, and macaque models of AD observed hyper-elongated mitochondria that were associated with DRP1 and FIS1^{226–228}. This was interpreted as evidence of failed DRP1-mediated fission. However, because the electron micrographs provide only snapshots of mitochondria at fixed moments of time, the possibility that these mitochondria would go on to divide – with their division being detrimental to cellular health – cannot be excluded.

Charcot-Marie-Tooth disease and autosomal dominant optic atrophy

We focused first on evidence for DRP1-dependent mitochondrial fission driving neuropathology in AD and PD, as they are the most common neurodegenerative diseases. Similar approaches have been used in other neurodegenerative conditions to implicate mitochondrial fission in neurodegeneration, including amyotrophic lateral sclerosis and Huntington’s disease^{219,229–245}. However, important evidence also comes from a few heritable neurodegenerative diseases caused by genetic mutations that directly result in mitochondrial fission/fusion imbalance. While these constitute perhaps the best evidence that unchecked mitochondrial fission is detrimental, it is important to note that the neuropathology in these diseases is tissue-specific—i.e., global neurodegeneration does not occur.

In the most prominent example, having one of more than 100 loss-of-function mutations in the pro-mitochondrial-fusion gene *MFN2* causes Charcot-Marie-Tooth disease type 2A (CMT2A), a pediatric peripheral neuropathy^{246,247}. *MFN2* encodes

mitofusin 2, a GTPase which localizes to the mitochondrial outer membrane and oligomerizes with mitofusins on other mitochondria, facilitating outer membrane fusion in opposition to DRP1 activity^{139,140}. In CMT2A, impaired mitochondrial fusion resulting from dysfunctional MFN2 causes CMT2A neurons to display a fragmented mitochondrial network²⁴⁸. This hallmark CMT2A feature is reversed in cell culture by pharmacological MFN2 reactivation²⁴⁹. A related disease, CMT4A, may be caused by mutations in *GDAP1*, a predominantly neuronal protein that induces mitochondrial fragmentation when overexpressed^{250–252}.

Autosomal dominant optic atrophy (ADOA), the most common hereditary optic neuropathy, also leads to phenotypes that appear to stem from unbalanced mitochondrial fission-fusion dynamics. ADOA is frequently caused by mutations in the gene *OPA1*, which encodes a GTPase that facilitates the fusion of the mitochondrial inner membrane when two mitochondria undergo fusion^{139,140,253–255}. Accordingly, ADOA-like symptoms are seen in mice with a heterozygous *OPA1* deletion²⁵⁶. Supporting that mitochondrial fission in excess of fusion contributes to ADOA, *DRP1* mutations have also been identified in families with isolated optic atrophy, with the same studies demonstrating that certain *DRP1* mouse mutants show ADOA-like symptoms¹⁵⁹. In one study of *OPA1* ADOA patient fibroblasts, mdivi-1 was able to reduce elevated DRP1 protein levels and mitochondrial ROS production while partially rescuing deficits in mitophagy and mitochondrial oxygen consumption²⁵⁷.

Synthesis

Taken as a whole, most evidence supports a deleterious role for abnormal or excessive DRP1-dependent mitochondrial fission in neurodegenerative processes. DRP1

knockdown and mdivi-1 inhibitor treatment are by far the most common experimental approaches employed in PD and AD, as well as in several other neurodegenerative diseases, e.g., Huntington's disease and amyotrophic lateral sclerosis. The use of both pharmacological and genetic approaches in many studies is a strength, but these may still suffer from some of the same limitations, as will be discussed below. Returning to the cautionary note that $DRP1 \neq$ mitochondrial fission, *DRP1* knockdown and mdivi-1 administration are approaches that more directly implicate a role for DRP1 than for mitochondrial fission in neurodegeneration. From a hypothesis-testing perspective, to show that neuroprotection due to DRP1 inhibition/loss is caused by the inhibition of mitochondrial fission, a way to restore fission downstream of DRP1 inhibition is required, which should lead to a reversal of the protective phenotype. Unfortunately, accomplishing this is not trivial. With these caveats noted, in the remaining sections of this introduction we discuss a few additional limitations that are common to many studies of mitochondrial fission in neurodegeneration.

1.4.3 Mdivi-1 Poorly Inhibits DRP1 GTPase Activity

Although other DRP1 inhibitors have been identified, the compound mdivi-1 has been used ubiquitously in studies implicating DRP1-dependent mitochondrial fission in neurodegeneration, with only a few studies employing the peptide-based inhibitor P110^{204,258–262}. Mdivi-1 was first identified as a potential DRP1 inhibitor in a 2008 chemical library screen for compounds influencing yeast mitochondrial morphology¹⁶⁸. In that study, mdivi-1 inhibited the self-assembly and GTPase activity of Dnm1, a yeast homolog of DRP1. However, it was unable to impair the GTPase activity of recombinant human DRP1, with the caveat that the recombinant DRP1 enzyme may not have folded

correctly because it was incapable of self-assembly. Nevertheless, mdivi-1 inhibited mitochondrial fission in a mammalian cell line and, based on evidence that included testing mdivi-1 on DRP1-overexpressing cells, it was assumed that the yeast Dnm1 antagonist inhibits mammalian DRP1 by the same mechanism.

Despite the continued widespread use of mdivi-1 as a specific DRP1 inhibitor, its inability to potently inhibit recombinant human DRP1-dependent GTP hydrolysis is a finding that has been replicated by multiple groups (but see Numadate et al. 2014; Rosdah et al. 2022 for conflicting reports)^{170,258,260,263,264}. The conclusion that mdivi-1 is ineffective as a DRP1 GTPase activity inhibitor is strengthened by the studies' inclusion of improved recombinant DRP1 preparations capable of self-assembly, as well as positive controls for GTPase activity inhibition (e.g., the non-hydrolyzable GTP analogue GTP γ S or newly identified potent DRP1 inhibitors). In addition, Bordt et al. reproduced the ability of mdivi-1 to inhibit yeast Dnm1 in parallel to showing its failed inhibition of DRP1²⁶³. Potentially explaining some of the literature disparities, a recent study showed that mdivi-1 exhibits colloidal aggregates affecting its inhibitor properties at aqueous solution concentrations above $\sim 20 \mu\text{M}$ ²⁶⁰. The specific concentration threshold depended on the content of dimethyl sulfoxide, the vehicle of the concentrated mdivi-1 stock. Partial ($\sim 50\%$) inhibition of DRP1 GTPase activity was seen at $5 \mu\text{M}$ mdivi-1, but disappeared at higher tested concentrations (e.g., $50 \mu\text{M}$)²⁶⁰. However, the investigators observed no direct interaction between mdivi-1 and recombinant human DRP1 by surface plasmon resonance at mdivi-1 concentrations ranging from $0.41 - 100 \mu\text{M}$ despite showing in parallel that the novel compound DRP1i27 binds and inhibits the enzyme.

Nevertheless, most evidence from in vitro and in vivo models still favors DRP1 interference as the main mechanism by which mdivi-1 suppresses mitochondrial fission. Regulation of either DRP1 protein level or the post-translational modifications promoting its association with mitochondria may, in many cases, explain the ability of mdivi-1 to induce or preserve elongated mitochondrial morphology. For example, one group used molecular modeling based on the DRP1 crystal structure to predict a direct interaction between mdivi-1 and DRP1 at serine 616 (S616), a phosphorylation site that regulates hypoxia-induced DRP1 translocation to mitochondria in vascular smooth muscle cells¹⁷⁰. Mdivi-1 suppressed the hypoxia-induced accumulation of endogenous DRP1 on mitochondria, but as predicted by an S616 interaction, failed to prevent mitochondrial DRP1 accumulation when a DRP1 S616-to-alanine mutant was ectopically expressed.

Finally, not all evidence points to an exclusively DRP1-dependent mechanism of mdivi-1 fission inhibition. One study found that mdivi-1 but not DRP1 knockdown prevents mitochondrial fragmentation and rescues cell viability in neurons treated with an excitotoxic concentration of NMDA²⁶⁵. Without excluding the putative inhibition of DRP1 by mdivi-1, this study suggests that mdivi-1 can suppress at least one form of mitochondrial division by a DRP1-independent mechanism.

1.4.4 Mdivi-1 is Not a Specific DRP1 Inhibitor

Though the precise mechanisms require further elucidation, the conclusion that mdivi-1 counteracts DRP1-dependent mitochondrial fission is supported by a preponderance of evidence. Yet, there are now many studies collectively demonstrating more than a dozen DRP1-independent mdivi-1 actions (Fig. 1.3, Table 1.1), some of which exhibit greater potency than DRP1/mitochondrial fission inhibition. This is

perhaps not surprising given that mdivi-1 has a reactive sulfhydryl group. In one study investigating the consequences of mdivi-1 treatment beyond potential DRP1 inhibition, the expression of 266 proteins and 97 phosphorylation sites were identified as mdivi-1-sensitive²⁶⁶. Among multiple studies reporting inhibition of mitochondrial oxygen consumption by mdivi-1, one observed inhibition of mitochondrial Complex I-dependent respiration without reproducing effects on mitochondrial length²⁶³. Another study suggested that this inhibitory effect on Complex I is a result of mdivi-1 directly binding to site IQ and impairing Complex I assembly²⁶⁷. However, mdivi-1 differs from the well-characterized IQ site inhibitor rotenone in its ability to induce ROS production, indicating that its effects on mitochondria may be more complex²⁶³. There is evidence from both yeast models and cell-free experiments that mdivi-1 may exhibit a moderate ability to scavenge free radicals^{268,269}. Nevertheless, in mammalian cells mdivi-1's effects on ROS appear to be primarily mediated through effects on endogenous proteins, including mitochondrial Complex I and the NRF2-dependent antioxidant response pathway^{170,263}.

Even in studies where mdivi-1 is reported to have the expected inhibitory effect on DRP1-mediated mitochondrial fission, unexpected off-target effects have been observed. In one case, mdivi-1 inhibited DRP1-dependent mitochondrial fission in oligodendrocytes, but also triggered DRP1-independent swelling of mitochondria and cell death, which the authors attributed to necrosis²⁷⁰. In another, mdivi-1 was reported to have inhibitory effects on DRP1-dependent fission only in the early stages following rodent ischemic/hypoxic injury; however, mdivi-1 improved survival outcomes in a DRP1-independent manner by increasing vascular reactivity and reducing injury-induced oxidative stress¹⁷⁰. A third study found inhibition of mitophagy by mdivi-1 that may be

due to failed autophagosome cargo loading, as an autophagy-inducing stimulus still increased autophagosome number and LC3-II to LC3-I ratio in the presence of mdivi-1, but with increased p62²⁷¹. Visual inspection of cells by electron microscopy identified increases in both empty and electron dense vesicles. Mdivi-1 inhibits not just mitophagy, but also macroautophagy in at least some cell types, as ATG7 overexpression restores mdivi-1-impaired autophagic flux²⁷².

Given the therapeutic interest in mdivi-1, understanding its specificity and mechanisms of action more completely is valuable for research into its potential applications – including those which may have targets other than DRP1. When considering mdivi-1's utility for improving our understanding of the possible role of DRP1-dependent mitochondrial fission in neurodegenerative processes however, it is important to keep its limitations in mind.

1.4.5 Mdivi-1 Treatment and DRP1 Knockout Each Impair Mitophagy and Induce Stress Response Pathways

The specificity of mdivi-1 for acting through inhibiting mitochondrial fission is frequently supported by genetic manipulations of DRP1 activity. However, the strength of this support is lessened if the two approaches have common alternative effects. Unfortunately, some of the same effects have been documented for each manipulation. In neurons, mitophagy is crucial for maintaining mitochondrial quality and energy production due to their high metabolic demand and low regenerative capacity^{273,274}. Extensive evidence indicates that mitophagy deficits in neurons contribute to neurodegenerative disorders, most notably, PD. Impaired mitophagy leads to the accumulation of damaged mitochondria, contributing to poor synaptic function, inflammation, and neurodegeneration^{273,274}. Mitophagy-inducing chemical compounds

such as urolithin A therefore comprise a major avenue of investigation for the treatment of multiple neurodegenerative diseases^{275,276}. Hence, it is paradoxical that despite the evidence that they are neuroprotective, mdivi-1 treatment and *DRPI* knockout each impair mitophagy^{149,271}.

While on the surface, mitophagy inhibition seems difficult to reconcile with the neuroprotective effects of these manipulations, the impaired removal of dysfunctional mitochondria by mitophagy may contribute to the induction of endogenous neuroprotection pathways that are activated by damaged mitochondria. The ATF4-mediated integrated stress response, specifically, is a cellular defense mechanism activated under infection, oxidative stress, nutrient deprivation, mitochondrial insult, and other forms of cellular damage^{277,278}. The integrated stress response involves the phosphorylation of eukaryotic initiation factor 2 alpha (eIF2 α), leading to a reduction in global protein synthesis and the selective translation of stress-response proteins including ATF4²⁷⁹. In the brain, ATF4 plays a key role in regulating the expression of genes that help protect neurons from damage, thereby facilitating neuronal survival and promoting adaptive changes during periods of stress²⁸⁰.

Both mdivi-1 and *DRPI* knockout induce the ATF4-dependent integrated stress response^{277,281}. However, whether this is due to their mitophagy inhibition, or conversely, whether their mitophagy inhibition is caused by the induction of the integrated stress response, is unclear. The interrelationship between mitophagy and the integrated stress response is complex, with evidence that the heme-regulated inhibitor (HRI) branch of the stress response may either trigger or inhibit mitophagy^{282,283}. Regardless, because the integrated stress response plays a critical role in maintaining neuronal homeostasis and

viability, the potential that this stress response pathway contributes to the neuroprotective effects of DRP1 interference should be considered²⁸⁴.

There are many other cellular stress response pathways that could be triggered by drug/knockdown manipulations, and some of these are also beginning to be investigated in the context of fission inhibition. Recently, a major mechanism of mdivi-1 protection against hypoxic-ischemic vascular injury was shown to be upregulation of antioxidant enzymes mediated in part by the transcription factor nuclear factor erythroid 2-related factor 2 (NRF2) driving the NRF2 Antioxidant Response Pathway¹⁷⁰. Interestingly, the NRF2 Antioxidant Response Pathway was also shown to cause DRP1 degradation, leading to mitochondrial hyper-fusion, which may explain the anti-fission effects of mdivi-1 in some models²⁸⁵. Another recent study identified the p53 transcriptional gene network as a major pathway upregulated by mdivi-1²⁸⁶. As the landscape of cellular responses to mdivi-1 and/or DRP1 knockdown continue to be revealed, the extent to which their neuroprotection can be attributed to the removal of a deleterious process (i.e., aberrant mitochondrial fission) vs. the induction of an endogenous protective response to disruption of a crucial biological process should become clearer.

1.4.6 A Fragmentated Mitochondrial Network Appearance Does Not Always Indicate Fission

A final caveat to the mitochondrial fission-neurodegeneration hypothesis is that, in some studies of mitochondrial fission dynamics, increased mitochondrial fission is inferred from a lower mitochondrial aspect ratio in static images. Measurements of mitochondrial size at a single time point, even when conducted rigorously, cannot differentiate between morphological remodeling, dynamic fission, or size reduction by alternative mechanisms, e.g., mitochondria-derived vesicle extrusion. Uncoupling of ATP

phosphorylation from electron transport is an example of a mitochondrial change that results in more circular/punctate mitochondria and appears to be caused by DRP1-independent swelling rather than DRP1-mediated fission²⁸⁷. Notably, *DRP1* knockdown is unable to prevent neuronal mitochondrial network fragmentation triggered by excitotoxic overactivation of N-methyl D-aspartate (NMDA) glutamate neurotransmitter receptors, a scenario to which mitochondrial swelling may contribute^{265,288}.

1.4.7 Conclusions

Numerous studies associate mitochondrial fragmentation phenotypes with neurodegeneration. However, rigorously falsifying alternative hypotheses to support causation is a tall task that requires multiple approaches. While mdivi-1, like DRP1 genetic loss-of-function, can often elongate mitochondria, mdivi-1 should not necessarily be employed as a specific inhibitor of DRP GTP hydrolysis and suppressor of mitochondrial fission. Mdivi-1 is not a potent DRP1 GTPase inhibitor, and it has targets beyond DRP1, with multiple studies demonstrating that mdivi-1 inhibits mitochondrial fission in DRP1-dependent and -independent manners and results in non-fission-associated effects that may be related to inhibition of Complex I, ROS regulation, or other targets. On the DRP1 side, DRP1 plays a GTP hydrolysis-mediated role in several different biological processes, meaning that the consequences of its inhibition are likely not restricted to reduced mitochondrial fission. Studies are beginning to use more sophisticated approaches, including bidirectional modulation of fission-fusion balance and DRP1 point mutants, to address the role of mitochondrial dynamics in neurodegeneration. As with any biological process, diversion from homeostasis is likely to lead to pathology in at least some contexts. While the field continues to test and—

perhaps support—the idea that abnormal or excessive mitochondrial fission contributes to neurodegeneration in many devastating diseases, a natural next question moves to the forefront: why?

Table 1.1. Biological Effects of Mdivi-1.

Biological Effect	Putative Target	Cell/Mito Type	Concentration(s) or IC₅₀	Reference(s)
Inhibition of Mitochondrial Fission	DRP1	Yeast, COS cells	50 μM (IC ₅₀)	(Cassidy-Stone et al. 2008) ¹⁶⁸
Inhibition of tBID-induced cytochrome <i>c</i> release	unknown	Yeast, HeLa cells	50 μM	(Cassidy-Stone et al. 2008; Kushnareva et al. 2012) ^{168,289}
Inhibition of rapidly activating delayed-rectifier K ⁺ current	KCNH2	HL-1 cells, GH ₃ cells	11.6 μM (IC ₅₀)	(So et al. 2012) ²⁹⁰
Inhibition of Puromycin-Sensitive Aminopeptidase (PSA)	PSA/NPEPPS	MOLT4 cell suspension	0.71 μM (IC ₅₀)	(Numadate et al. 2014) ²⁶⁴
Inhibition of DNA replication	Unknown	MDA-MB-231 cells	20 μM	(Qian et al. 2014) ²⁹¹
Mitotic arrest	Unknown	WT and DRP1 ^{-/-} SV40-immortalized MEF cells, MDA-MB-231 cells	Doses between 10 μM and 50 μM	(Wang et al. 2015; Fang et al. 2021) ^{292,293}
Inhibition of mitochondrial respiration	Complex I	WT and DRP1 ^{-/-} MEFs, H1299 cells, primary rat cortical neurons, isolated brain and heart mito, permeabilized adult cardiomyocytes	50 μM	(Qian et al. 2014; Bordt et al. 2017; Zhang et al. 2017) ^{227,263,291}
Inhibition of succinate-dependent mitochondrial ROS production	Complex I	Isolated brain mitochondria	50 μM	(Bordt et al. 2017) ²⁶³
Induction of glycolysis	Unknown	MCF-7 and HDQ-P1 cells	1 μM	(Lucantoni, Dussmann, and Prehn 2018) ²⁹⁴
Impaired glucose and glutamine metabolism	Unknown but involving increased ROS	DRP1-WT DRP1-KO H460 lung cancer cells and MEFs	20 and 50 μM	(Dai et al. 2020) ²⁹⁵

Table 1.1, continued.

Inhibition of tubulin polymerization	Tubulin	MDA-MB-231 cells	Doses above 50 μ M	(Fang et al. 2021) ²⁹³
Free radical scavenging	N/A	N/A	25 μ M	(Bordt et al. 2022) ²⁶⁹
Metabolic regulation of yeast-to-hyphae transition	Unknown but involved decreasing NO	<i>Candida albicans</i>	30 μ M (IC ₅₀)	(Koch et al. 2018) ²⁶⁸
Vasorelaxation	Cav1.2 channel (blocker) K _{Ca} 1.1 channel (stimulation)	Smooth muscle cells isolated from Wistar rats	Doses between 3 μ M and 20 μ M	(Ahmed et al. 2022; Ahmed et al. 2023) ^{296,297}
Mitochondrial Complex I assembly	Complex I	HeLa cells, cultured neural progenitor cells and neurons	50 μ M for 24 hours and 10 μ M for 1 week	(Marx et al. 2024) ²⁶⁷
Extracellular matrix detachment	Complex I	MCF-7, MDA-MB-231, HCT116 cell lines (breast and cell cancer lines)	50 μ M	(Silva-Pavez et al. 2024) ²⁹⁸

Chapter 2: HAP1 *TPCNI* Knockout Cells Exhibit Impaired Mitochondrial Bioenergetics

2.1 Introduction

Intronic variants in the gene *TPCNI*, which encodes the endosomal cation channel Two-Pore Channel 1 (TPC1), have been identified as a disease risk factor in genome-wide association studies (GWAS) of AD and LBD patients^{78,80–82}. The functional consequences of these variants have not been reported. Within the brain, TPC1 is highly expressed in microglia and astrocytes, where its expression decreases in AD and LBD; in one AD dataset, the *TPCNI* mRNA decrease in a disease-relevant astrocyte population was correlated with the Braak score of pathological severity (see Figure 1.2C)^{69,91–95}. Genetic and pharmacological loss of TPC1 function has been shown to play both protective and pathological roles in peripheral immunity, including blocking Ebola infection, promoting the proliferation of Treg cells, and elevating the exocytosis of histamine during an anaphylactic response^{63,69–73}. Mitochondrial roles for TPC1 are less studied, but suggest that TPC1 may regulate mitochondrially-mediated death or mitochondrial turnover via mitophagy or impact mitochondrial function indirectly via Ca^{2+} and Fe^{2+} release from acidic organelle stores^{74,75,299}.

HAP1 cells are derived from the first near-haploid leukemia cell line, KBM-7, and are haploid for all chromosomes except for a disomal portion of chromosome 15 encoding 330 genes^{300–302}. Both the original KBM-7 line and the subsequent HAP1 line were developed for their utility in human genetic analysis, and the near-haploid status of both KBM-7 and HAP1 cells has been frequently exploited for its utility in knockout studies^{301–305}. Limitations of both haploid cell line chromosomal instability and of off-target edits in genetically engineered cell lines are well-known^{306–309}. However, important

attention must also be paid to the potential risks of *de novo* mutations in cell lines, especially haploid models where there is no redundancy for the functional consequences of those mutations. Furthermore, while a reference genome has been developed for the derived eHAP1 cell line, none exists for the parental HAP1 cell line³¹⁰. Despite this, we were only able to identify one report describing a *de novo* mutation in HAP1 cells, a splice-site inhibition in *TDPI* which causes HAP1 cells to be more sensitive to topoisomerase 1 inhibition³¹¹.

We employed a commercially available HAP1 *TPCNI* knockout (KO) to model the effects of TPC1 loss on mitochondrial dysfunction. Our results support that these cells exhibit deficits in oxidative phosphorylation and in the expression of several electron transport chain subunits. However, our inability to rescue these phenotypes TPC1 re-expression and subsequent whole-genome sequencing results question whether TPC1 loss is responsible for these mitochondrial phenotypes. Additionally, these results reinforce the need for a high standard of rigor when using haploid cell KO models.

2.2 Materials and Methods

2.2.1 HAPI cell culture

HAPI cells were cultured in Dulbecco's Modified Eagle Medium supplemented with 10% heat-inactivated fetal bovine serum and 1% penicillin/streptomycin. Cells were maintained in 95% air and 5% CO₂ at 37°C. Only cells under passage 30 were utilized in this study.

2.2.2 Quantitative real-time polymerase chain reaction (PCR)

RNA was extracted from HAP1 cells using an RNeasy mini Kit (Qiagen) with on-column DNase treatment (Qiagen) according to the manufacturer's recommended protocol. cDNA amplification was performed using a High-Capacity cDNA Reverse Transcription Kit (Thermo Scientific, catalogue #4368814) according to manufacturer's protocol, with 1 µg of input RNA for each sample. qPCR was performed using PowerUp™ SYBR™ Green Master Mix (Thermo Scientific, catalog #A25741) on a QuantStudio 3 real-time PCR system (Applied Biosystems) according to manufacturer's protocol. Primers against *Tpcn1*, *Tpcn2*, and *Ccdc127* were purchased as described in the following table from Integrated DNA Technologies (Coralville, IA). Gene expression was normalized to coiled-coil domain containing 127 (*Ccdc127*) and expressed relative to vehicle control samples to yield a relative quantity value ($2^{-\Delta\Delta C_t}$).

Table 2.1. qPCR Primers to detect *Tpcn1* and *Tpcn2* expression levels.

Transcript	Forward Primer	Reverse Primer
<i>Tpcn1</i>	CAAACGGACCGCCATCCA	AAGCGTTCCTTGCACTCAT
<i>Tpcn2</i>	GTGGACTGGATCGTTTCGCT	CAATAGGAAACTGTGCACTGGG
<i>Ccdc127</i>	TGGGAGAAGCTCTCGAGGAA	ACAGATGTGCGCACCAGTAA

2.2.3 HAP1 cell culture

Immortalized *TPCNI* KO HAP1 cells (catalog number (Cat#) HZGHC007874c010) were acquired from Horizon Discovery (Waterbeach, United Kingdom) at passage 9, along with the wild-type parental line (passage 7). The reported *TPCNI* knockout CRISPR edit was validated by next-generation sequencing at the University of Maryland, Baltimore Translational Genomics Core using forward primer CCTGATGTTGGCAGGAAGTGT and reverse primer ACCTCATCACTAACTGACTCACAA. HAP1 cells were cultured at 37°C under 5%

CO₂ in Iscove's Modified Dulbecco's Medium supplemented with 10% heat-inactivated fetal bovine serum (FBS) and 1% penicillin/streptomycin. Only cells under passage 20 were utilized.

2.2.4 HT1080 cell culture

Immortalized wild-type, *TPCN1* knockout, and *TPCN2* knockout HT1080 cells were generously provided by Drs. Spencer Freeman and Sergio Grinstein (Peter Gilgan Centre for Research and Learning, Hospital for Sick Children, Toronto, ON, Canada). These cells were cultured at 37°C under 5% CO₂ in Dulbecco's Modified Eagle Medium supplemented with 10% heat-inactivated FBS and 1% penicillin/streptomycin. Only cells under passage 10 were utilized.

2.2.5 TPCN1 overexpression

Wild-type and dominant-negative pLV-CMV-TPCN1-3xGS-HA-Neo constructs were designed and purchased via VectorBuilder (Chicago, IL). Virus was transduced into wild-type or *TPCN1* KO HAP1 cells using 5 MOI of virus and 1 mg/mL Kolliphor. The selection of successfully transduced cells was performed using 400 µg/mL G418.

2.2.6 Western blotting

HAP1 or HT1080 cells were lysed one day after plating in ice-cold RIPA buffer plus protease/phosphatase inhibitor (Thermo Fisher Scientific; Waltham, MA), sonicated for 10 seconds on ice, and centrifuged at 13,300 x g for 20 minutes at 4°C to remove insoluble material. The supernatant was collected for western blot. For experiments employing a proteasome or autophagy inhibitor, cells were treated on the day after plating with 15 µM epoxomicin or 10 µM chloroquine, respectively, for 24 hours prior to

the lysate collection and processing. Protein levels were quantified via bicinchoninic acid assay³¹².

Protein samples (30-50 µg) were prepared in 1X sodium dodecyl sulfate (SDS) loading buffer (LI-COR; Lincoln, NE) containing 0.1M dithiothreitol and heated for 10 minutes at 95°C before loading onto Novex 4-20% Tri-Glycine Plus SDS-polyacrylamide gel electrophoresis (PAGE) gels (Thermo Fisher Scientific). SDS-PAGE was run at 160V for 35 minutes and then protein was transferred to polyvinylidene fluoride membranes. Total protein levels were imaged using Revert 700 (LI-COR). Blocking was performed in Tris-buffered saline containing 0.1% (v/v) Tween-20 (TBS-T) that was supplemented with 2.5% non-fat milk and 2.5% bovine serum albumin (BSA). The following primary antibodies at the indicated dilutions were used: 1:5,000 human rhodamine-conjugated anti-tubulin (Bio-Rad Cat# 12004165, RRID:AB_2884950; Hercules, CA), 1:200 rabbit anti-TPC1 (Proteintech Cat# 23758-1-AP, RRID:AB_2879317; Rosemont, IL), 1:500 mouse anti-human OxPhos Cocktail (Thermo Fisher Scientific Cat# 45-8199, RRID:AB_2533836), 1:1,000 mouse anti-HA (BioLegend Cat# 901513, RRID:AB_2565335; San Diego, CA), 1:1000 rabbit anti-p62/SQSTM1 (Proteintech Cat# 18420-1-AP, RRID:AB_10694431), and 1:1,000 rabbit anti-MCL-1 (Proteintech Cat# 16225-1-AP, RRID:AB_2143977). The secondary antibodies used were IRDye 680RD goat anti-mouse (LI-COR Biosciences Cat# 926-68070, RRID:AB_10956588) and IRDye 800CW goat anti-rabbit (LI-COR Biosciences Cat# 926-32211, RRID:AB_621843), both at 1:20,000. Imaging was performed on a LI-COR Odyssey FC imager.

2.2.7 Immunocytochemistry

HAP1 cells transduced with either wild-type or dominant-negative TPC1-HA were seeded onto two coverslips each at 150,000 cells/well in a 24-well plate and cultured overnight. The next day, the cells were fixed in 4% paraformaldehyde in phosphate-buffered saline (PBS). Following fixation, cells were washed three times with PBS and permeabilized for 20 minutes in PBS containing 0.15% Triton-X-100. Cells were then blocked in 7.5% BSA and 0.15% Triton-X-100-containing PBS for 45 minutes, followed by 90 minutes of immunostaining with 1:200 rabbit-anti NDUFB8 (Proteintech Cat# 14794-1-AP, RRID:AB_2150970) and 1:1,000 mouse anti-HA (BioLegend Cat# 901513, RRID:AB_2565335). Cells were then washed twice in PBS before one hour of incubation with an an Alexa Fluor 488 goat anti-mouse IgG secondary antibody (Life Technologies, catalog #A11029, RRID:AB_2354088) and an Alex Fluor 555 goat anti-rabbit IgG secondary antibody (Invitrogen, catalog# A32732, RRID:AB_2633281) at a dilution of 1:2,000 each. Cells were finally washed twice with PBS, mounted with ProLong Diamond with 4',6-diamidino-2-phenylindole, dihydrochloride (DAPI; Thermo Fisher, Cat# P36971), and allowed to cure for 24 hours before imaging. Images were acquired on a Nikon W1 spinning disk confocal microscope at the University of Maryland, Baltimore Confocal Microscopy Facility.

2.2.8 Seahorse microplate-based respirometry

Cellular oxygen consumption rates (OCR) and extracellular acidification rates (ECAR) were assessed using a Seahorse XFe24 Extracellular Flux Analyzer (Agilent Technologies; Santa Clara, CA). Briefly, the principle behind this technology is the quantification of flux in extracellular oxygen and pH from adherent cells by recording real-time changes in the oxygen and proton composition of cell culture media in a

transient microcompartment created between the XF assay cartridge and probes and a specialized cell culture plate. Oxygen and proton composition is quantified by fluorescent emission signal (oxygen excitation/emission = 532nm/650 nm; proton excitation/emission = 470 nm/530 nm), and the cartridge contains four programmable delivery chambers for the serial injection of test compounds, which can be leveraged to selectively assess the function of individual ETC subunits^{313,314}. Measurements were performed in an assay medium comprised of 120 mM NaCl, 3.5 mM KCl, 1.3 mM CaCl₂, 0.4 mM KH₂PO₄, 1 mM MgCl₂, 5 mM 4-(2-hydroxyethyl)-1-piperazineethanesulfonic acid (HEPES), 15 mM glucose, and 4 mg/mL fatty acid-free bovine serum albumin, pH 7.4.

2.2.9 Whole-Genome Sequencing

Passage 9 (WT parental) and 11 (*TPCNI* KO) HAP1 cells were submitted for whole-genome sequencing and variant call analysis through the University of Maryland Institute for Genome Sciences. The following description details how these procedures were done by the core facility. Genomic DNA libraries were constructed for sequencing on the Illumina NovaSeq 6000 (Illumina, San Diego, CA) using the KAPA EVOPlus II Kit (Roche, Indianapolis, IN). Libraries were prepared using a modified version of the manufacturer's protocol. A custom adapter was used for adapter ligation. Ligated fragments were size-selected using calibrated SPRIselect beads (Beckman Coulter Genomics, Danvers, MA). Unique dual indexes of 10 nucleotides in length were added to each sample during a final library amplification step. Final libraries were assessed using the GX Touch II (Revity, Waltham, MA). The libraries were pooled, assessed by qPCR

using the KAPA Library Quantification Kit (Kapa Biosystems, Woburn, MA), and sequenced on an Illumina NovaSeq 6000 using 150bp PE reads.

Raw data from the sequencer were processed using Illumina and Maryland-Genomics-developed pipelines for sequence assessment and quality control. Following base-calling by Illumina pipelines, our quality control pipeline assessed base-call quality and truncated reads when the median Phred-like quality score fell below Q20. Further analysis of the resulting sequence reads was performed using our human whole genome analysis pipeline based upon the Burrows-Wheeler Aligner (BWA-0.7.4) and the Genome Analysis Toolkit (GATK-4.2.4.1).

Initial alignment to the human reference genome (human_g1k_v37_decoy) was performed using BWA and followed by preliminary evaluation to assess coverage. The Picard package was used to clean up any mapping artifacts and to identify sequence reads that result from duplicated library fragments. Removal of these duplicated reads prevents artificially high coverage and reduces false-positive variant calling. The alignments were processed using GATK to recalibrate base qualities. Haplotypecaller in GATK was used to call indels and SNVs. Variants were filtered to identify false positives due to poor mapping, strand bias, read position bias and variant confidence. The resulting sets of high confidence variants were annotated and their effects on genes (e.g., amino acid change) predicted using ANNOVAR³¹⁵.

2.3. Results

2.3.1 HAPI microglia-like cells exhibit lower levels of *Tpcn1* mRNA following pro-inflammatory activation

To evaluate changes to *Tpcn1* gene expression in pro-inflammatory microglia, we utilized an immortalized mouse microglia cell line (HAPI) and induced pro-inflammatory activation by culturing the cells for 18 hours in the presence of 100 ng/mL lipopolysaccharide (LPS) and 10 ng/mL mouse interferon-gamma (IFN γ). We then ran qPCR to test for changes in mRNA encoding either *Tpcn1* or the other mammalian two-pore channel, *Tpcn2*, relative to *Ccdc127* as a housekeeping control. These results demonstrated a significant ($p = 0.011$) decrease in *Tpcn1* mRNA in pro-inflammatory microglia relative to controls, but no change in *Tpcn2* mRNA (Figure 2.1.).

2.3.2 TPCN1 KO HAPI cells exhibit decreased mitochondrial bioenergetic function

To determine the impact of TPC1 loss on mitochondrial bioenergetic function, we employed a commercially available human near-haploid *TPCN1* knockout cell line (HAP1) because HAPI cells and other microglial cell lines are difficult to genetically manipulate^{109–111}. This cell line is reported to have a deletion in exon 7 of *TPCN1*, which we validated by next generation sequencing (Figure 2.2) OCR and ECAR were measured using a Seahorse XFe24 Extracellular Flux Analyzer (Agilent Technologies) to evaluate mitochondrial respiration and glycolysis, respectively. To interrogate mitochondrial ETC function, we employed two injection paradigms. In the first paradigm, we performed serial injections as follows:

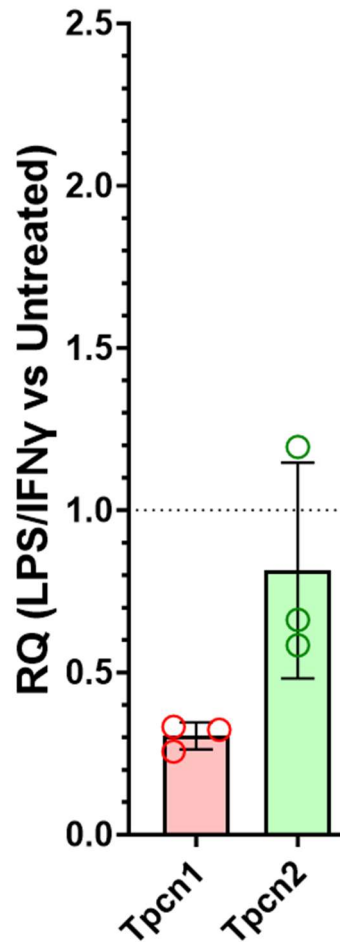


Figure 2.1. LPS/IFN γ suppresses mRNA expression of *Tpcn1* in HAPI cells.

Tpcn1, but not *Tpcn2*, mRNA transcript expression is decreased in HAPI cells following 18 hours of pro-inflammatory activation with 100 ng/mL LPS and 10 ng/mL IFN γ

1. FCCP + pyr, where FCCP uncouples ETC Complex I-IV activity from that of ATP synthase, and pyr supplies additional substrate to overcome glycolysis rate-limitation of OCR. This induces “maximal” mitochondrial respiration, and the difference between this maximal OCR and basal OCR is understood as the spare or reserve capacity of mitochondria^{316,317}.

2. Additional FCCP, to confirm attainment of maximal OCR following the first injection.
3. Antimycin A, a Complex III inhibitor. Electron transport flows from Complexes I and II separately into Complex III; by inhibiting the ETC at Complex III, we can quantify the remaining OCR as contributions from non-mitochondrial biological and chemical processes^{316,317}.
4. TMPD/asc, where TMPD donates electrons to cytochrome *c*, which under physiological conditions transfers electrons from Complex III to Complex IV. Quantification of OCR following TMPD/asc injection allows us to calculate the respiratory capacity of ETC Complex IV in isolation from other subunits³¹⁷.

In the second injection paradigm, we employed serial titration of the ATP synthase inhibitor oligomycin followed by antimycin a, which allows for further calculation of OCR linked to the production of ATP and due to “proton leak,” where protons enter the mitochondrial process without contributing to the production of ATP³¹⁶. *TPCNI* KO HAP1 cells exhibited decreased basal, ATP-linked (oligomycin-sensitive), and maximal (FCCP-induced) OCR relative to WT parental controls (Figure 2.3A-B; Table 2.2) but did not display basal or maximal (oligomycin-induced) ECAR alterations (Figure 2.3C; Table 2.2). These results are consistent with *TPCNI* KO cells having decreased oxidative phosphorylation and unaltered glycolysis as compared with WT cells.

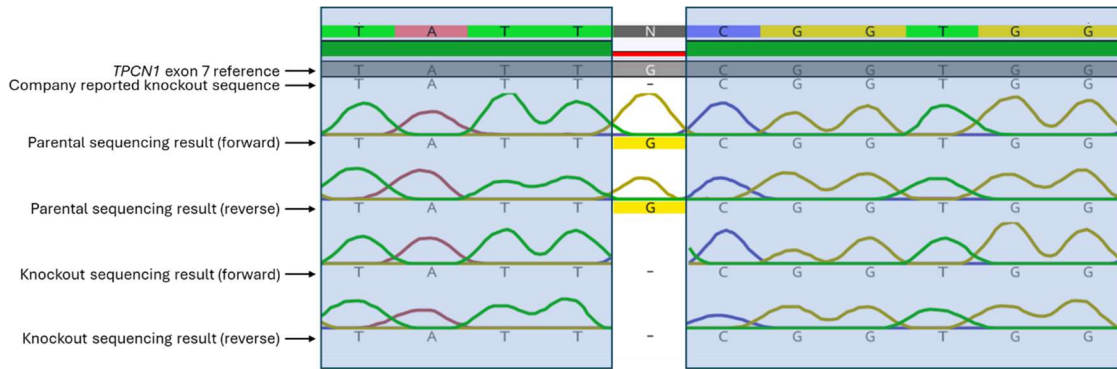


Figure 2.2. Next generation sequencing validation of *TPCN1* KO.

Chromatograms showing next generation sequencing results of exon 7 of *TPCN1*, comparing *TPCN1* KO and WT parental HAP1 genomic DNA against the reported sequence in the human reference genome (gray reference sequence) and the reported deletion provided by the commercial cell line supplier (Horizon Discovery; “company reported knockout sequence”).

We examined the protein expression of several mitochondrial electron transport chain (ETC) subunits to determine whether ETC alterations may contribute to the reduced respiration of *TPCN1* KO cells. We evaluated five independent lysate collections from *TPCN1* KO or WT HAP1 cells by western blot using an OxPhos antibody cocktail to detect a representative subunit of each ETC complex. A subset of ETC subunits that included the Complex I subunit NDUFB8, the Complex III subunit UQCX2, and the complex IV subunit MT-CO2 were severely depleted in *TPCN1* KO cells, whereas the Complex II subunit SDHB and the Complex V subunit ATP5A were unaltered (Figure 2.4A-B). We were surprised by the severity of the ETC complex protein deficiencies relative to the more moderate deficits in mitochondrial oxygen consumption, so we sought to examine the Complex I subunit NDUFB8 by fluorescence microscopy. In parallel, we overexpressed WT TPC1 conjugated to an HA tag to resolve if TPC1 colocalizes with mitochondria. The resulting images reveal that the NDUFB8 that is present in *TPCN1* KO displays a WT distribution pattern consistent with mitochondrial

localization, and that overexpressed TPC1 protein does not predominantly colocalize with NDUFB8 in either WT or KO cells (Figure 2.4C).

2.3.3 The ETC subunit loss in *TPCN1* KO HAP1 cells is not rescued by an autophagy or proteasome inhibitor

Pharmacological inhibition of two-pore channels, nonspecific to isoform, is reported to decrease autophagic flux in cardiomyocytes and astrocytes, causing accumulation of the autophagy substrate p62^{318,319}. Impaired mitophagy can lead to mitochondrial ETC protein degradation through the enhanced activity of matrix proteases³²⁰. The levels of some mitochondrial ETC proteins are reported to be regulated by ubiquitin-dependent proteasome turnover^{320,321}. Thus, either altered autophagy or enhanced proteasomal degradation might contribute to the loss of ETC subunits observed in *TPCN1* KO HAP1 cells. To investigate these possibilities, WT and *TPCN1* KO cells were cultured for 24 hours in the presence of either the autophagy inhibitor chloroquine or the proteasome inhibitor epoxomicin prior to the western blot evaluation of ETC subunits. All five representative ETC subunits were unaltered by chloroquine or epoxomicin treatment in each cell type (Figure 2.5A).

Figure 2.3. *TPCN1* knockout HAP1 cells exhibit impaired respiration.

(a) Oxygen consumption rate (OCR) trace for wild-type (WT) parental and *TPCN1* knockout (KO) HAP1 cells receiving serial injections of 2 μ M FCCP plus 10 mM pyruvate, 1 μ M FCCP, 1 μ M antimycin A, and 0.4 mM TMPD plus 2 mM ascorbate. Traces are mean \pm SD from three independent experiments, with 2-3 technical replicates per experiment. (b) OCR and (c) ECAR traces for WT parental and *TPCN1* KO HAP1 cells receiving serial injections of 0.5 μ g/ml oligomycin, 0.25 μ g/ml oligomycin, 0.25 μ g/ml oligomycin, and 1 μ M antimycin A. Traces are mean \pm SD from three independent experiments, with 2-3 technical replicates per experiment.

Figure 2.3, continued.

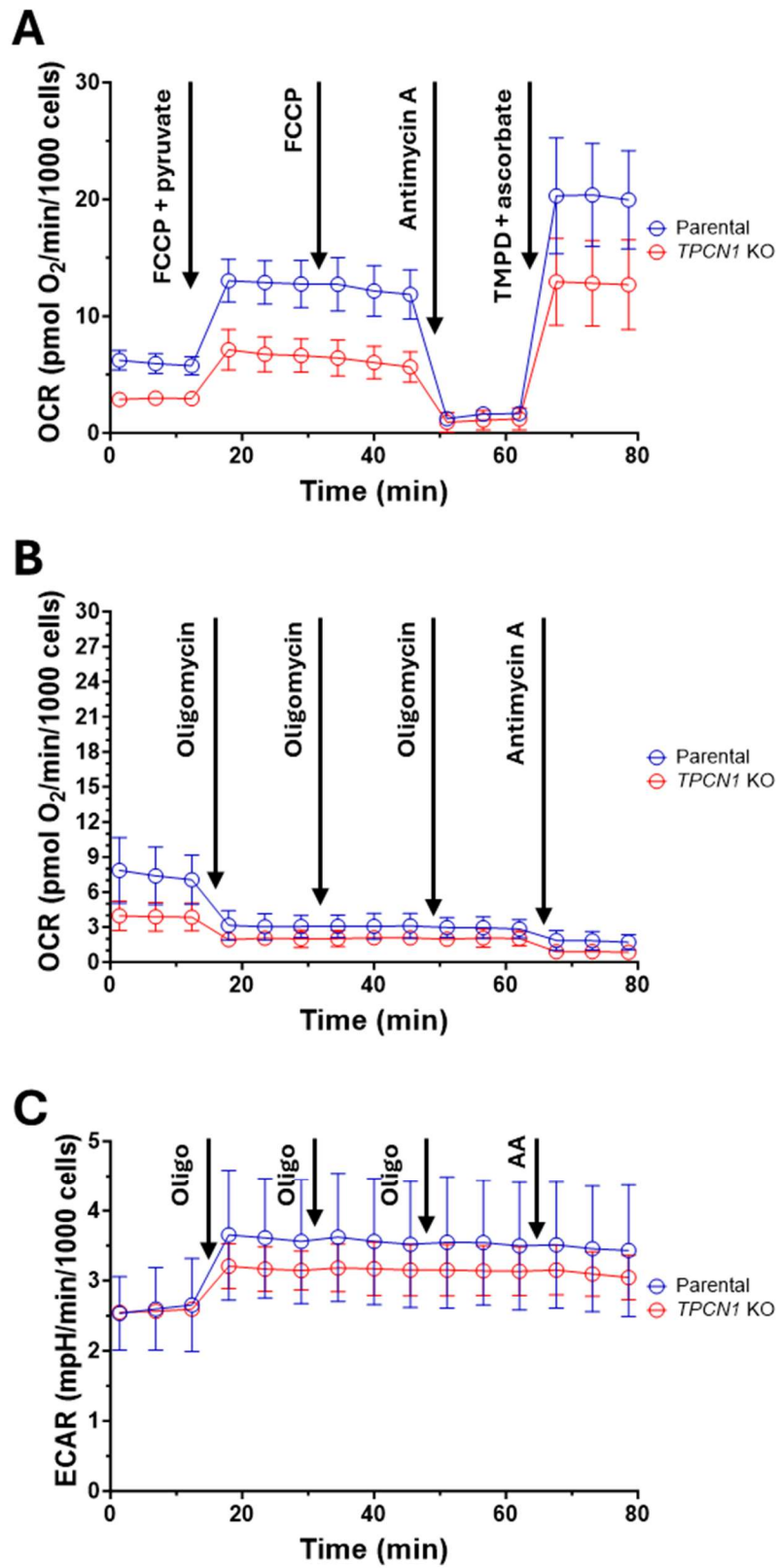


Table 2.2. *TPCNI* knockout HAP1 cells exhibit impaired oxidative phosphorylation.

Calculated components of mitochondrial bioenergetic function derived from the data in Figure 2.1.

Parameter (pmol O ₂ /min/1000 cells)	Parental	<i>TPCNI</i> KO	Significance
Basal Mitochondrial OCR	4.40	2.35	p = 0.0117
Maximal Mitochondrial OCR	11.38	5.76	p = 0.0380
Non-Mitochondrial OCR	1.58	0.89	n.s.
ATP-Linked OCR	3.60	1.62	p = 0.0208
Proton Leak	1.07	0.90	n.s.
Complex IV Capacity	17.94	12.33	n.s.
Basal ECAR (mpH/min/1000 cells)	2.59	2.57	n.s.
Maximal ECAR (mpH/min/1000 cells)	3.47	3.01	n.s.

Neither the level of the autophagy substrate p62 nor the level of the proteasome-regulated mitochondrial protein MCL-1 differed between WT and *TPCNI* KO cells at baseline. In WT cells, chloroquine increased p62 expression while epoxomicin increased MCL-1 expression, consistent with the expected inhibition of autophagy and the proteasome, respectively (Figure 2.5A, C). However, in the KO cells, p62 and MCL-1 were not increased by chloroquine and epoxomicin, respectively, making the lack of effect on ETC subunits difficult to interpret (Figure 2.5A, C). Thus, we repeated this experiment in *TPCNI* KO cells only, including additional, higher concentrations of chloroquine and epoxomicin, as well as a chloroquine/epoxomicin co-treatment group. The expected stabilization of MCL-1 by epoxomicin was now clearly observed at both the 15 μ M and 30 μ M concentrations (Figure 2.5B). However, we failed to see p62 stabilization in

TPCN1 KO HAP1 cells even when employing a five-fold higher concentration of chloroquine (Figure 2.5B, C).

2.3.4 Genetic manipulations of *TPC1* levels or activity fail to rescue or recreate the mitochondrial phenotypes seen in *TPCN1* KO HAP1 cells

To validate that the mitochondrial deficits observed in *TPCN1* KO HAP1 cells are in fact due to loss of TPC1 function, we employed multiple strategies. First, we overexpressed either wild-type or dominant negative HA-tagged TPC1 in both wild-type and *TPCN1* KO cells using lentiviral constructs^{64,66}. Surprisingly, although successful overexpression of TPC1 was confirmed via western blot, no rescue of ETC subunits via WT TPC1 overexpression or loss of subunits via dominant-negative TPC1 was observed (Figure 2.6A). We then acquired HT1080 cells of wild-type, *TPCN1* KO, and *TPCN2* KO backgrounds, and probed for ETC subunit expression. Again, while we confirmed *TPCN1* KO, we were unable to identify any changes in ETC subunit expression in either the *TPCN1* KO or *TPCN2* KO HT1080 cell lines (Figure 2.6B).

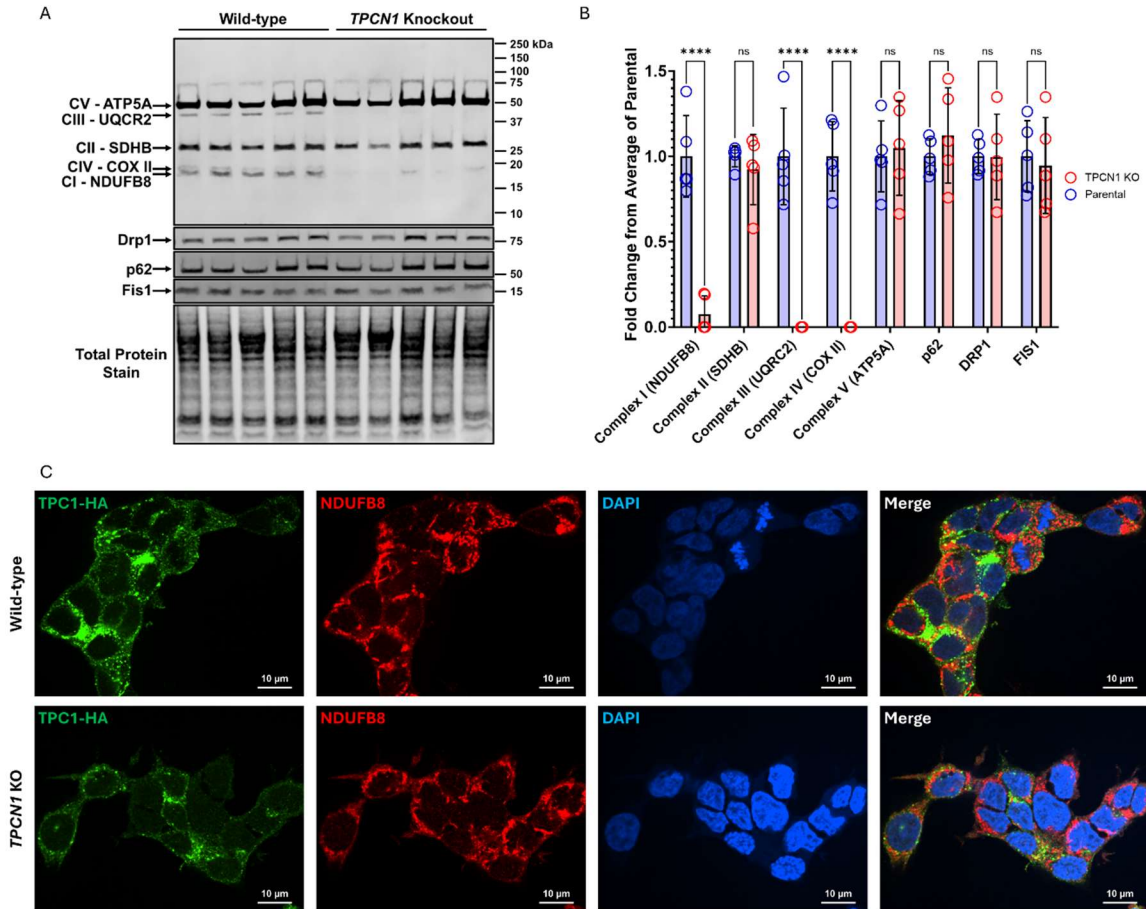


Figure 2.4. *TPCN1* knockout cells exhibit decreased levels of several mitochondrial electron transport chain proteins but overexpressed TPC1-HA does not predominantly localize to mitochondria.

(a) NDUFB8, SDHB, UQCR2, COX II, and ATP5A protein levels in WT and *TPCN1* KO HAP1 cells. Five independent lysate collections per genotype. (b) Quantification of ETC subunits in panel (a) (c) Localization of HA and NDUFB8 proteins and double-stranded DNA (DAPI) in WT and *TPCN1* KO HAP1 cells overexpressing a WT TPC1-HA construct.

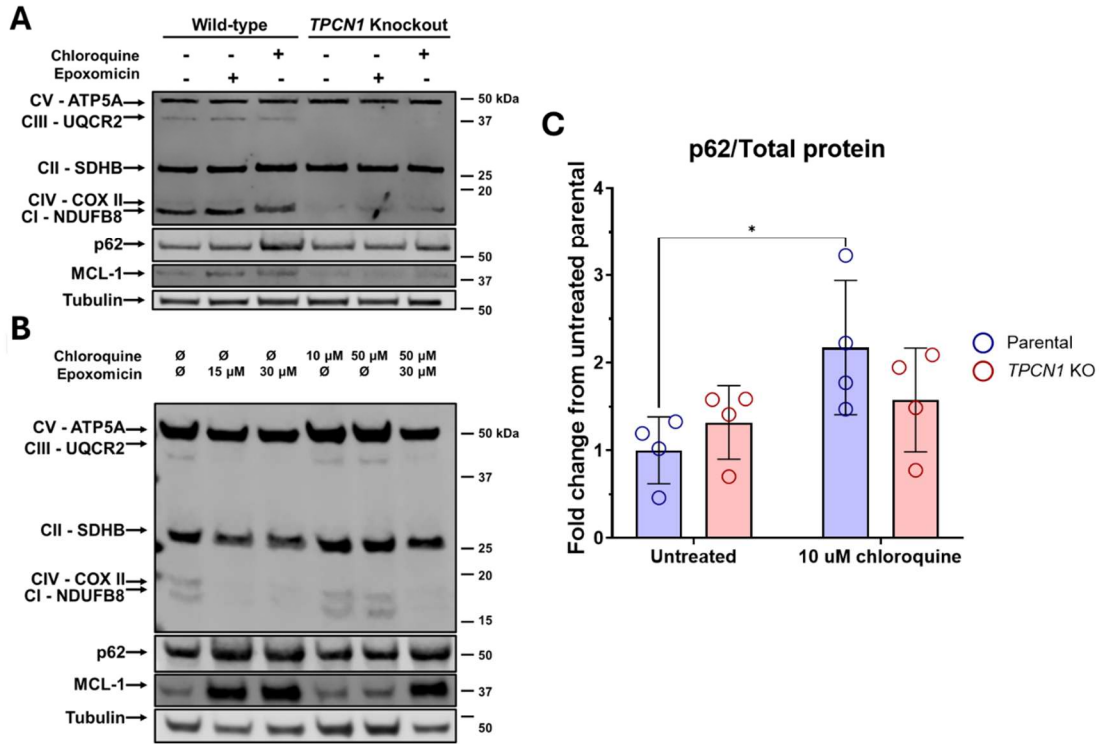


Figure 2.5. Inhibition of autophagy or proteasomal activity does not recapitulate or rescue the mitochondrial ETC protein loss observed in TPCN1 KO HAP1 cells.

(a) NDUFB8, SDHB, UQCR2, COX II, ATP5A, p62, MCL-1, and tubulin protein levels in WT and *TPCN1* KO HAP1 cells cultured with or without 10 μM chloroquine to inhibit autophagy or 15 μM epoxomicin to inhibit proteasomal activity for 24 hours. The results with chloroquine are representative of four independent experiments whereas as a single experiment with epoxomicin is shown. (b) Experimental paradigm in (a) repeated in *TPCN1* KO HAP1 cells only, with the addition of 50 μM chloroquine, 30 μM epoxomicin, and chloroquine/epoxomicin co-treatment groups. (c) Quantification of p62 stabilization by chloroquine in wild-type parental but not *TPCN1* KO over four identical lysate collections, as described in (a).

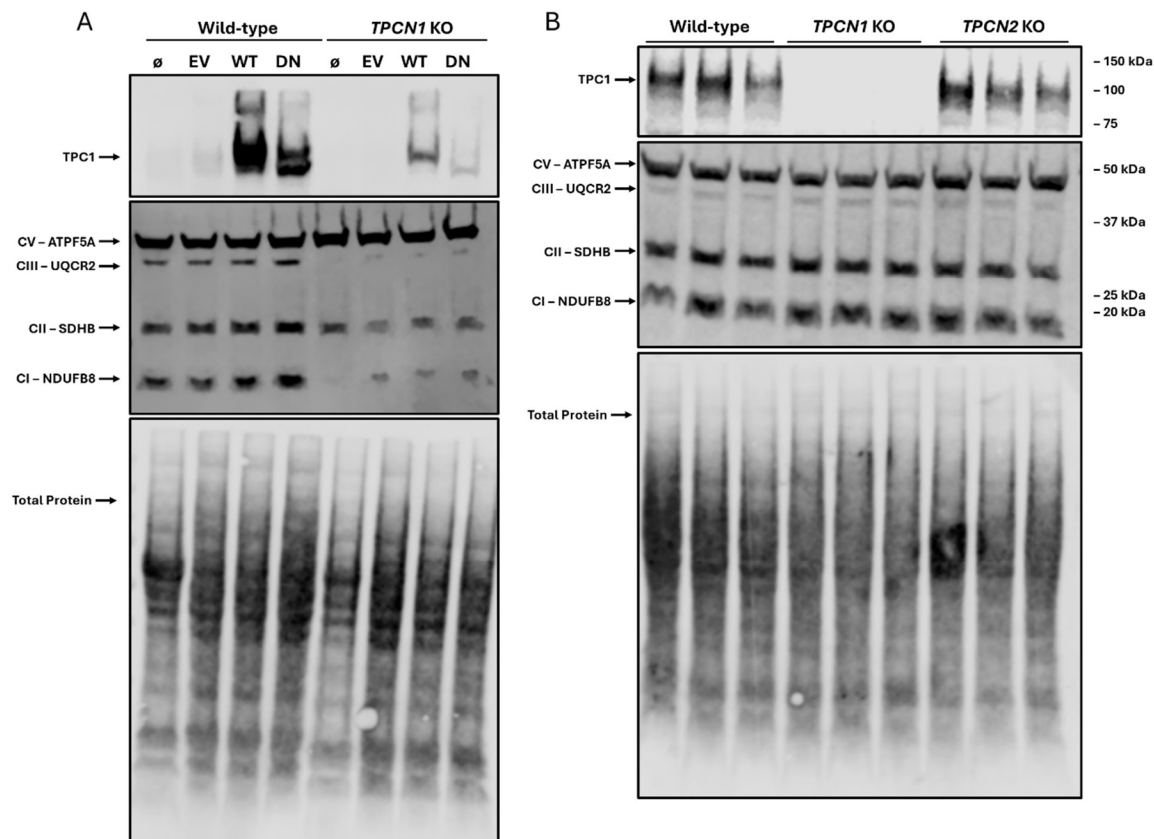


Figure 2.6. Other genetic manipulations of TPC1 levels or activity fail to rescue or recreate the mitochondrial phenotypes seen in *TPCN1* KO HAP1 cells.

(a) NDUFB8, SDHB, UQCR2, ATP5A, and HA tag protein levels in WT parental or *TPCN1* KO HAP1 cells with either no viral transduction (\emptyset), transduction with an ORF stuff construct (EV), or transduction with either WT TPC1 or dominant negative (DN) TPC1 p.L273P conjugated to an HA tag. (b) NDUFB8, SDHB, UQCR2, ATP5A, and TPC1 protein levels in WT, *TPCN1* KO, or *TPCN2* KO HT1080 cells. Three independent lysate collections per genotype are shown.

2.3.5 HAP1 cells exhibit many *de novo* mutations that could alter the functional interpretations of KO studies

To identify alternative mutations in *TPCN1* KO HAP1 cells that could cause or contribute to the loss of mitochondrial ETC subunits, we carried out whole-genome sequencing (WGS) and variant call analysis on both WT parental and *TPCN1* KO HAP1 cells relative to the human reference genome (Table 2.3), which was done through the

UMB Institute for Genome Sciences Core Facility. The resulting variants were identified in known protein-encoding genes and then filtered for genes encoding proteins included within the MitoCarta3.0 database of mitochondrially localized proteins³²². This analysis revealed 557 variants from the human reference genome that are present in *TPCNI* KO cells but not WT parental HAP1 cells, including the introduced frameshift-inducing amino acid deletion in *TPCNI* itself. Of these 557 variants, 185 altered the primary amino acid sequence of the encoded protein, and 20 were in genes encoding proteins found in the MitoCarta3.0 database. Among the MitoCarta genes, five – *FDXI*, *NUPBL*, *POLG*, *TRAP1*, and *MTFMT* – had DNA variation that would result in a nonsynonymous amino acid sequence (Table 2.4). Because the *MTFMT* p.R332X mutation encodes the most severely altered predicted variant and is present in the disomal region of HAP1 chromosome 15, we conducted next-generation sequencing on both WT parental and *TPCNI* KO HAP1 cells to test for this variant and evaluate hetero- vs homozygosity. Unexpectedly, we found that both genetic backgrounds are heterozygous for *MTFMT* p.R332X (Figure 2.7), suggesting that this mutation is unlikely to cause the *TPCNI* KO cells' bioenergetic deficits. Surprisingly, we also identified 672 variants – 242 of which alter the primary amino acid sequence of the encoded protein – present in WT parental cells but not in *TPCNI* KO cells (Table 2.3). The two DNA samples were sequenced at the lowest available passage of each cell line, differing only by two passages (P9 for WT and P11 for *TPCNI* KO, respectively). The similarly large variant number in the WT and KO cells suggests that HAP1 cells have a high propensity for *de novo* mutations – i.e., it is unlikely that most of the variants in the *TPCNI* KO line are off-target CRISPR editing effects, since the unedited line showed the same level of variation. A further 29,414

variants from the human reference genome, 7,339 of which are nonsynonymous, were present in both genetic backgrounds (Table 2.3).

Table 2.3. Prevalence of genetic variants from the human reference genome in protein-encoding genes of HAP1 cell lines.

Total, nonsynonymous, and frameshift or stop gain variants predicted by WGS and variant call analysis in HAP1 cells, subdivided into those variants found only in *TPCNI* KO cells, only in WT parental cells, or shared by both genetic backgrounds.

Genotype	Total variants	Predicted nonsynonymous variants	Predicted frameshift or stop gain variants
<i>TPCNI</i> KO	557	185	15
Wild-type	672	242	12
Both	29,414	7,339	183

Table 2.4. MitoCarta3.0 variants found in *TPCNI* KO HAP1 cells.

List of all genes with variants, and location of those variants, for genes encoding proteins found in the MitoCarta3.0 database.

Gene	Location
<i>LRPPRC</i>	3' UTR
<i>SUCLG1</i>	Intronic
<i>ALDH7A1</i>	3' UTR
<i>PARK2</i>	Intronic
<i>GDAP1</i>	Downstream
<i>CYP11B2</i>	Intronic
<i>ALDH1L2</i>	Intronic
<i>CYP11A1</i>	Upstream
<i>TTC19</i>	3' UTR
<i>TTC19</i>	3' UTR
<i>TTC19</i>	3' UTR
<i>CLPP</i>	Upstream
<i>TIM44</i>	Upstream
<i>TIM44</i>	Upstream
<i>TXN2</i>	Upstream
<i>FDX1</i>	Missense p.R41P
<i>NUPBL</i>	Missense p.K167T
<i>POLG</i>	Missense p.Q1236H
<i>TRAP1</i>	Missense p.R307G
<i>MTFMT</i>	Premature stop p.R332X

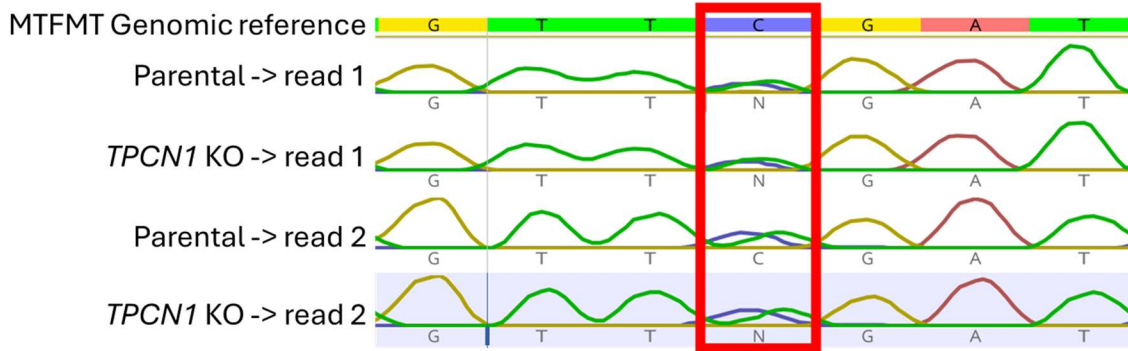


Figure 2.7. NGS validation of *MTFMT* sequencing

Chromatogram of NGS sequencing results from both WT parental and *TPCN1* KO HAP1 cells for the predicted premature p.R332X stop variant of *MTFMT*. Chromatograms labeled as “read 1” and “read 2” correspond to forward and reverse primer pairs. Note double peaks for cytosine (blue) and thymine (green) in the highlighted region in both WT parental and *TPCN1* KO cells, suggesting both lines are heterozygous for the p.R332X mutation, which is caused by a cytosine to thymine mutation at cDNA position 994 relative to the *MTFMT* reference sequence³²³.

2.4 Discussion

TPC1 has previously been ascribed both initiating and restraining roles in immune responses, either independently or in concert with the other two-pore channel, TPC2^{63,69–73}. More limited evidence suggests that TPC1, specifically, may also regulate interactions between the endolysosomal system and mitochondria^{74,75}. In the brain, TPC1 is highly expressed in microglia, in which mitochondrial bioenergetic deficiencies are thought to be key contributing factors to the progression of Alzheimer's Disease and Lewy Body Dementia^{1,42,43,47–49}. As TPC1 is a druggable target, a better understanding of the impacts of TPC1 loss on mitochondrial function may provide a point of intervention in difficult-to-treat neurological conditions.

After confirming that *Tpcn1* mRNA is lost upon pro-inflammatory insult in an immortalized mouse microglia line, we found that *TPCN1* KO HAP1 cells exhibit

impaired mitochondrial oxygen consumption and ETC subunit expression, consistent with TPC1 being required for homeostatic oxidative phosphorylation. We did not find evidence for a role of autophagy or proteasomal activity in regulating the levels of the investigated mitochondrial ETC subunits in WT cells, suggesting that known roles for two-pore channels in these protein quality control pathways may not be involved in *TPCNI* KO cells. However, the effects of the autophagy inhibitor chloroquine on *TPCNI* KO cells was difficult to interpret because it did not cause the expected stabilization of p62 even when added at a concentration five-fold higher than that showing efficacy in WT cells. One potential explanation for this discrepancy may be due to TPC1's homeostatic role as a proton-permeable ion channel regulating endosomal and lysosomal pH, as sufficiently acidic lysosomal environments are required for efficient autophagy and proteolysis^{324,325}. Thus, *TPCNI* KO cells may already partially recapitulate the effects of pharmacological inhibition of autophagy already. Notably, while we do not see evidence for altered p62 levels in *TPCNI* KO vs WT parental cells under basal conditions (Figure 2.4A-B), small interfering RNA-based knockdown of *TPCNI* has previously been reported to impair autophagy in cardiomyocytes and astrocytes^{318,319}. Additionally, confounding effects of non-specific interactions are always an important consideration when employing pharmacological inhibitors. Future studies should test other autophagy inhibitors and measure the lysosomal pH in *TPCNI* KO cells to address the surprising lack of chloroquine effect.

Unexpectedly, we found that overexpression of WT TPC1 in *TPCNI* KO HAP1 cells does not rescue ETC protein levels, and that overexpression of dominant negative TPC1 in WT HAP1 cells is not sufficient to reduce the expression of ETC subunits. In

addition, CRISPR-Cas9-mediated KO of *TPCNI* in HT1080 cells does not recapitulate the mitochondrial phenotype seen in the HAP1 *TPCNI* KO line. These results suggest that either an alternative mutation in *TPCNI* KO HAP1 cells is responsible for the observed mitochondrial phenotypes, or that the regulation of mitochondrial homeostasis by TPC1 occurs through a more complex balance of processes (e.g. both over- and under-expression of TPC1 may be detrimental, or TPC1 loss may only be detrimental in certain genetic backgrounds or cell types).

To begin to address these possibilities, we also show that HAP1 cells carry tens of thousands of variants from the human reference genome, including thousands which are predicted to result in nonsynonymous protein translation. Further, the identification of hundreds of variants unique to the unedited WT parental line suggests that HAP1 cells have a propensity for *de novo* mutations.

Overall, our results suggest that *TPCNI* KO HAP1 cells exhibit substantial deficits in oxidative phosphorylation, but the attribution of these deficits to TPC1 loss is premature. More broadly, our findings suggest that a higher standard of rigor must be applied to genetic studies in HAP1 cells and other haploid models compared to conventional practices, as whole-genome sequencing is not standard. This need results from the increased propensity for spontaneous genetic variants outside the scope of study to exert functional impacts that may cause or contribute to the phenotype of interest.

Chapter 3: Recharacterization of HAPI Cells as Mouse Microglia-like Cells Useful for Immunometabolism Studies

3.1 Introduction

Since first being reported in 2001, HAPI cells have become a popular *in vitro* microglial model system; as of August 20, 2025, we identified 99 results for “HAPI microglia*” in a search of PubMed¹⁰³. The capacity of HAPI cells for phagocytosis, induction of inducible nitric oxide synthase (iNOS) and TNF α , and secretion of NO and other pro-inflammatory molecules in response to LPS and/or the type II interferon IFN- γ has been independently replicated many times^{103,104,120–135}. These findings, as well as direct comparisons of HAPI cells to primary microglia and another immortalized microglial cell line, BV-2, supported the use of HAPI cells for studying microglial immune responses¹⁰⁴. However, HAPI cells were first reported as spontaneously immortalized rat microglia, isolated from a 3-day old rat brain¹⁰³.

We performed next generation sequencing of multiple genes while conducting experiments with HAPI cells and the results suggested that HAPI cells have a mouse, rather than rat, origin. Subsequently, we found that the HAPI cells are listed on the International Cell Line Authentication Committee’s Register of Misidentified Cell Lines as mouse, not rat, cells based on personal communication with their former suppliers, MilliporeSigma (Burlington, MA). Despite this, we have not identified any peer-reviewed publications referring to HAPI cells as mouse cells, and almost all recent publications continue to refer to HAPI cells as rat microglia^{326–335}. Therefore, the goals of our study were two-fold: 1) to recharacterize HAPI cells as a microglia-like mouse cell line by evaluating typical microglial cell markers and using the gold standard method of short tandem repeat (STR) profiling and 2) to help re-establish and extend the utility of HAPI

cells for *in vitro* studies of microglial immune responses by measuring the morphological and bioenergetic changes induced by common immune stimuli.

In both *ex vivo* and *in vitro* primary microglia treated with the pro-inflammatory stimuli LPS, alone or in combination with IFN γ , a suppression of maximal mitochondrial oxygen consumption and spare respiratory capacity is observed⁴⁷⁻⁴⁹. These metabolic shifts are thought to be TLR4-mediated and to contribute to the pro-inflammatory reprogramming of microglia in a range of neurological conditions, including multiple neurodegenerative diseases and following brain injury⁴⁷. As such, we tested whether HAPI cells, like primary microglia, demonstrate pro-inflammatory suppression of mitochondrial respiration. We then sought to extend these studies by investigating the effects of the type I interferon IFN- α on mitochondrial oxygen consumption, which has not been reported from primary microglia or microglia-derived cell lines.

3.2 Materials and Methods

3.2.1 Materials

Universal™ Type I interferon, a hybrid human interferon- α protein exhibiting bioactivity across multiple species including mice, was from PBL Assay Science (Piscataway, NJ; Cat# 11200).

Mouse-origin interferon- γ recombinant protein was from SinoBiological (Paoli, PA; Cat# 50709-MNAH)

Rat-origin interferon- γ recombinant protein was from ThermoFisher (Waltham, MA; Cat# 400-20). All other reagents were purchased from Sigma-Aldrich (St. Louis, MO) unless otherwise noted.

3.2.2 Cell Culture

HAPI cells and SIM-A9 cells were cultured in Dulbecco's Modified Eagle Medium supplemented with 10% heat-inactivated fetal bovine serum and 1% penicillin/streptomycin. Neuro2a cells were cultured in Eagle's Minimum Essential Medium supplemented with 10% heat-inactivated fetal bovine serum and 1% penicillin/streptomycin. Bone-marrow derived macrophages (BMDMs) were isolated from male C57BL/6 mice as per Haag and Murthy 2021³³⁶ and cultured for 8 days in Dulbecco's Modified Eagle Medium supplemented with 10% heat-inactivated fetal bovine serum, 1% penicillin/streptomycin, and 20% DMEM conditioned from Ladamac929 cells with a full media change every other day. All cells were maintained in 95% air and 5% CO₂ at 37°C. For the cell lines, only cells under passage 30 were utilized in this study.

3.2.3 Cortex Tissue Isolation

Messenger RNA from the brain cortex of an adult male C57BL6/J mouse was extracted using a Qiagen (Germantown, MD, USA) RNA extraction kit.

3.2.4 Short Tandem Repeat (STR) Profiling

HAPI DNA was submitted to American Type Culture Collection (ATCC; Manassas, VA) for STR profiling. Eighteen mouse STR loci were analyzed by ATCC and two markers (Human D8 and D4) were used to screen for the presence of human or African green monkey species. Samples, including appropriate positive and negative controls, were processed using an ABI Prism® 3500xl Genetic Analyzer and data were analyzed using GeneMapper® ID-X v1.2 software (Applied Biosystems; Waltham, MA). Comparison to entries in the ATCC Mouse STR Database were conducted by ATCC according to the Tanabe algorithm³³⁷.

3.2.5 mRNA Expression

RNA from HAPI cells, SIM-A9 cells, C57BL/6 mouse cortex, C57BL/6 mouse BMDMs, and Neuro2a cells was extracted and isolated using an RNAeasy Minikit (Qiagen, Cat# 74104) according to the manufacturer's recommended protocol. cDNA amplification was performed using a High-Capacity cDNA Reverse Transcription Kit (Thermo Scientific, Cat# 4368814) according to manufacturer's protocol, with 300 ng of input RNA for each sample. Primers against *Tmem119* (expected product length: 119 bp) and *Cx3cr1* (expected product length: 109 bp) as described in the following table were purchased from Integrated DNA Technologies (Coralville, IA). PCR amplification was performed using a 50 μ L reaction mix containing 25 μ L of GoTaq 2x MasterMix (Promega, Cat# M7132), 10 μ M each of the corresponding forward and reverse primers, 4 μ L of cDNA template, and nuclease-free water added to 50 μ L. For both target transcripts, the PCR amplification consisted of a two-minute initial denaturation at 95°C, 30 cycles of 30 second denaturation at 95°C, 1 minute annealing at 55°C, and 1 minute extension at 72°C, and a final 5-minute extension at 72°C. PCR products were then prepared with 2 μ L of 6x TriTrack DNA loading buffer (Thermo Scientific, catalogue #R1161) and 10 μ L sample and run in a 2% agarose Tris-borate EDTA (TBE) gel. Product size was visualized by emission at 600 nm in a LI-COR Odyssey Fc imager (LI-COR Biotechnology, Lincoln, NE) and evaluated by comparison to a GeneRuler 100 bp Plus DNA ladder (Thermo Scientific, Cat# SM0321).

Table 3.1. Primers against transcripts preferentially expressed by microglia and macrophages.

Transcript	Forward Primer	Reverse Primer
<i>Tmem119</i>	ATGGGGACAATGACAGCTCTTC	GGGAGTGACACAGAGTAGGC
<i>Cx3cr1</i>	TCGTCTTCACGTTTCGGTCTG	CTCAAGGCCAGGTTTCAGGAG

3.2.6 Immunocytochemistry

HAPI cells were seeded on glass coverslips and fixed in 4% paraformaldehyde in phosphate-buffer saline (PBS) for 20 minutes on the following day. Cells were then washed three times with PBS, permeabilized with 0.15% Triton-X-100 in PBS for 20 minutes, and blocked with 7.5% bovine serum albumin (BSA) in PBS for 45 minutes. Primary immunostaining was performed with 1:200 mouse-anti- Tmem119 antibody (Thermo Fisher, Cat# MA5-35043, RRID:AB_2848948) for 90 minutes in PBS containing 7.5% BSA and 0.15% Triton-X-100. Cells were then washed twice in PBS, before 60 minutes of incubation with an Alexa Fluor 488 goat anti-mouse IgG secondary antibody (Life Technologies, Cat# A11029, RRID:AB_2534088) at a 1:1000 dilution. Cells were then washed twice more in PBS before mounting coverslips and allowing to cure overnight in ProLong Diamond + DAPI antifade media (Thermo Fisher, Cat# P36971). Imaging was performed on a Nikon W1 spinning disk confocal mounted on a Nikon Ti2 inverted microscope at the University of Maryland, Baltimore Confocal Microscopy Facility. All steps were performed at room temperature.

3.2.7 Quantification of Nitric Oxide

HAPI microglial cells were stimulated for 18 hours with lipopolysaccharide (LPS; 100 ng/ml), interferon-gamma (IFN- γ ; 10 ng/ml), or Universal™ Type I interferon (10 ng/ml) alone, or LPS in combination with IFN- γ or Type I interferon at the same concentrations. Nitrite, a stable, non-volatile breakdown product of nitric oxide, was quantified in cell culture media by Griess assay according to the manufacturer's protocol (Thermo Fisher Scientific). The Griess assay relies on the extremely short half life (<1 second in blood) of NO, which breaks down into nitrite (NO₂⁻) and nitrate (NO₃⁻), the latter of which can then be reduced to nitrite. Sulfanilic acid and N-(1-

(1-Naphthyl)ethylenediamine dihydrochloride are then added to the test solution, where sulfanilic acid reacts with nitrite to form a diazonium salt, which then reacts with the N-(1-Naphthyl)ethylenediamine dihydrochloride to produce a purple azo dye that can be quantified via absorbance at 548 nm^{338,339}. In this way, the Griess assay leverages nitrite in the test solution – in this case, microglia conditioned media – as an indirect measure of NO secretion.

3.2.8 Morphology

Phase contrast images of cells were acquired using an EVOS® FL Auto Cell Imaging System (Thermo Fisher).

3.2.9 XF24 microplate-based respirometry

HAPI oxygen consumption and extracellular acidification rates were assessed using a Seahorse XF24 Extracellular Flux Analyzer (Agilent Technologies)(as described in Chapter 2 (2.2.8))^{313,314}. Measurements were performed in a pH 7.4 aCSF assay medium comprised of 120 mM NaCl, 3.5 mM KCl, 1.3 mM CaCl₂, 0.4 mM KH₂PO₄, 1 mM MgCl₂, 5 mM 4-(2-hydroxyethyl)-1-piperazineethanesulfonic acid (HEPES), 15 mM glucose, and 4 mg/mL fatty acid-free bovine serum albumin.

3.3 Results

3.3.1 HAPI cells are mouse cells expressing microglia selective markers

We performed next generation sequencing of multiple genes in HAPI cells during the process of designing small guide RNAs for CRISPR knockout. Sequencing results suggested that HAPI cells have a mouse, rather than rat, origin based on DNA homology. HAPI cells were identified as mouse cells in a public database, but the mouse strain or cell line they originated is unknown. To validate that HAPI cells are mouse cells and identify if they have a match in the ATCC cell database, we submitted HAPI cells to

ATCC's Mouse Cell Line Authentication Service, which uses short tandem repeat (STR) profiling by a multiplex PCR assay established by the Mouse Cell Line Authentication Consortium³⁴⁰. STRs are short sequences of DNA that are repeated in tandem at specific locations (loci) in the genome. The number of repeats varies greatly among cell lines, making STRs highly useful for identification by providing a cell line "fingerprint." Even an earlier method based on only nine rather than 18 STRs was able to distinguish among three different Balb/c-derived cell lines, demonstrating the utility of STR profiling for cell line identification³⁴¹.

STR profiling revealed that HAPI cells are an exact (100% STR) match for SIM-A9 cells, a mouse microglial cell line in the ATCC database (Figure 3.1; Table 3.2.). However, HAPI cells were first reported in 2001, while SIM-A9 cells were initially reported in 2014^{102,103}. Additionally, the HAPI cells used in this study were obtained from the original reporting lab in 2014. Therefore, it is unlikely that HAPI cells originated from mischaracterized SIM-A9 cells; rather, it is more likely that both cell lines were mischaracterized from a common ancestor.

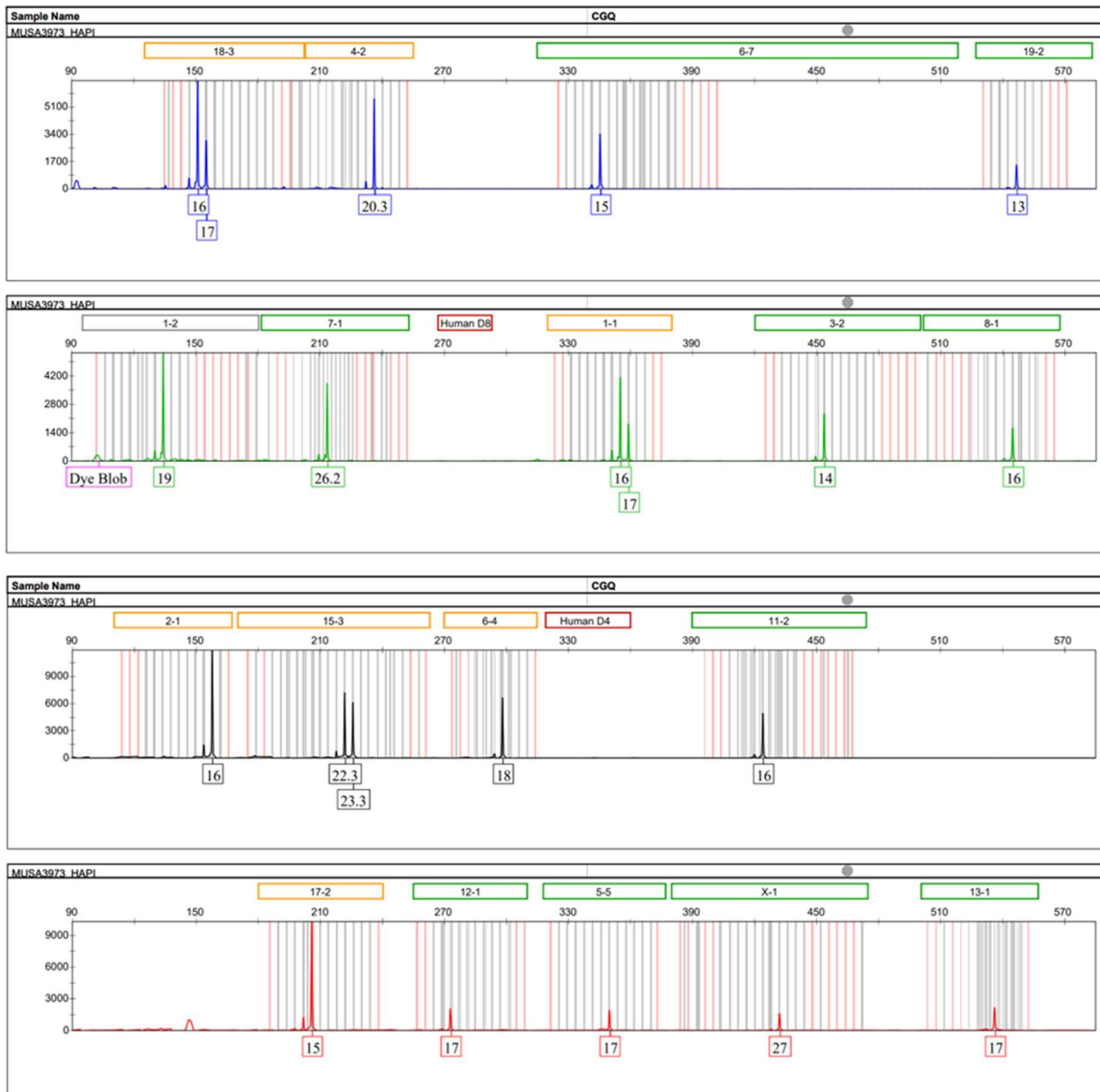


Figure 3.1. HAPI cell STR profiling results.

Electropherograms of each allele used for HAPI STR profiling.

Table 3.2. HAPI cells are mouse cells closely related to SIM-A9 cells.

Comparative STR allele results for submitted HAPI cells and the SIM-A9 cell record present in the ATCC Mouse STR Database.

Locus	HAPI Results	SIM-A9 Reference Profile
18-3	16,17	16,17
4-2	20.3	20.3
6-7	15	15
19-2	13	13
1-2	19	19
7-1	26.2	26.2
1-1	16,17	16,17
3-2	14	14
8-1	16	16
2-1	16	16
15-3	22.3,23.3	22.3,23.3
6-4	18	18
11-2	16	16
17-2	15	15
12-1	17	17
5-5	17	17
X-1	27	27
13-1	17	17

Next, to evaluate if HAPI cells have a microglia-like cell identity, we tested for the expression of the microglia-selective marker *Tmem119*, and the microglia- and macrophage-selective marker *Cx3cr1*. Polymerase chain reaction (PCR) amplification of primers specific to the mRNA transcripts of these genes was carried out on cDNA samples amplified from RNA isolated from HAPI cells, SIM-A9 cells, mouse cortex (as a microglia-containing positive control), bone marrow-derived macrophages, and Neuro2a neuroblastoma cells (as a non-microglia negative control). We found that HAPI cells, like SIM-A9 cells and the microglia-containing cortex samples, but unlike BMDMs and Neuro2a cells, expressed mRNA for the microglia-selective marker *Tmem119* (Figure 3.2A). Similarly, we found that HAPI cells also expressed the microglia-/macrophage-selective marker *Cx3cr1*, as did SIM-A9, cortex, and BMDM samples, but not samples

collected from Neuro2a cells (Figure 3.2B). Finally, we conducted immunocytochemistry for Tmem119 on fixed HAPI cells to provide a protein-level validation of Tmem119 expression. Universal staining of our cell population was observed (Figure 3.2C). These results support that HAPI cells are a microglia-like cell line, most likely originating from a mouse microglial origin.

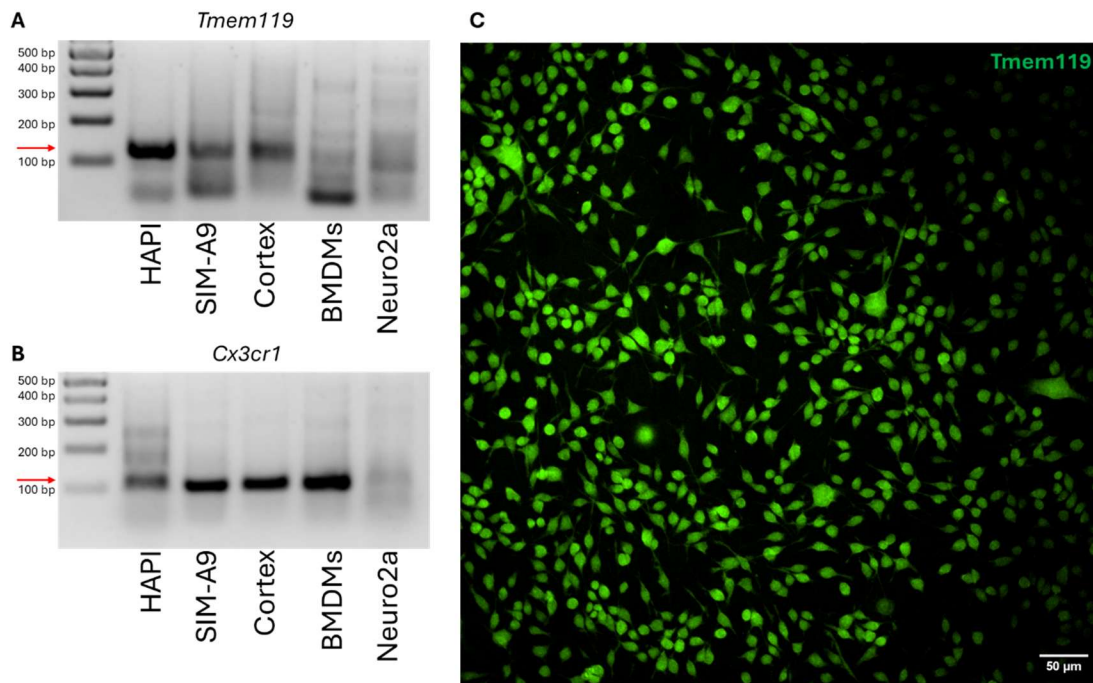


Figure 3.2. HAPI cells exhibit microglia-specific markers.

(A) Expression of *Tmem119* PCR products (expected band size: 119 bp, indicated in red) in samples prepared from HAPI cells, SIM-A9 cells, mouse cortical tissue, BMDMs, and Neuro2a cells. (B) Expression of *Cx3cr1* PCR products (expected band size: 109 bp, indicated in red) in samples prepared from HAPI cells, SIM-A9 cells, mouse cortical tissue, BMDMs, and Neuro2a cells. (C) Representative image of HAPI cells immunostained for Tmem119. Scale bar = 50 μM.

3.3.2 LPS, IFN γ , and IFN α induce activation-associated morphological changes in HAPI cells

Past studies support that treatment of HAPI cells with LPS or the type II interferon IFN γ can induce morphological changes and production of nitric oxide (NO) associated with pro-inflammatory remodeling of microglia^{103,104,121–129,131–135,342}. We sought to replicate these findings and extend them to the effects of the type I interferon IFN α . Because these past reports assumed that HAPI cells were of rat origin, we first compared their production of NO in response to rat- or mouse-origin IFN γ via the Griess assay. Our results indicate that HAPI cells reach a similar maximum NO release in response to 18 hours of treatment with similar doses of rat- or mouse-origin IFN γ (Figure 3.3), supporting the common usage of the rat cytokine for these mouse cells.

To test the ability of these stimuli to induce morphological changes in HAPI cells, a previous lab member imaged cultured cells treated with LPS, IFN γ , IFN α , or LPS/IFN γ or LPS/IFN α co-treatments for 18 hours using brightfield microscopy. Qualitatively, all treatments induced a morphological change relative to control cells, characterized by a rounding of cell bodies and the development of thin processes (Figure 3.4). These results support that HAPI cells undergo reactive changes in response to LPS or Type I or Type II interferons.

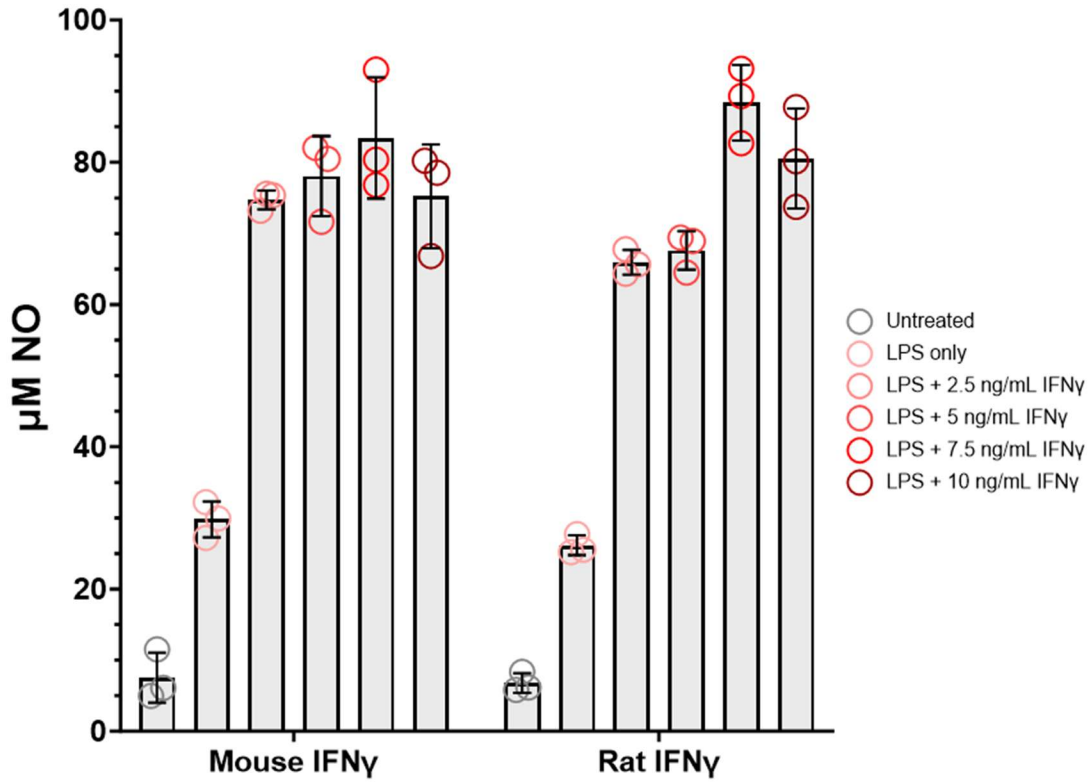


Figure 3.3. HAPI cells exhibit similar sensitivity and magnitude of response to mouse- and rat-origin IFN γ in their release of nitric oxide.

NO concentration after 18 hours of stimulation, as quantified by Griess assay.

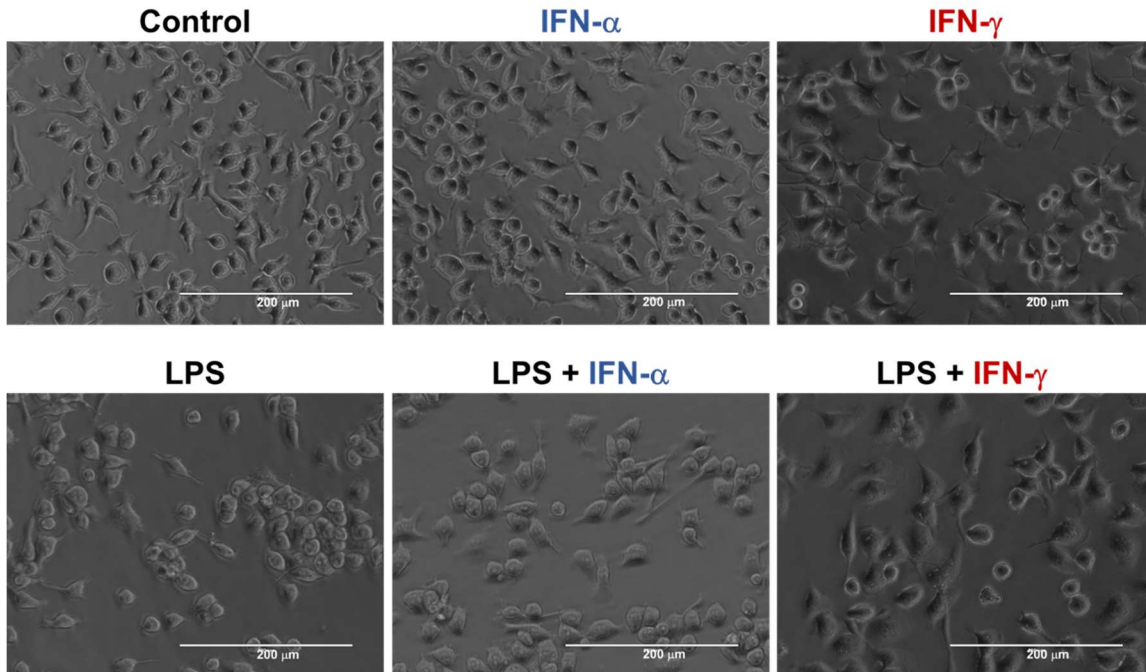


Figure 3.4. LPS, IFN α , and IFN γ induce synergistic morphological changes in HAPI cells.

Representative phase-contrast images of HAPI cells following 18 hours of stimulation with 100 ng/mL LPS, 10 ng/mL IFN α , 10 ng/mL IFN γ , or combined LPS/IFN α or LPS/IFN γ .

3.3.3 IFN γ and IFN α each synergize with LPS to suppress mitochondrial oxygen consumption in HAPI cells

To test the effect of pro-inflammatory activation on mitochondrial respiration, we utilized Agilent Seahorse respirometry to quantify OCR of HAPI cells after 18 hours of treatment with LPS, IFN γ , IFN α , LPS/IFN γ , or LPS/IFN α . This experiment was done by a previous lab member, but I analyzed the data and prepared the figures. We found that the treatment of HAPI cells with either LPS or IFN α suppressed OCR, and while treatment with both LPS and either IFN γ or IFN α resulted in a greater decrease than the single-stimuli conditions (Figure 3.5A-B). IFN γ treatment caused only a trend toward OCR suppression but it strongly synergized with LPS to decrease basal and maximal

OCR as was reported for primary microglia⁴⁷⁻⁴⁹. Nitric oxide has been implicated in the pro-inflammatory suppression of mitochondrial respiration³⁴³. The NO scavenger cPTIO was added after uncoupler to test for rescue of mitochondrial respiratory capacity. However, we found that it had little ability to reverse the stimuli-induced reduction in maximal OCR that was observed (Figure 3.5A).

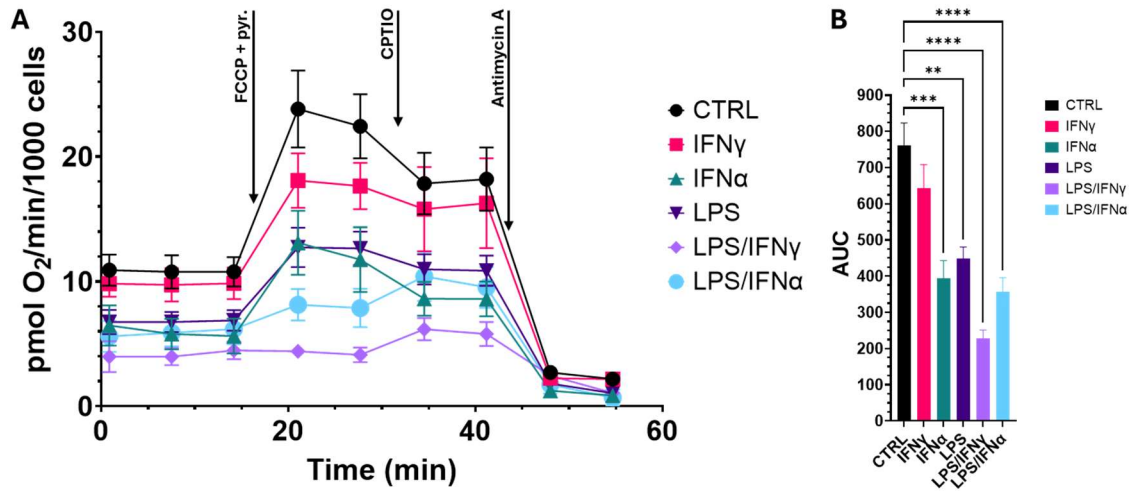


Figure 3.5. LPS, IFN α , and IFN γ suppress mitochondrial oxygen consumption in HAPI cells.

(A) Average OCR trace for HAPI cells over n=5 experiments. Arrows represent serial injections with 4 μ M carbonyl cyanide 4-(trifluoromethoxy)phenylhydrazone plus 10 mM sodium pyruvate (“FCCP + pyr.”), 200 μ M 2-(4-carboxyphenyl)-4,4,5,5-tetramethylimidazole-1-oxyl-3-oxide potassium salt (“CPTIO”), and 1 μ M Antimycin A. (B) Cumulative all-point area under the curve for OCR traces across n=5 experiments.

3.4 Discussion

The use of HAPI cells to model pro-inflammatory microglial responses in vitro has been widespread since their initial description in 2001¹⁰³. However, given the misidentification of HAPI cells as rat cells, it is important to reassess if they recapitulate a cellular identity and pro-inflammatory responses similar to those seen in primary microglia. Here, we present sequencing supporting that HAPI cells are a mouse cell line

sharing a common origin with the SIM-A9 microglial cell line, and express markers consistent with a microglia-like cell identity. We also found that HAPI cells recapitulate primary microglia findings that the pro-inflammatory stimuli LPS and IFN γ induce NO production and a shift in morphology^{103,104,121–129,131–135,342}. We then extend these results to show that HAPI cells, as in *ex vivo* and *in vitro* models of primary microglia, exhibit a synergistic suppression of mitochondrial oxygen consumption after LPS and IFN γ treatment^{47–49}. These findings support that HAPI cells represent a mouse microglia-like cell line useful for studies of pro-inflammatory microglial activation, including studies of microglial immunometabolism.

Further, we build upon these results to show that treatment of HAPI cells with the type I interferon IFN α can induce morphological changes and suppression of mitochondrial oxygen consumption in synergy with LPS. As the NO scavenger cPTIO failed to substantially rescue the reduction of mitochondrial respiratory capacity, work remains to identify how IFN α signaling mediates this suppression. Type I interferon signaling has recently been implicated in several neurological conditions, including AD and neuroinflammation induced by malaria and HIV infection^{344–346}. Additionally, inhibiting type I interferon signaling appears to mitigate the release of mitochondrial-origin damage associated molecular patterns in a model of neuropathic pain³⁴⁷. However, whether mitochondrial bioenergetic changes contribute to type I interferon signaling in any of these neurological conditions remains to be seen.

Chapter 4: Mdivi-1 Inhibits Pro-Inflammatory Microglial Activation Without Preventing Mitochondrial Fission

4.1. Introduction

Microglial mitochondria undergo changes in size and morphology following activation triggered by LPS treatment, both *in vitro* and *in vivo*^{348–350}. Most mitochondrial fission is achieved through translocation of the GTPase DRP1 to the mitochondrial outer membrane¹⁴¹. DRP1 recruitment initiates organellar constriction, leading to the pinching off of two separate daughter mitochondria from the constricted parent¹⁶⁸. Mdivi-1 is a quinazolinone derivative that was suggested to antagonize DRP1-dependent mitochondrial fission because it inhibited the GTPase activity of the yeast DRP1 homologue and caused mitochondrial elongation in mammalian cells¹⁶⁸. Both mdivi-1 treatment and DRP1 siRNA knockdown attenuated pro-inflammatory cytokine expression in the BV2 microglial cell line, suggesting that mitochondrial fission may causatively contribute to the pro-inflammatory phenotype. It was hypothesized that fragmentation of the mitochondrial network leads to increased ROS production, resulting in enhanced mitogen-activation protein kinase (MAPK)-dependent nuclear factor kappa-light-chain-enhancer of activated B cells (NFκB) phosphorylation³⁴⁹. NFκB phosphorylation promotes its translocation to the nucleus, where it initiates the transcription of target genes³⁵¹. Although this model is attractive, the reported timing of microglial mitochondrial fragmentation (2-12 hours after LPS treatment) does not appear consistent with a role in NFκB translocation, which is generally observed within two hours of the pro-inflammatory trigger. In addition, mdivi-1 has DRP1-independent actions on cells that include inhibition of electron transport chain Complex I and modulation of mitochondrial ROS²⁶³.

Consequently, we predicted that mdivi-1 inhibits the pro-inflammatory microglial activation phenotype independently of effects on mitochondrial fragmentation. Consistent with this possibility, we found that mdivi-1 suppresses the LPS/IFN γ -induced release of NO *in vitro* but fails to rescue full-length mitochondrial networks. We also employed a recently developed and putatively more specific and potent DRP1 inhibitor, Drpitor1a, to test if it would mimic mdivi-1's suppressive effects on pro-inflammatory activation, but found instead that Drpitor1a fails to suppress NO release and synergizes with LPS and IFN γ to induce dose-dependent cell death²⁵⁹.

Finally, given evidence that the anti-inflammatory mdivi-1 effects are independent of the mitochondrial fragmentation phenotype, we initiated an exploratory investigation of fibroblast growth factor receptor 3 (FGFR3) as a potential alternative target based on proteomic evidence that FGFR3 signaling may be affected by mdivi-1. FGFR3 was shown to have increased expression in pro-inflammatory microglia, and the use of FGFR inhibitors reduced pro-inflammatory activation in microglial models of TBI and multiple sclerosis³⁵²⁻³⁵⁴. Fibroblasts growth factor receptor substrate 2 (FRS2), also affected by mdivi-1 in the proteomics study, is an adaptor of FGFRs, and is required to initiate FGFR3-mediated signaling^{355,356}. Therefore, we tested if the FGFR inhibitor infigratinib could mimic the ability of mdivi-1 to inhibit iNOS induction in LPS/IFN γ -treated HAPI cells³⁵⁷. Our results indicate that infigratinib suppresses LPS/IFN γ -induced induction of iNOS protein expression and NO secretion in a dose-dependent manner, providing exploratory support for further investigation of inhibition of FGFR3 signaling as an alternative mdivi-1 mechanism of action.

4.2. Materials and Methods

4.2.1 HAPI Cell Culture

HAPI cells were cultured in Dulbecco's Modified Eagle Medium supplemented with 10% heat-inactivated fetal bovine serum and 1% penicillin/streptomycin. Cells were maintained in 95% air and 5% CO₂ at 37°C. Only cells under passage 30 were utilized in this study.

4.2.2 Immunocytochemistry

HAPI cells were seeded on Nunc Lab-Tek Chambered Coverglass slides (Thermo Scientific) and treated the following day for nine hours with either 10 ng/mL each of LPS and IFN γ , 75 μ M mdivi-1, a combination of LPS, IFN γ , and mdivi-1, or a control, before being fixed in 4% paraformaldehyde in phosphate-buffer saline (PBS) for 20 minutes. Cells were then washed three times with PBS, permeabilized with 0.15% Triton-X-100 in PBS for 20 minutes, and blocked with 7.5% bovine serum albumin (BSA) in PBS for 45 minutes. Primary immunostaining was performed with 1:1000 mouse-anti-cytochrome *c* (BD Biosciences, Cat# 556432, RRID:AB_396416) and 1:1000 rabbit-anti-Tomm20 (Proteintech, Cat# 11802-1-AP, RRID:AB_2207530) for 90 minutes in PBS containing 7.5% BSA and 0.15% Triton-X-100. Cells were then washed twice in PBS, before 60 minutes of incubation with an Alexa Fluor 488 goat anti-mouse IgG secondary antibody (Life Technologies, Cat# A11029, RRID:AB_2354088) and an Alex Fluor 555 goat anti-rabbit IgG secondary antibody (Invitrogen, Cat# A32732, RRID:AB_2633281), both at a 1:1000 dilution. Cells were then washed twice more in PBS, mounted on coverslips, and allowed to cure overnight in ProLong Diamond + DAPI antifade media (Thermo Fisher, Cat# P36971). Imaging was performed with a Zeiss LSM 880 microscope (Zeiss MicroImaging) equipped with an Airyscan superresolution imaging module, using

63/1.40 Plan-Apochromat Oil DIC M27 objective lens (Zeiss MicroImaging). All steps were performed at room temperature.

4.2.3 Quantification of Mitochondrial Morphology

Because the density and overlap of mitochondria in our acquired images impeded image segmentation, we developed a three-category classification system describing mitochondria as “long tubular” (elongated and narrow), “short tubular” (short and narrow), or “rounded” (circular, sometimes negative for cytochrome *c* staining). Two volunteers, blinded to the experimental conditions and the expected results, were asked to classify each imaged cell by its predominant mitochondrial morphology. The fraction of cells with each predominant morphology in each image was then quantified, and the assessments of the two volunteers were averaged.

4.2.4 Phase-Contrast Imaging

Phase contrast images of cells were acquired using the 20X objective of an ImageXPress Pico Automated Cell Imaging System (Molecular Devices; San Jose, CA).

4.2.5 Proteomics

The proteomics experiment was done through the Mass Spectrometry Center at the University of Maryland School of Pharmacy. Protein quantification by mass spectrometry was performed on a mitochondria-enriched heavy membrane fraction of HAPI cells treated for 18 hours with 100 ng/mL LPS and 10 ng/mL IFN γ \pm 75 μ M mdivi-1 or vehicle control \pm 75 μ M mdivi-1. The heavy membrane fraction was isolated by resuspending pelleted cells in fractionation buffer (10 mM HEPES, 10 mM NaCl, 1.5 mM MgCl₂, and 1x protease inhibitor, diluted in water), and passing the resulting cell suspension through a 25-gauge syringe twelve times before centrifuging at 1000 x *g* for 5

minutes. The resulting supernatant was then isolated and centrifuged again at 1000 x g for 5 minutes, then isolated and centrifuged for 10 minutes at 3500 x g. Supernatant was removed, and the remaining heavy membrane pellet was washed with 50 μ L of PBS and centrifuged again for 10 minutes at 3500 x g. After aspirating excess supernatant, the heavy membrane pellet was resuspended in 50 μ L HDP buffer (10 mM HEPES, 1 mM DTT, 100 μ M phenylmethylsulfonyl fluoride) and incubated on ice for 30 minutes. Samples were then sonicated via four 10-second bouts and centrifuged at 9000 x g for 30 minutes. The resulting supernatant was considered the soluble heavy membrane protein fraction. The pellet of insoluble heavy membrane proteins was resuspended in 500 μ L of ME buffer (20 mM Tris-HCL, 0.4 M NaCl, 15% glycerol, 1 mM DTT, 100 μ M phenylmethylsulfonyl fluoride, 1.5% Triton-X-100) and incubated at room temperature on a rocker for 30 minutes. The insoluble fraction solution was then centrifuged for 30 minutes at 9000 x g. The resulting supernatant was collected and combined with the heavy membrane soluble fraction for mass spectroscopy analysis. All centrifugation steps were performed at 4°C.

4.2.6 *Quantification of Nitric Oxide*

HAPI microglial cells were stimulated for 24 hours with lipopolysaccharide (LPS; 10 ng/ml) in combination with interferon-gamma (IFN- γ ; 10 ng/ml). Nitrite, a stable, non-volatile breakdown product of nitric oxide, was quantified in cell culture media by Griess assay according to the manufacturer's protocol (Thermo Fisher Scientific). Cells were treated at the time of stimulation with 75 μ M mdivi-1, Drpitor1a in doses ranging from 10 nM to 25 μ M, or a DMSO vehicle control. For experiments using infigratinib, treatment times were instead 18 hours, with infigratinib doses ranging from 1.25 μ M to

10 μ M. For a more detailed discussion of the principles behind the Griess assay, please refer to Chapter 3 (3.2.7).

4.2.7 Western Blotting

After 18 hours of treatment with 10 ng/mL each of LPS plus IFN γ , HAPI cells were lysed in ice-cold RIPA buffer containing protease/phosphatase inhibitor cocktail (Thermo Fisher Scientific; Waltham, MA), sonicated for 10 seconds on ice, and centrifuged at 13,300 x g for 20 minutes at 4°C to remove insoluble material. The supernatant was collected for western blot. Protein levels were quantified via bicinchoninic acid assay³¹².

Protein samples (30 μ g) were prepared in 1X sodium dodecyl sulfate (SDS) loading buffer (LI-COR; Lincoln, NE) containing 0.1M dithiothreitol and heated for 10 minutes at 95°C before loading onto Novex 4-20% Tri-Glycine Plus SDS-polyacrylamide gel electrophoresis (PAGE) gels (Thermo Fisher Scientific). SDS-PAGE was run at 160V for 35 minutes and then protein was transferred to polyvinylidene fluoride membranes. Total protein levels were imaged using Revert 700 (LI-COR). Blocking was performed in Tris-buffered saline containing 0.1% (v/v) Tween-20 (TBS-T) that was supplemented with 2.5% non-fat milk and 2.5% bovine serum albumin (BSA). The following primary antibodies at the indicated dilutions were used: 1:5,000 human rhodamine-conjugated anti-tubulin (Bio-Rad Cat# 12004165, RRID:AB_2884950; Hercules, CA), 1:1000 rabbit anti-iNOS (Arigo, Cat# 1ARG56509) and 1:1000 mouse anti-Rodent OxPhos Cocktail (Abcam, Cat# 1ab110413, RRID:AB_2629281) The secondary antibodies used were IRDye 680RD goat anti-mouse (LI-COR Biosciences Cat# 926-68070, RRID:AB_10956588) and IRDye 800CW goat anti-rabbit (LI-COR Biosciences Cat#

926-32211, RRID:AB_621843), both at 1:20,000. Imaging was performed on a LI-COR Odyssey FC imager.

4.3 Results

4.3.1 Mdivi-1 fails to rescue the mitochondrial length shortening induced by LPS/IFN γ treatment

Mdivi-1 is reported as a mitochondrial fission inhibitor; however, this effect is not seen in all cell types²⁶³. To determine if mdivi-1 blocked mitochondrial fragmentation in HAPI microglia-like cells, we quantified mitochondrial morphology following pro-inflammatory activation with LPS and IFN γ . As expected, non-activated control cells exhibited mostly long tubular mitochondria, a morphology lost upon LPS/IFN γ -mediated activation. Mdivi-1 treatment did not rescue this morphology and caused an increase in the fraction of cells with shortened mitochondrial morphology even in non-activated cells. However, we noted that the predominant morphology induced by LPS/IFN γ treatment was not short tubules, but instead a rounded structure; this morphology was less prevalent in mdivi-1 treated cells (Figure 4.1). We interpret these results to mean that mdivi-1 does not prevent mitochondrial fragmentation in LPS/IFN γ -activated HAPI cells and speculate that the rounded morphology is caused by a process other than Drp1-mediated mitochondrial fragmentation.

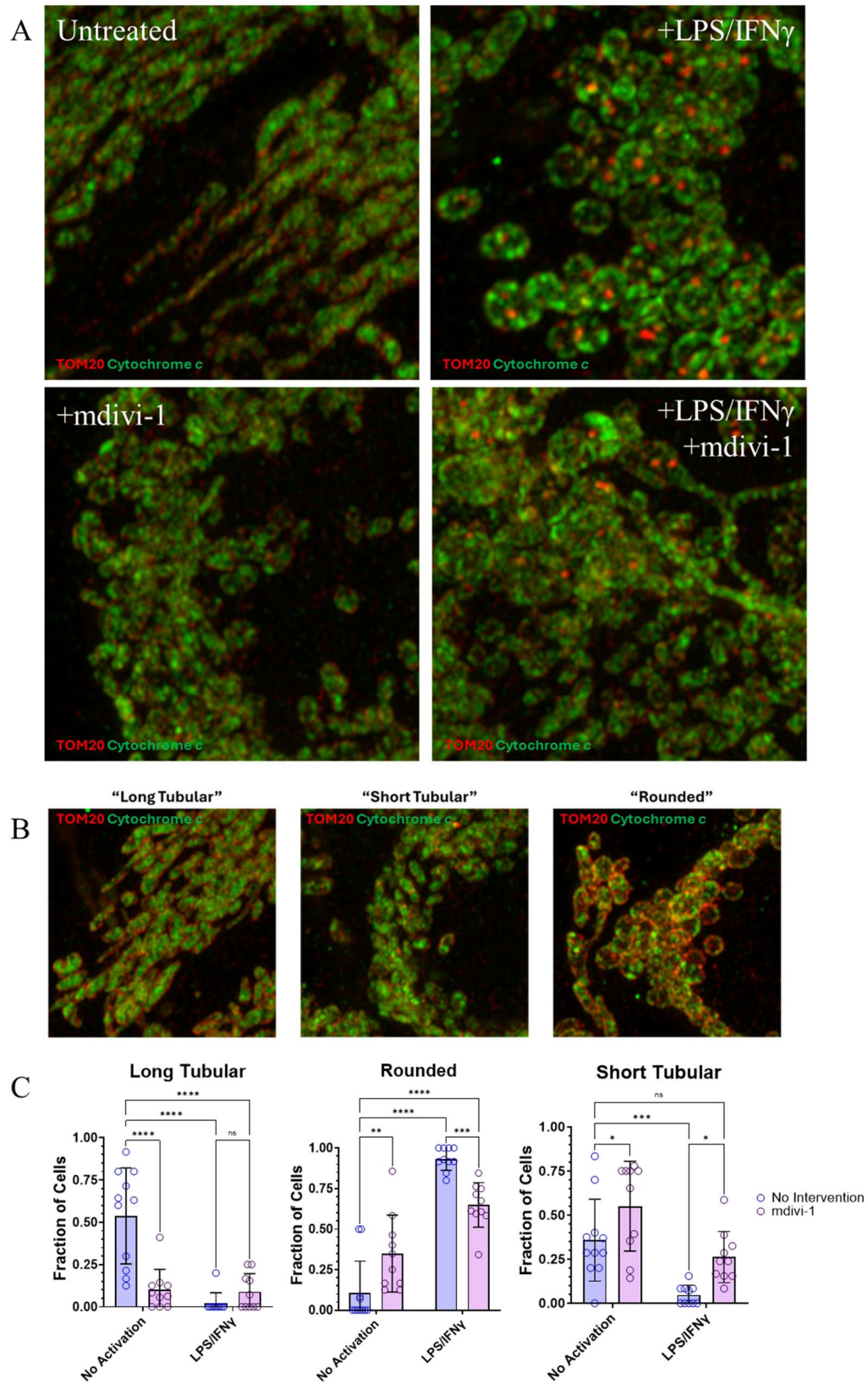
4.3.2 The structurally distinct DRP1 inhibitor, Drpitor1a, does not mimic mdivi-1's protective effect against microglial pro-inflammatory activation

To further investigate if mdivi-1's suppressive effect on LPS/IFN γ -induced pro-inflammatory activation may be DRP1-mediated, we employed a more recently developed and putatively more specific and potent DRP1 inhibitor, Drpitor1a²⁵⁹. Surprisingly, we found in our initial dose-response testing that Drpitor1a synergized with LPS/IFN γ to increase microglial cell death, despite being nontoxic in non-activated cells (Figure 4.2). Following Drpitor1a re-titration, we then quantified NO release as a proxy for pro-inflammatory activation using non-toxic doses of Drpitor1a, and found that – unlike mdivi-1 – Drpitor1a does not suppress LPS/IFN γ -induced secretion of NO (Figure 4.3). Together, these results suggest that DRP1 inhibition may not be the mechanism of action by which mdivi-1 exhibits protective effects against pro-inflammatory microglial activation.

Figure 4.1. Mdivi-1 slightly suppresses LPS/IFN γ -induced rounding of mitochondria in activated HAPI cells, but does not restore long tubular mitochondrial morphology.

(A) Representative images of immunostained HAPI cells acquired from each treatment group. Green = cytochrome *c*, red = Tomm20. Conditions are untreated controls, 75 μ M mdivi-1, 100 ng/mL LPS + 10 ng/mL IFN γ , or mdivi-1 + LPS/IFN γ , all after nine hours of treatment. (B) Representative images used to classify mitochondrial morphology as “long tubular,” “short tubular,” or “rounded.” (C) Quantification of the fraction of cells in each treatment group exhibiting long tubular, short tubular, or rounded mitochondrial morphologies.

Figure 4.1, *continued*.



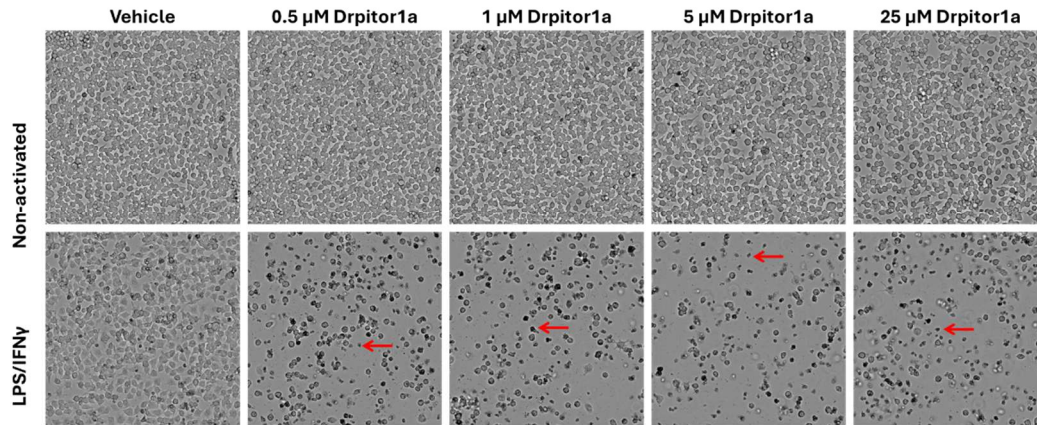


Figure 4.2. Drpitor1a synergizes with LPS/IFN γ to induce HAPI cell death

Phase contrast images showing viable HAPI cells following 24 hours of treatment with Drpitor1a alone in doses as high as 25 μM (top), and loss of viable cells when Drpitor1a was added to LPS/IFN γ -stimulated HAPI cells at doses \geq 0.5 μM (bottom). The red arrows denote examples of cell debris.

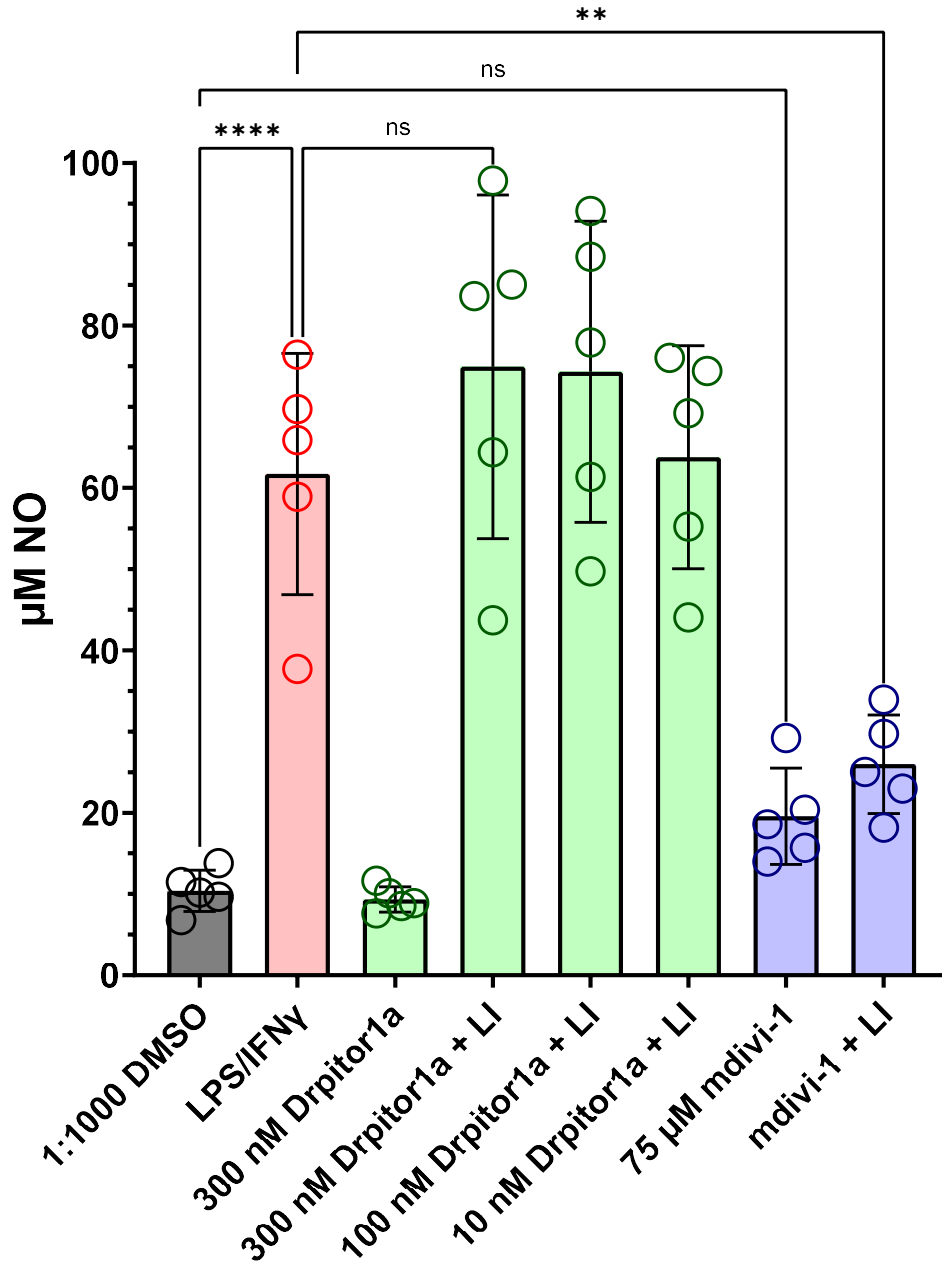


Figure 4.3. Mdivi-1, but not Drpitor1a, suppresses LPS/IFN γ -induced NO secretion

Quantification of NO secreted by HAPI cells following 18 hours of treatment with 75 μ M mdivi-1 or Drpitor1a in doses ranging from 10 nM – 300 nM, with or without LPS/IFN γ stimulation (10 ng/mL each).

4.3.3 The FGFR inhibitor infgratinib blocks iNOS induction but not ETC deficits in LPS/IFN γ -activated HAPI cells

We next examined potential alternative targets to DRP1 in mediating mdivi-1's protective effect against pro-inflammatory microglial activation. A previous student in the lab had performed proteomics analysis of mitochondria-enriched heavy membrane fractions from HAPI cells treated with LPS/IFN γ or vehicle control, with the goal of identifying proteins translocating into or out of mitochondria following pro-inflammatory activation. Because the treatments were also done with and without mdivi-1 (75 μ M), we evaluated this old lab dataset to determine whether additional insight into mdivi-1's mechanism(s) of action could be obtained. In the proteomics analysis of mitochondria-enriched heavy membrane fractions, FGFR3 expression was decreased and FRS2 expression increased by LPS/IFN γ stimulation, which mdivi-1 treatment reversed (Figure 4.4). FRS2 is required for the initiation of FGFR3 signaling and FGFR3 inhibitors were reported to reduce neuronal death and the expression of genes associated with pro-inflammatory microglial activation in mouse models of TBI and multiple sclerosis³⁵²⁻³⁵⁷. Hypothesizing that mdivi-1 may block the LPS/IFN γ -induced FRS2 increase by causing an inactivating aggregation of FGFR3 in the heavy membrane fraction, we sought to determine if an FGFR inhibitor, infgratinib, conferred similar protection as mdivi-1 against pro-inflammatory HAPI cells activation. Pending additional replication, our results suggest that infgratinib may confer dose-dependent protection against both the secretion of NO (Figure 4.5B) and the expression of iNOS protein (Figure 4.5A) following LPS/IFN γ -mediated activation, but without protecting against the loss of ETC subunit proteins (Figure 4.5A). These results are consistent with infgratinib exhibiting a protective effect against microglial activation independent of mitochondrial dysfunction.

The inability of infigratinib to rescue LPS/IFN γ -induced loss of ETC subunit protein expression is also concordant with a past report that mdivi-1 treatment is unable to reverse LPS/IFN γ -induced suppression of mitochondrial oxygen consumption in primary microglia^{358,359}.

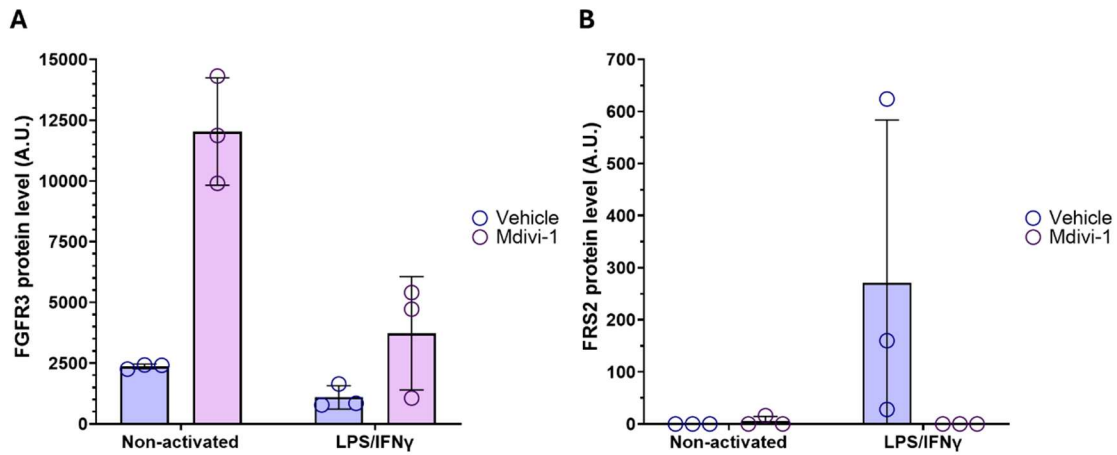


Figure 4.4. Proteomics reveals mdivi-1 as a possible inhibitor of FGFR3 signaling

Quantification of FGFR3 (A) and FRS2 (B) protein abundance in HAPI cells following treatment with 75 μ M mdivi-1 in both non-activated cells and cells stimulated with 100 ng/mL LPS and 10 ng/mL IFN γ for 18 hours. The proteomics experiment was conducted by a former lab member, and the data were provided by the University of Maryland School of Pharmacy's Mass Spectrometry Center.

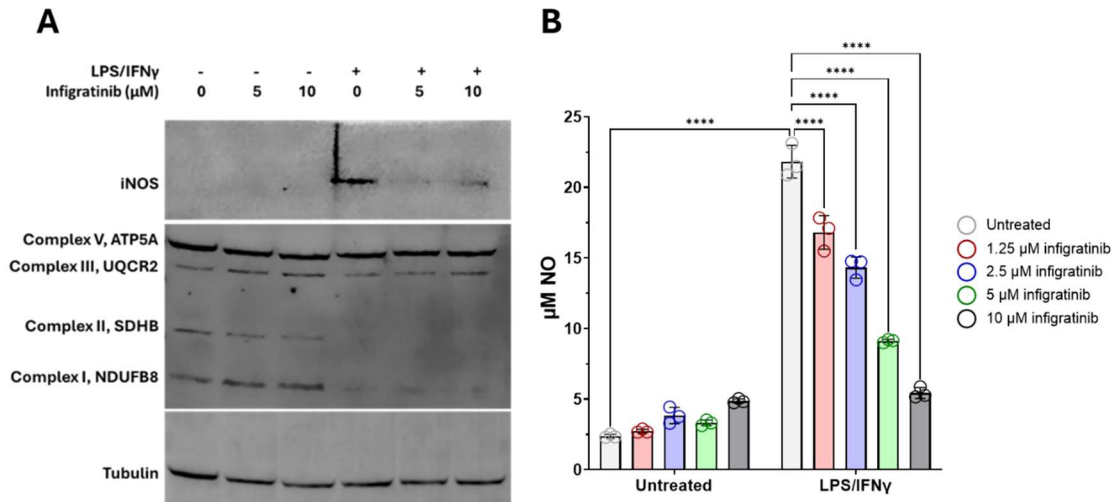


Figure 4.5. The FGFR inhibitor ifingratinib confers dose-dependent protection against NO secretion in HAPI cells following LPS/IFN γ treatment

(A) Western blot showing the expression of iNOS, select ETC subunits, and tubulin following 18 hours of stimulation with LPS/IFN γ in the presence of 0, 5, or 10 μ M ifingratinib. (B) NO release as quantified by Griess assay following 18 hours of stimulation with LPS/IFN γ in the presence of ifingratinib doses ranging from 1.25 – 10 μ M (representative of n = 3 biological replicates).

4.4. Discussion

Since its initial identification, mdivi-1 has been primarily used as a selective inhibitor of mitochondrial fission, putatively via impairing DRP1 GTPase activity. It is through this mechanism that mdivi-1 was suggested to suppress pro-inflammatory microglial activation^{349,358–362}. However, previous reports support that mdivi-1 has many DRP1- and fission-independent effects, including impairing mitochondrial Complex I-dependent respiration²⁶³. Contrary to the suggestion that mdivi-1 accomplishes suppression of pro-inflammatory phenotypes via impairing DRP1-mediated mitochondrial fission, we find that mdivi-1 treatment is unable to rescue mitochondrial length or morphology in vitro following LPS/IFN γ treatment. While we do not directly test mdivi-1 inhibition of DRP1 GTPase activity in this study, our results indicate that

impaired mitochondrial fission cannot be an explanation for mdivi-1's observed effect on microglial activation. Furthermore, we find that an alternative and putatively more specific DRP1 inhibitor, Drpitor1a, confers no protective effect against secretion of NO in pro-inflammatory microglia and, in fact, synergizes with LPS/IFN γ to induce cell death²⁵⁹. Future studies should test if Drpitor1a inhibits mitochondrial fragmentation at concentrations that do not synergize with LPS/IFN γ to induced cytotoxicity; i.e. doses \leq 300 nM. If Drpitor1a does prevent fragmentation at these doses, it would suggest that DRP1-mediated mitochondrial fragmentation is not required for pro-inflammatory iNOS induction. If Drpitor1a fails to inhibit LPS/IFN γ -induced mitochondrial fragmentation, that result, together with mdivi-1's failure, would support the possibility that DRP1 activity is not required for the microglial activation-associated mitochondrial size reduction.

We then present exploratory studies towards identifying an alternative target for mdivi-1's suppression of microglial NO secretion. We identify LPS/IFN γ -induced changes in FGFR3 and FRS2 protein abundance which are reversed by mdivi-1 treatment and determine that the FGFR inhibitor infigratinib blocks the secretion of NO from LPS/IFN γ in a dose-dependent manner. Further work is required to elucidate the site of mdivi-1 action leading to potentially altered FGFR signaling and whether it is anti-inflammatory. Additionally, because infigratinib is similarly as potent against FGFR1 and FGFR2 and is it is against FGFR3, additional validation should be employed to confirm that infigratinib-mediated suppression of NO secretion is a result of FGFR3 inhibition specifically; e.g. by siRNA knockdown³⁶³. However, collectively, our findings support

that mdivi-1 suppresses microglial pro-inflammatory activation in a mitochondrial fission-independent manner.

Chapter 5: Assessment of Human Induced Microglia Models for Bioenergetic Studies

5.1. Introduction

Human-derived neurodegenerative disease cell models enable the study of genetic risk factors while avoiding species-specific complications. Species-specific differences between humans and rodent models are known in studies of both neurodegenerative disease and of microglial immune response, and the extent to which animal models are reflective of human physiology is a matter of contention in both fields³⁶⁴⁻³⁷¹. In particular, an NO-mediated suppression of mitochondrial oxygen consumption is thought to promote pro-inflammatory, neurotoxic microglial phenotypes similar to those seen in many neurodegenerative conditions³⁴³. However, human microglia and macrophages are reported to show impaired NO production in response to LPS/IFN γ treatment relative to their rodent cell counterparts, which may reduce or eliminate activation-associated mitochondrial respiratory suppression³⁷⁰⁻³⁷². To date, very few studies have been performed assessing mitochondrial oxygen consumption in human iMGs³⁷³⁻³⁷⁶. In addition, while LPS/IFN γ stimulation is thought to induce microglial pro-inflammatory activation broadly reflective of neurodegenerative disease-like states via its initiation of TLR4 signaling, evidence suggests that there are substantive differences between the transcriptional states induced by LPS and those induced by endogenous DAMPs like HMGB1 that are released in AD and other neurodegenerative disease and injury conditions¹¹⁹. The goal of this exploratory study was to assess the utility of several human iMG models for use in bioenergetic studies and to test the prediction that, like their rodent counterparts, human microglia-like cells suppress mitochondrial respiration in response to neurodegenerative disease-relevant pro-inflammatory stimulation.

5.2. Materials and Methods

5.2.1 Differentiation of MDMs from PBMCs

Human PBMCs were commercially sourced (STEMCELL Technologies, Cat# 70025) and differentiated using the protocol described by Ryan et al³⁷⁷. Briefly, cells were seeded onto Geltrex- (Invitrogen, Cat# A159601) coated plates and cultured in RPMI-1640 media (Sigma, Cat# R0883) supplemented with 1X Glutamax, 1% penicillin/streptomycin, 0.1 ug/mL IL-34 (Peprotech, Cat# 200-034), 0.1 ug/mL CCL2 (BioLegend, Cat# 571406), 0.01 ug/mL GM-CSF (Peprotech, Cat# 300-03), 0.01 ug/mL M-CSF (Peprotech, Cat# 300-25), and 0.01 ug/mL NGF-b (Sino Biological, Cat# 11050-HNAC). Media was replaced every other day until day 10, at which point cells were used for experiments.

5.2.2 Differentiation of microglia from iPSCs

iPSCs expressing inducible microglial transcription factors were previously reported by Dräger et al. and were obtained courtesy of Dr. Li Gan (Weill Cornell Medicine, New York, NY); iPSC culture was performed as originally described¹¹⁷. For differentiation, iPSCs were seeded on poly-D-lysine- (Invitrogen, Cat# A3890401) and Matrigel- (Corning, Cat# 47743-722) coated plates in an initial D0 medium of E8 (Gibco, Cat# A15169-01) + 2 µg/mL doxycycline (Sigma, Cat# D5207) + 10 nM ROCK inhibitor Y-27632 (Tocris, Cat# 125410). An MG basal media was prepared from 100 mL BrainPhys Neuronal Media (StemCell Technologies, Cat# 05790), supplemented with 1 mL B27 (Gibco, Cat# 17504044), 500 uL N2 (Gibco, Cat# 17502048), 10 ng/mL NT-3 (Peprotech, Cat# 450-03), 10 ng/mL BDNF (Peprotech, Cat# 450-02), and 1 ug/mL mouse laminin (Thermo Fisher Scientific, Cat# 23017-015). Media changes were performed using MG basal media supplemented with 2 ug/mL doxycycline, 100 ng/mL

IL-34, and 10 ng/mL GM-CSF on day 2; supplemented with 2 ug/mL doxycycline, 100 ng/mL IL-34, 10 ng/mL GM-CSF, 50 ng/mL M-CSF, and 50 ng/mL TGFB-1 (Peprotech, Cat# 100-21C) on day 4; and supplemented with 100 ng/mL IL-34, 10 ng/mL GM-CSF, 50 ng/mL M-CSF, and 50 ng/mL TGFB-1 on days 8 and 12. Differentiated iTF-Microglia were used in terminal experiments on day 15 for all experiments.

5.2.3 Immunocytochemistry

MDMis or iTF-Microglia cultured on glass coverslips were fixed in 4% paraformaldehyde in phosphate-buffered saline (PBS). Following fixation, cells were washed three times with PBS and permeabilized for 20 minutes in PBS containing 0.15% Triton-X-100. Cells were then blocked in 7.5% BSA and 0.15% Triton-X-100-containing PBS for 45 minutes, followed by 90 minutes of immunostaining with 1:500 rabbit-anti P2RY12 (Abclonal, Cat# A1710, RRID:AB_2763672) (both models) and 1:200 mouse anti-CX3CR1 (Abnova, Cat# H0001524-B01P, RRID:AB_1672835) (MDMis only). Cells were then washed twice in PBS before one hour of incubation with an Alexa Fluor 488 goat anti-mouse IgG secondary antibody (Life Technologies, Cat# A11029, RRID:AB_2354088) (both iMG models) and an Alex Fluor 555 goat anti-rabbit IgG secondary antibody (Invitrogen, Cat# A32732, RRID:AB_2633281) (MDMis) at a dilution of 1:2,000 each. Cells were finally washed twice with PBS, mounted with ProLong Diamond with 4',6-diamidino-2-phenylindole, dihydrochloride (DAPI) (Thermo Fisher, Cat# P36971), and allowed to cure for 24 hours before imaging. Images were acquired on a Nikon Eclipse E200 upright microscope (MDMis) or an ImageXPress Pico Automated Cell Imaging System for iTF-Microglia (Molecular Devices; San Jose, CA).

5.2.4 Seahorse microplate-based respirometry

Cellular oxygen consumption rates (OCR) and extracellular acidification rates (ECAR) were assessed using a Seahorse XFe24 Extracellular Flux Analyzer for iTF-Microglia or a Seahorse XF24 Extracellular Flux Analyzer for MDMis (Agilent Technologies; Santa Clara, CA)(as described in Chapter 2 (2.2.8)^{313,314}. Measurements were performed in an assay medium comprised of 120 mM NaCl, 3.5 mM KCl, 1.3 mM CaCl₂, 0.4 mM KH₂PO₄, 1 mM MgCl₂, 5 mM 4-(2-hydroxyethyl)-1-piperazineethanesulfonic acid (HEPES), 15 mM glucose, and 4 mg/mL fatty acid-free bovine serum albumin, pH 7.4. Principles governing the selection of serial injections employed in this study were as described in Chapter 2 (2.3.2).

5.3. Results

5.3.1 Differentiation and bioenergetic assessment of MDMis

A key limitation of using MDMi is the lack of a consensus differentiation protocol^{112,118,377-380}. Consistent shared aspects of existing protocols are the culturing of PBMCs, or monocytes isolated from PBMCs, for a period of approximately 10 days in media containing, at a minimum, IL-34 and GM-CSF to induce differentiation into a microglia-like population (Figure 5.1). The resulting MDMi population recapitulates phagocytic, transcriptional, and immune activation phenotypes of primary human microglia^{118,377-379}. However, we were unable to identify any bioenergetic studies using MDMis. Employing a differentiation protocol described by Ryan et al, we were able to induce the generation of human MDMis expressing the microglia-specific marker P2RY12 and the microglia/macrophage marker CX3CR1 from commercially sourced PBMCs without need for an initial monocyte isolation step (Figure 5.2)³⁷⁷. We then treated terminally differentiated MDMis for period of 18 or 48 hours with either HMGB1

or IL-1 β , proteins which act as endogenous pro-inflammatory signaling molecules in AD and other neurodegenerative disorders⁶. Following activation, basal and maximal oxygen consumption was assessed. At both 18- and 48-hours post-treatment, HMGB1 treatment suppressed maximal OCR (Figure 4.3). These results are consistent with correlative studies suggesting an association between high levels of HMGB1 expression and decreased mitochondrial bioenergetic in human peripheral immune cell types, and with the suppression of mitochondrial oxygen consumption induced by LPS in primary mouse microglia^{47-49,381,382}. However, heterogeneity in both yield and morphology of terminally differentiated MDMis limited our ability to replicate this finding and diminished their utility as a model for studying microglial bioenergetic function.

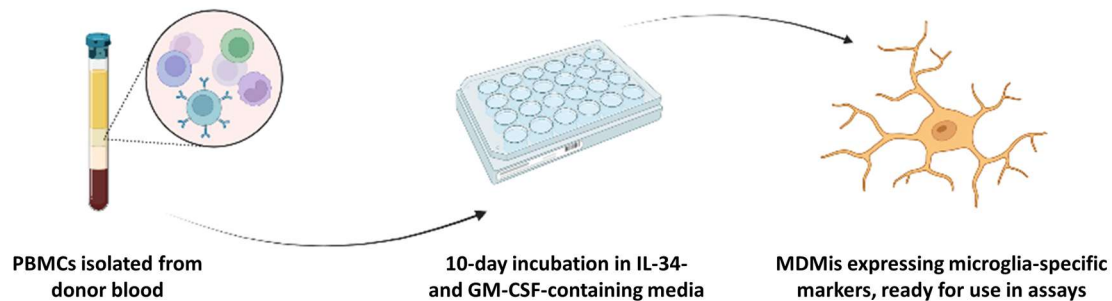


Figure 5.1. Differentiation of MDMis

Cartoon depicting the process for differentiating MDMis from PBMCs.

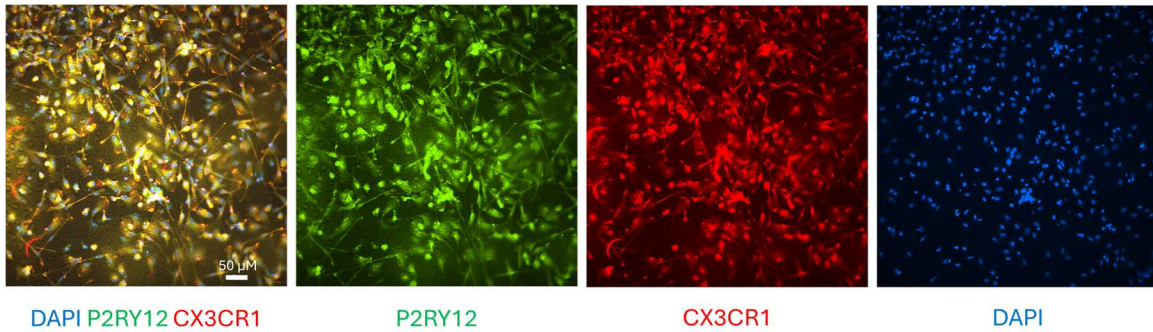


Figure 5.2. MDMi express microglia-selective markers

Immunocytochemistry depicting the expression of the microglia-selective marker P2RY12 and the microglia/macrophage-selective marker CX3CR1 in terminally differentiated MDMi.

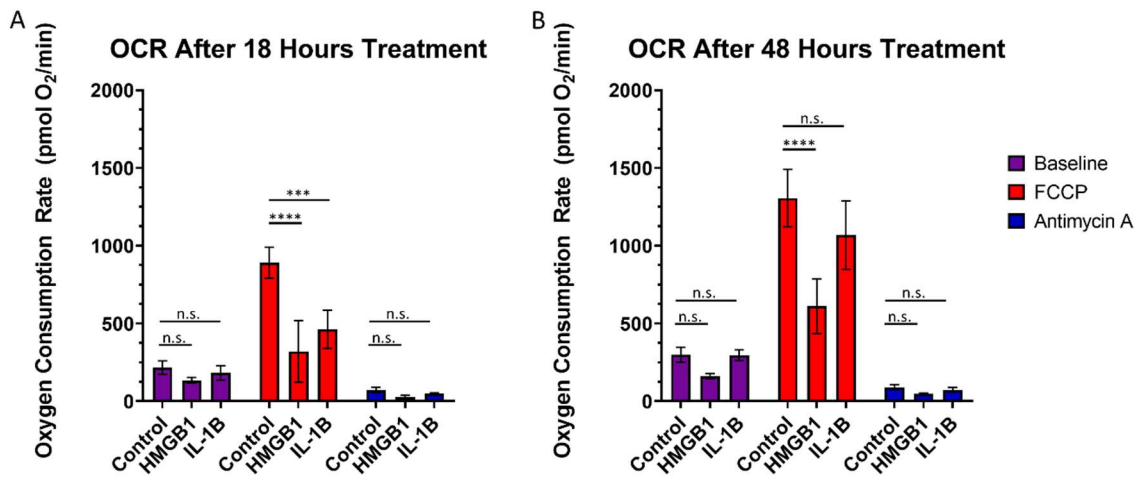


Figure 5.3. MDMi oxygen consumption rates following HMGB1 or IL-1 β treatment

Quantification of MDMi OCR following (A) 18 or (B) 48 hours of stimulation with 500 ng/mL HMGB1 or 50 ng/mL IL-1 β . Results are three technical replicates per condition from a single male donor.

5.3.2 Differentiation and bioenergetic assessment of iTF-Microglia

We next sought to employ a recently developed iPSC line containing six doxycycline-inducible microglial transcription factors, a system which was originally developed to enable rapid differentiation and scalability for high-throughput genomic screening¹¹⁷. Using a modified version of the originally published differentiation protocol, we were able to consistently generate morphologically homogenous populations of iTF-Microglia expressing the microglia-selective marker P2RY12 (Figure 5.4). However, even when cells were cultured to confluency using the reported differentiation media, negligible mitochondrial oxygen consumption was detectable from these cells. As doxycycline is known to impair mitochondrial translation, we adjusted the differentiation protocol to remove doxycycline on day 8, by which time iTF-Microglia already have acquired microglial identity at an early stage of maturity^{117,383,384}. By doing so, we were able to generate a population of iTF-Microglia that displayed low but quantifiable mitochondrial OCRs that responded as expected to the addition of the uncoupling agent FCCP, the complex III inhibitor antimycin A, and the complex IV electron donor TMPD (Figure 5.5). However, these cells did not exhibit changes in mitochondrial OCR in response to LPS, HMGB1, or IFN γ treatment (Figure 5.5). While the conventional interpretation of this result may be that iTF-Microglia are useful for bioenergetic studies but do not demonstrate the immunometabolic changes seen in primary microglia, we caution that all assessments of mitochondrial oxygen consumption in microglia that we could identify were performed in rodent cells, and studies in alternative human iMG models have found profound differences in LPS-stimulated oxygen consumption as compared to mouse primary microglia³⁷⁶.

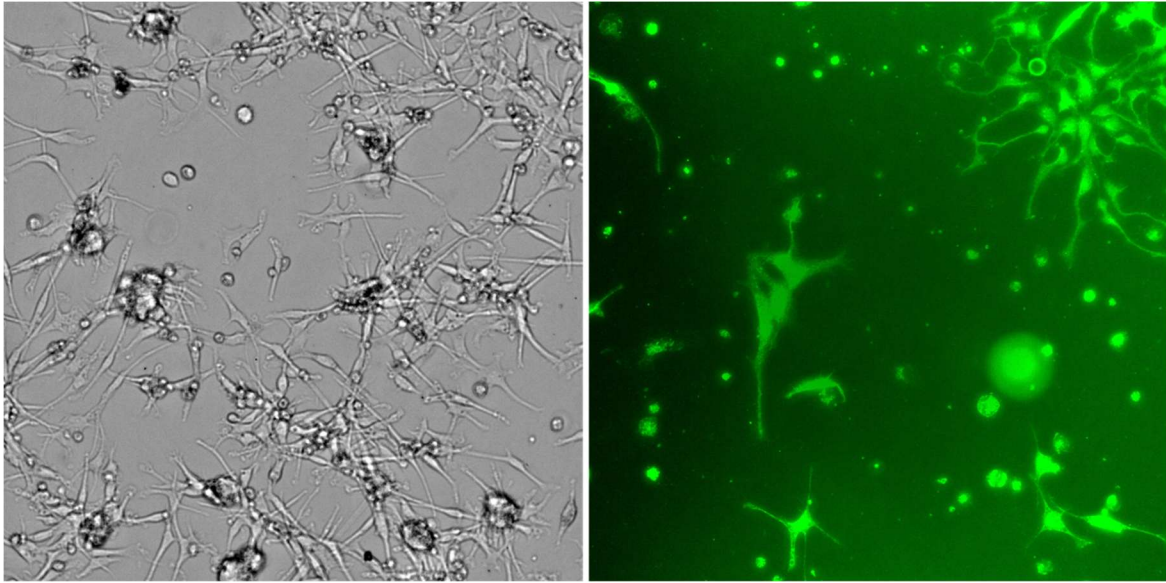


Figure 5.4. iTF-Microglia differentiation yields morphologically homogeneous cells expressing the microglia-specific marker P2RY12

Phase contrast image (left panel) and immunofluorescent P2RY12 staining (right panel) of terminally differentiated iTF-Microglia. Note that the two panels do not depict the same field of cells.

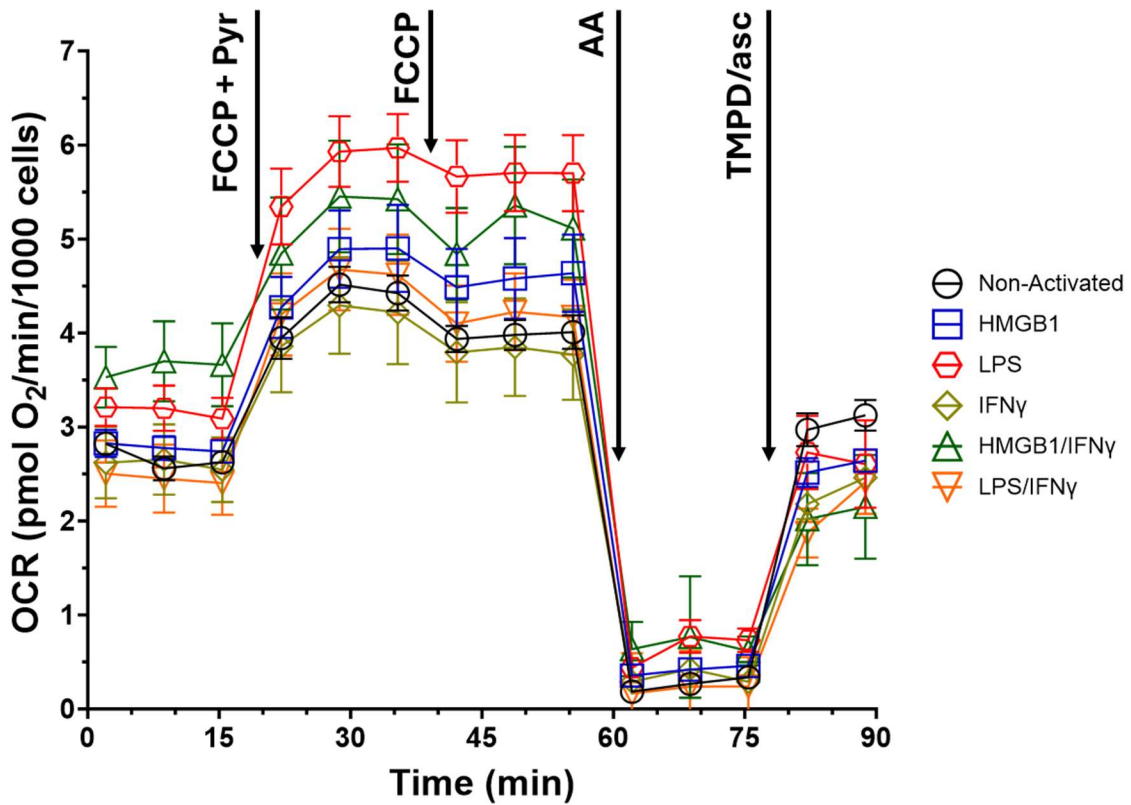


Figure 5.5. Oxygen consumption rate of iTF-Microglia following treatment with various pro-inflammatory stimuli.

Quantification of iTF-Microglia OCR following 18 hours of stimulation with 500 ng/mL HMGB1, 100 ng/mL LPS, 10 ng/mL IFN γ , or combinations of HMGB1/IFN γ or LPS/IFN γ . Results are 2-4 technical replicates per condition from a single differentiation. Arrows represent serial injections with 3 μ M carbonyl cyanide 4-(trifluoromethoxy)phenylhydrazone plus 10 mM sodium pyruvate (“FCCP + pyr.”), 1 μ M FCCP, 1 μ M Antimycin A (“AA”), and 0.4 mM N,N,N',N'-Tetramethyl-p-phenylenediamine plus 2 mM sodium ascorbate (“TMPD/asc”).

5.4. Discussion

Primary and immortalized *in vitro* cell culture models are valuable for the study of immunometabolism, but the available systems restrict our ability to compare human and non-human bioenergetic responses to pro-inflammatory stimuli. Induced microglia systems enable functional studies of human microglial response to pro-inflammatory insults associated with neurodegenerative disease and brain injury, but the capability of these cells to recapitulate bioenergetic changes seen in primary isolated microglia has largely not been assessed. Here, we present pilot immunometabolism studies from two human iMG systems, an MDMi differentiation protocol based upon Ryan et al and a modified iTF-Microglia differentiation protocol based upon Dräger et al^{117,377}. Following differentiation, expression of the microglia marker P2RY12 is robust in both systems, as originally reported, and we were able to obtain measurements of mitochondrial OCR via Agilent Seahorse technology in both models. Further, preliminarily, we found a suppression of maximal mitochondrial OCR in MDMis following 18 or 48 hours of pro-inflammatory stimulation with HMGB1, an endogenous DAMP implicated in AD and other neurodegenerative diseases. However, substantial batch-to-batch variability in MDMi yield and morphology limited our ability to follow up on this study. By contrast, we found that iTF-Microglia generated more consistent microglial morphology and yield

after terminal differentiation. Furthermore, following the removal of doxycycline from terminal culture media, the cells could be cultured at sufficient density for assessment of OCR by Seahorse respirometry. However, iTF-Microglia failed to demonstrate the expected metabolic shifts in response to a range of pro-inflammatory stimuli, including LPS and HMGB1. Whether this lack of altered mitochondrial oxygen consumption in response to LPS and HMGB1 is a limitation of iTF-Microglia as a model system or a result of species-specific differences in microglial immunometabolism is difficult to assess, given the absence of bioenergetic studies in primary human microglia; further comparative studies are thus warranted. These results provide insight into the advantages and limitations of current human iMG systems for functional use in (immuno)metabolism studies. Additionally, they highlight the need for novel model systems to enable species-specific studies of changes in mitochondrial metabolism that are associated with neurodegeneration-associated neuroinflammation.

Chapter 6: Discussion

This dissertation described two key findings; first, that a *TPCNI* knockout cell line exhibits mitochondrial bioenergetic deficits and severe depletion of several ETC subunit proteins that is not attributable to autophagy or proteasomal degradation (Chapter 2), and second, that the DRP1 inhibitor mdivi-1 confers protection against microglial pro-inflammatory secretion of NO in a mitochondrial fission-independent manner while failing to protect against LPS/IFN γ -induced loss of long tubular mitochondrial morphology entirely (Chapter 4). Substantial portions of the dissertation were also dedicated to evaluation and re-evaluation of *in vitro* systems used for the study of microglial immunometabolism relevant to neurodegenerative disease, with Chapter 3 recharacterizing HAPI cells as a mouse microglia-like cell line sharing a recent common origin with SIM-A9 cells and exhibiting a suppression of mitochondrial oxygen consumption in response to the type I interferon, IFN α , and Chapter 5 presenting our assessment of the utility and limitations of two human iMG systems, MDMis and iTF-Microglia, for the functional study of microglial immunometabolism.

Chapter 1 served as a literature review introducing the foundations of the remaining chapters of this dissertation. We first presented a general overview of the centrality of chronic pro-inflammatory microglia activation and mitochondrial bioenergetic deficits to neurodegenerative diseases, and of the bidirectional interactions between immune response pathways and cellular bioenergetic function collectively understood as immunometabolism. We then proceed to introduce the gene *TPCNI* and its encoded protein TPC1, including an overview of TPC1's known roles in immune responsiveness, mitochondrial function, and links to neurodegenerative disease. We made

a case based upon these known functional roles and brain cell type expression profiles of TPC1, and their changes in AD and LBD, that loss-of-function models of TPC1 are worth exploring in the context of immunometabolism and mitochondrial bioenergetic studies, including those we performed in Chapter 2. The following section highlighted existing *in vitro* microglial monoculture systems, and their strengths and limitations for use in studies of mitochondrial response to immune insult; assessing the utility of these models and addressing some of their limitations formed the rationale for the work performed in Chapters 3 and 5. Finally, in Chapter 4, we presented an in-depth overview of studies employing pharmacological or genetic manipulations of DRP1 to study mitochondrial fission and its dysfunction in neurodegenerative diseases, and made the case that alternative targets of the popular DRP1 inhibitor mdivi-1 warrant the consideration of non-fission mechanisms of action – for example in suppressing pro-inflammatory microglial activation.

In Chapter 2, we investigated the hypothesis that the endolysosomal cation channel TPC1 is required for mitochondrial bioenergetic function. We first demonstrate that pro-inflammatory activation of a microglial cell line, HAPI, results in a decrease in *Tpcn1* mRNA similar to the correlative findings that *TPCNI* mRNA expression is decreased in the microglia and astrocytes of AD and LBD patients. We then utilize a commercially available *TPCNI* KO near-haploid human cell line, HAPI cells, to study the consequences of genetic ablation of TPC1. In doing so, we found that *TPCNI* KO HAPI cells exhibit lower levels of mitochondrial respiration, but not glycolysis, compared to their WT parental counterparts, and that the abundance of select subunits of ETC complexes I, III, and IV are severely depleted at the protein level. We further

demonstrated that the inhibition of autophagy or proteasomal activity does not alter ETC subunit expression in either HAP1 cell line. However, unexpectedly, we found that the overexpression of a dominant negative form of TPC1 in WT HAP1 cells did not result in reduced ETC subunit expression, and the overexpression of wild-type TPC1 in *TPCNI* KO HAP1 cells failed to rescue ETC protein levels. Additionally, a second *TPCNI* KO model, in the HT1080 cell line, does not display ETC subunit deficits. These findings prompted an investigation of the genetic background of HAP1 cells via whole-genome sequencing and variant analysis, which found that both *TPCNI* KO and WT parental HAP1 cells carried an abundance of *de novo* mutations in protein-coding genes, including genes encoding proteins known to localize to mitochondria. As human HAP1 cells are widely used to conduct functional genetic studies and, as a haploid cell line, are more susceptible to functional consequences of individual mutations than are diploid cell lines with two gene copies, our findings indicate that higher standards of rigor are necessary for functional genetic studies conducted in haploid models. A key limitation of the study described in this chapter comes from the lack of a CRISPR gene-edited revertant of the *TPCNI* KO back to the WT form of the gene, which would provide a definitive answer regarding the potential role of TPC1 in mediating the observed mitochondrial phenotypes; multiple CRISPR attempts have failed and the successful generation of this revertant is an ongoing effort and part of our future directions.

Chapter 3 continued the theme of critically assessing our model systems by re-evaluating HAP1 cells, the microglia-like system we employed to demonstrate *Tpcn1* mRNA loss upon pro-inflammatory insult in Chapter 2. HAP1 cells are well-validated as possessing immune and phagocytic responses consistent with microglia and related

immune cell types, such as macrophages. However, they were initially misreported as rat microglia, and since have been recognized by commercial suppliers as cells of mouse origin. Despite this, HAPI cells continue to be specified as rat cells in recent publications. We used STR profiling to identify HAPI cells as a cell line of mouse origin displaying identical an STR profile to another mouse microglial cell line, SIM-A9, which was described many years after HAPI cells were first published. Both cell lines were reported to originate from primary microglia cultures via spontaneous immortalization. Contamination of both cultures with the same microglial cell line is a possible alternative explanation that would account for their identical STR profile.

Aiming to establish the continued usefulness of the HAPI microglial model despite the continued uncertainty regarding their exact origin, we then showed that HAPI cells express mRNA for the microglia-selective marker *Tmem119* in common with both SIM-A9 cells and mouse cortex samples containing microglia. They were also demonstrated to express the microglia/macrophage-selective marker *Cx3r1*, which they share with SIM-A9 cells, cortex samples, and BMDMs. These results suggest that HAPI cells are more reflective of microglia than macrophages. We further demonstrate that HAPI cells exhibit a suppression of mitochondrial bioenergetic function in response to the type I interferon, $IFN\alpha$, that is synergistically enhanced by LPS. This result is significant because microglial immunometabolic responses to type I interferons have not been previously reported, despite their secretion as part of neuroinflammatory responses in AD and other neurodegenerative diseases.

In Chapter 4, we tested the hypothesis that the widely used Drp1 inhibitor, mdivi-1, confers protection against microglial pro-inflammatory activation without suppressing

LPS/IFN γ -induced mitochondrial fission. We found that HAPI cells treated with mdivi-1 did not retain a long tubular mitochondrial structure following LPS/IFN γ stimulation. However, mdivi-1 treatment did result in a larger fraction of pro-inflammatory microglia exhibiting short tubular mitochondria and a decreased fraction of microglia containing rounded mitochondria compared with control-treated cells. This prompted us to ask if mdivi-1's anti-inflammatory mechanism of action might be entirely DRP1-independent. We found that a putatively more specific DRP1 inhibitor, Drpitor1a, not only failed to protect against LPS/IFN γ -induced NO secretion, but also synergized with LPS/IFN γ to induce dose-dependent microglial cell death at concentrations $\geq 0.5 \mu\text{M}$. We also identified an inverse correlation between mdivi-1- and LPS/IFN γ -induced changes in the abundance of FGFR3 and its required signaling adaptor, FRS2, that led us to speculate that inhibition of FGFR3 signaling could be an alternative target mediating mdivi-1's protective effect against pro-inflammatory microglia NO secretion. Our follow-up experiments suggested that the FGFR inhibitor infigratinib inhibits LPS/IFN γ -induced NO secretion in a dose-dependent manner, and that infigratinib also confers a dose-dependent attenuation of iNOS protein expression following pro-inflammatory HAPI cell activation. However, infigratinib did not protect against LPS/IFN γ -mediated loss of ETC subunits, suggesting that its suppression of iNOS induction is unrelated to signaling pathways by which LPS/IFN γ -mediated activation disrupts mitochondrial function. The significance of the work in this chapter is demonstrating that mdivi-1's anti-inflammatory effect on microglia is independent of its ability to suppress mitochondrial fission, and establishing an alternative potential target for future investigation. A future goal is the introduction of a dominant negative DRP1 mutant, DRP1 K38A, to HAPI cells, which

will allow for a more rigorous determination of whether DRP1-dependent mitochondrial fission is required for the LPS/IFN γ -induced mitochondrial morphology changes and/or NO secretion.

A key limitation in the studies present in Chapters 2-4 is the lack of a human microglial model; instead, we employed either mouse microglial cell lines or non-microglial immortalized human cells. This limitation is reflective of the paucity of human-specific *in vitro* monoculture systems that are both scalable to functional studies and validated as useful for assessment of mitochondrial bioenergetic changes induced by pro-inflammatory responses. In Chapter 5, we adopted and assessed two previously reported human iMG systems – one differentiated from monocytes present among human PBMCs, and the other from an iPSC line genetically engineered to contain doxycycline-inducible microglial transcription factors – for use in Agilent Seahorse mitochondrial oxygen consumption assays^{117,377}. We were able to differentiate iMGs expressing the microglia-selective marker P2RY12 and found that, with some modifications to the existing protocols, it was possible to quantify mitochondrial OCR in both systems by Seahorse respirometry. This is the first reported use of these specific systems to assess mitochondrial bioenergetics that we could identify. We further found in an n-of-1 exploratory study that an endogenous DAMP associated with neurodegenerative disease and brain injury, HMGB1, suppressed maximal mitochondrial OCR in MDMi following 18 or 48 hours of stimulation. If supported by further replication, this finding would suggest that HMGB1 may be a disease-relevant stimulus for assessing microglial immunometabolic shifts associated with AD, LBD, and other forms of neurodegeneration. However, we identified key limitations in the inconsistency of MDMi

yield and morphology from batch to batch, and the lack of iTF-Microglia response to HMGB1 and other pro-inflammatory stimuli, highlighting the need for further iteration upon existing iMG protocols before they can be readily adapted for immunometabolism studies.

Taken together, the results described in this dissertation showcase advances in the rigor of modeling microglial immunometabolism *in vitro* and demonstrate both a mitochondrial fission-independent mechanism of mdivi-1-mediated protection against microglial pro-inflammatory activation and a novel finding of mitochondrial bioenergetic deficits in a *TPCNI* knockout cell line. Future work remains to identify the target of mdivi-1 action in suppressing NO release, and to validate the role of *TPCNI* in mediating mitochondrial phenotypes seen in HAP1 cells.

References

1. Wilson, D. M. *et al.* Hallmarks of neurodegenerative diseases. *Cell* **186**, 693–714 (2023).
2. Surendranathan, A., Rowe, J. B. & O'Brien, J. T. Neuroinflammation in Lewy body dementia. *Parkinsonism Relat Disord* **21**, 1398–1406 (2015).
3. Mackenzie, I. R. Activated microglia in dementia with Lewy bodies. *Neurology* **55**, 132–134 (2000).
4. Loveland, P. M., Yu, J. J., Churilov, L., Yassi, N. & Watson, R. Investigation of Inflammation in Lewy Body Dementia: A Systematic Scoping Review. *Int J Mol Sci* **24**, 12116 (2023).
5. Edison, P., Donat, C. K. & Sastre, M. In vivo Imaging of Glial Activation in Alzheimer's Disease. *Front Neurol* **9**, 625 (2018).
6. Castro-Gomez, S. & Heneka, M. T. Innate immune activation in neurodegenerative diseases. *Immunity* **57**, 790–814 (2024).
7. Graykowski, D. & Cudaback, E. Don't know what you got till it's gone: microglial depletion and neurodegeneration. *Neural Regen Res* **16**, 1921–1927 (2021).
8. Neal, M. L. *et al.* Pharmacological inhibition of CSF1R by GW2580 reduces microglial proliferation and is protective against neuroinflammation and dopaminergic neurodegeneration. *FASEB J* **34**, 1679–1694 (2020).
9. Mancuso, R. *et al.* CSF1R inhibitor JNJ-40346527 attenuates microglial proliferation and neurodegeneration in P301S mice. *Brain* **142**, 3243–3264 (2019).
10. Oh, S. J. *et al.* Evaluation of the Neuroprotective Effect of Microglial Depletion by CSF-1R Inhibition in a Parkinson's Animal Model. *Mol Imaging Biol* **22**, 1031–1042 (2020).
11. Asai, H. *et al.* Depletion of microglia and inhibition of exosome synthesis halt tau propagation. *Nat Neurosci* **18**, 1584–1593 (2015).
12. Loane, D. J. *et al.* Novel mGluR5 Positive Allosteric Modulator Improves Functional Recovery, Attenuates Neurodegeneration, and Alters Microglial Polarization after Experimental Traumatic Brain Injury. *Neurotherapeutics* **11**, 857–869 (2014).
13. Loane, D. J., Stoica, B. A., Pajoohesh-Ganji, A., Byrnes, K. R. & Faden, A. I. Activation of Metabotropic Glutamate Receptor 5 Modulates Microglial Reactivity and Neurotoxicity by Inhibiting NADPH Oxidase. *J Biol Chem* **284**, 15629–15639 (2009).

14. Guerreiro, R. *et al.* TREM2 Variants in Alzheimer's Disease. *N Engl J Med* **368**, 117–127 (2013).
15. Jonsson, T. *et al.* Variant of TREM2 Associated with the Risk of Alzheimer's Disease. *N Engl J Med* **368**, 107–116 (2013).
16. Adav, S. S., Park, J. E. & Sze, S. K. Quantitative profiling brain proteomes revealed mitochondrial dysfunction in Alzheimer's disease. *Mol Brain* **12**, 8 (2019).
17. Minjarez, B. *et al.* Identification of proteins that are differentially expressed in brains with Alzheimer's disease using iTRAQ labeling and tandem mass spectrometry. *J Proteomics* **139**, 103–121 (2016).
18. Zhang, L. *et al.* Potential hippocampal genes and pathways involved in Alzheimer's disease: a bioinformatic analysis. *Genet Mol Res* **14**, 7218–7232 (2015).
19. Mastroeni, D. *et al.* Nuclear but not mitochondrial-encoded oxidative phosphorylation genes are altered in aging, mild cognitive impairment, and Alzheimer's disease. *Alzheimer's & dementia : the journal of the Alzheimer's Association* **13**, 510 (2016).
20. Brooks, W. M. *et al.* Gene expression profiles of metabolic enzyme transcripts in Alzheimer's disease. *Brain Research* **1127**, 127–135 (2007).
21. Liang, W. S. *et al.* Alzheimer's disease is associated with reduced expression of energy metabolism genes in posterior cingulate neurons. *Proc Natl Acad Sci U S A* **105**, 4441–4446 (2008).
22. Wang, W., Zhao, F., Ma, X., Perry, G. & Zhu, X. Mitochondria dysfunction in the pathogenesis of Alzheimer's disease: recent advances. *Mol Neurodegener* **15**, 30 (2020).
23. Kish, S. J. *et al.* Brain cytochrome oxidase in Alzheimer's disease. *J Neurochem* **59**, 776–779 (1992).
24. Parker, W. D., Filley, C. M. & Parks, J. K. Cytochrome oxidase deficiency in Alzheimer's disease. *Neurology* **40**, 1302–1303 (1990).
25. Yao, J. *et al.* Mitochondrial bioenergetic deficit precedes Alzheimer's pathology in female mouse model of Alzheimer's disease. *Proc Natl Acad Sci U S A* **106**, 14670–14675 (2009).
26. Javitch, J. A., D'Amato, R. J., Strittmatter, S. M. & Snyder, S. H. Parkinsonism-inducing neurotoxin, N-methyl-4-phenyl-1,2,3,6 -tetrahydropyridine: uptake of the metabolite N-methyl-4-phenylpyridine by dopamine neurons explains selective toxicity. *Proc Natl Acad Sci U S A* **82**, 2173–2177 (1985).
27. Langston, J. W. The MPTP Story. *J Parkinsons Dis* **7**, S11–S19 (2017).

28. Langston, J. W., Ballard, P., Tetrud, J. W. & Irwin, I. Chronic Parkinsonism in humans due to a product of meperidine-analog synthesis. *Science* **219**, 979–980 (1983).
29. Langston, J. W., Irwin, I., Langston, E. B. & Forno, L. S. 1-Methyl-4-phenylpyridinium ion (MPP⁺): identification of a metabolite of MPTP, a toxin selective to the substantia nigra. *Neurosci Lett* **48**, 87–92 (1984).
30. Ramsay, R. R., Salach, J. I. & Singer, T. P. Uptake of the neurotoxin 1-methyl-4-phenylpyridine (MPP⁺) by mitochondria and its relation to the inhibition of the mitochondrial oxidation of NAD⁺-linked substrates by MPP⁺. *Biochem Biophys Res Commun* **134**, 743–748 (1986).
31. Ramsay, R. R. *et al.* Interaction of 1-methyl-4-phenylpyridinium ion (MPP⁺) and its analogs with the rotenone/piericidin binding site of NADH dehydrogenase. *J Neurochem* **56**, 1184–1190 (1991).
32. Esteves, A. R. F. *et al.* Mitochondrial function in Parkinson’s disease cybrids containing an nt2 neuron-like nuclear background. *Mitochondrion* **8**, 219–228 (2008).
33. González-Rodríguez, P. *et al.* Disruption of mitochondrial complex I induces progressive parkinsonism. *Nature* **599**, 650 (2021).
34. Hatton, C. *et al.* Complex I reductions in the nucleus basalis of Meynert in Lewy body dementia: the role of Lewy bodies. *Acta Neuropathol Commun* **8**, 103 (2020).
35. Crugnola, V. *et al.* Mitochondrial respiratory chain dysfunction in muscle from patients with amyotrophic lateral sclerosis. *Arch Neurol* **67**, 849–854 (2010).
36. Cheng, M. *et al.* Mitochondrial respiratory complex IV deficiency recapitulates amyotrophic lateral sclerosis. *Nat Neurosci* **28**, 748–756 (2025).
37. Liao, Y.-C. *et al.* RNA Granules Hitchhike on Lysosomes for Long-Distance Transport, Using Annexin A11 as a Molecular Tether. *Cell* **179**, 147-164.e20 (2019).
38. De Pace, R. *et al.* Messenger RNA transport on lysosomal vesicles maintains axonal mitochondrial homeostasis and prevents axonal degeneration. *Nat Neurosci* **27**, 1087–1102 (2024).
39. Altman, T. *et al.* Axonal TDP-43 condensates drive neuromuscular junction disruption through inhibition of local synthesis of nuclear encoded mitochondrial proteins. *Nat Commun* **12**, 6914 (2021).
40. Sörensen, A. *et al.* Prognosis of conversion of mild cognitive impairment to Alzheimer’s dementia by voxel-wise Cox regression based on FDG PET data. *Neuroimage Clin* **21**, 101637 (2018).

41. Reiman, E. M. *et al.* Functional brain abnormalities in young adults at genetic risk for late-onset Alzheimer's dementia. *Proc Natl Acad Sci U S A* **101**, 284–289 (2004).
42. Wilkins, H. M. *et al.* Mitochondrial Lysates Induce Inflammation and Alzheimer's Disease-Relevant Changes in Microglial and Neuronal Cells. *J Alzheimers Dis* **45**, 305–318 (2015).
43. Wilkins, H. M. *et al.* Extracellular Mitochondria and Mitochondrial Components Act as Damage-Associated Molecular Pattern Molecules in the Mouse Brain. *J Neuroimmune Pharmacol* **11**, 622–628 (2016).
44. Aarreberg, L. D. *et al.* Interleukin-1 β Induces mtDNA Release to Activate Innate Immune Signaling via cGAS-STING. *Mol Cell* **74**, 801-815.e6 (2019).
45. Rongvaux, A. *et al.* Apoptotic caspases prevent the induction of type I interferons by mitochondrial DNA. *Cell* **159**, 1563–1577 (2014).
46. White, M. J. *et al.* Apoptotic Caspases Suppress mtDNA-Induced STING-Mediated Type I IFN Production. *Cell* **159**, 1549–1562 (2014).
47. Orihuela, R., McPherson, C. A. & Harry, G. J. Microglial M1/M2 polarization and metabolic states. *Br J Pharmacol* **173**, 649–665 (2016).
48. Jaber, S. M. *et al.* Sex differences in the mitochondrial bioenergetics of astrocytes but not microglia at a physiologically relevant brain oxygen tension. *Neurochemistry International* **117**, 82–90 (2018).
49. Bordt, E. A. *et al.* Gonadal hormones impart male-biased behavioral vulnerabilities to immune activation via microglial mitochondrial function. *Brain, Behavior, and Immunity* **115**, 680–695 (2024).
50. Lauro, C. & Limatola, C. Metabolic Reprogramming of Microglia in the Regulation of the Innate Inflammatory Response. *Front Immunol* **11**, 493 (2020).
51. Gimeno-Bayón, J., López-López, A., Rodríguez, M. J. & Mahy, N. Glucose pathways adaptation supports acquisition of activated microglia phenotype. *J Neurosci Res* **92**, 723–731 (2014).
52. Murphy, M. P. & O'Neill, L. A. J. Krebs Cycle Reimagined: The Emerging Roles of Succinate and Itaconate as Signal Transducers. *Cell* **174**, 780–784 (2018).
53. Tannahill, G. M. *et al.* Succinate is an inflammatory signal that induces IL-1 β through HIF-1 α . *Nature* **496**, 238–242 (2013).
54. Jha, A. K. *et al.* Network Integration of Parallel Metabolic and Transcriptional Data Reveals Metabolic Modules that Regulate Macrophage Polarization. *Immunity* **42**, 419–430 (2015).

55. Peruzzotti-Jametti, L. *et al.* Mitochondrial complex I activity in microglia sustains neuroinflammation. *Nature* **628**, 195–203 (2024).
56. Lampropoulou, V. *et al.* Itaconate Links Inhibition of Succinate Dehydrogenase with Macrophage Metabolic Remodeling and Regulation of Inflammation. *Cell Metab* **24**, 158–166 (2016).
57. B, B. *et al.* Pro-inflammatory macrophage activation does not require inhibition of oxidative phosphorylation. *EMBO Reports* <https://doi.org/10.1038/s44319-024-00351-y> (2025) doi:10.1038/s44319-024-00351-y.
58. Liu, N. *et al.* Itaconate restrains acute proinflammatory activation of microglia after traumatic brain injury in mice. *Science Translational Medicine* **17**, eadn2635 (2025).
59. Palmieri, E. M. *et al.* Nitric oxide orchestrates metabolic rewiring in M1 macrophages by targeting aconitase 2 and pyruvate dehydrogenase. *Nat Commun* **11**, 698 (2020).
60. Van den Bossche, J. *et al.* Mitochondrial Dysfunction Prevents Repolarization of Inflammatory Macrophages. *Cell Rep* **17**, 684–696 (2016).
61. S, F.-B. *et al.* Two-pore channels (TPCs): Novel voltage-gated ion channels with pleiotropic functions. *Channels (Austin, Tex.)* **11**, (2017).
62. Jašlan, D., Böck, J., Krogsaeter, E. & Grimm, C. Evolutionary Aspects of TRPMLs and TPCs. *Int J Mol Sci* **21**, 4181 (2020).
63. Ruas, M. *et al.* Purified TPC Isoforms Form NAADP Receptors with Distinct Roles for Ca²⁺ Signaling and Endolysosomal Trafficking. *Curr Biol* **20**, 703–709 (2010).
64. Brailoiu, E. *et al.* Essential requirement for two-pore channel 1 in NAADP-mediated calcium signaling. *J Cell Biol* **186**, 201–209 (2009).
65. Calcrafft, P. J. *et al.* NAADP mobilizes calcium from acidic organelles through two-pore channels. *Nature* **459**, 596–600 (2009).
66. Fernández, B. *et al.* Iron overload causes endolysosomal deficits modulated by NAADP-regulated 2-pore channels and RAB7A. *Autophagy* **12**, 1487–1506 (2016).
67. Krogsaeter, E., Tang, R. & Grimm, C. JPT2: The missing link between intracellular Ca²⁺ release channels and NAADP? *Cell Calcium* **97**, 102405 (2021).
68. Patel, S., Yuan, Y., Gunaratne, G. S., Rahman, T. & Marchant, J. S. Activation of endo-lysosomal two-pore channels by NAADP and PI(3,5)P₂. Five things to know. *Cell Calcium* **103**, 102543 (2022).

69. Davis, L. C., Morgan, A. J. & Galione, A. Acidic Ca²⁺ stores and immune-cell function. *Cell Calcium* **101**, 102516 (2022).
70. Cen, J., Hu, N., Shen, J., Gao, Y. & Lu, H. Pathological Functions of Lysosomal Ion Channels in the Central Nervous System. *Int J Mol Sci* **25**, 6565 (2024).
71. Sakurai, Y. *et al.* Two-pore channels control Ebola virus host cell entry and are drug targets for disease treatment. *Science* **347**, 995–998 (2015).
72. He, T. *et al.* Inhibition of two-pore channels in antigen-presenting cells promotes the expansion of TNFR2-expressing CD4⁺Foxp3⁺ regulatory T cells. *Sci Adv* **6**, eaba6584 (2020).
73. Arlt, E. *et al.* TPC1 deficiency or blockade augments systemic anaphylaxis and mast cell activity. *Proc Natl Acad Sci U S A* **117**, 18068–18078 (2020).
74. Davidson, S. M. *et al.* Inhibition of NAADP signalling on reperfusion protects the heart by preventing lethal calcium oscillations via two-pore channel 1 and opening of the mitochondrial permeability transition pore. *Cardiovasc Res* **108**, 357–366 (2015).
75. Halcrow, P. W. *et al.* HIV-1 gp120-Induced Endolysosome de-Acidification Leads to Efflux of Endolysosome Iron, and Increases in Mitochondrial Iron and Reactive Oxygen Species. *J Neuroimmune Pharmacol* **17**, 181–194 (2022).
76. Dixon, S. J. *et al.* Ferroptosis: An Iron-Dependent Form of Non-Apoptotic Cell Death. *Cell* **149**, 1060–1072 (2012).
77. Endlicher, R., Drahotová, Z., Štefková, K., Červinková, Z. & Kučera, O. The Mitochondrial Permeability Transition Pore—Current Knowledge of Its Structure, Function, and Regulation, and Optimized Methods for Evaluating Its Functional State. *Cells* **12**, 1273 (2023).
78. Bellenguez, C. *et al.* New insights into the genetic etiology of Alzheimer’s disease and related dementias. *Nat Genet* **54**, 412–436 (2022).
79. Carrigan, M. *et al.* A novel approach to resilience and its links with education and Alzheimer’s disease genetics. *Alzheimers Dement* **21**, e70379 (2025).
80. Katsumata, Y. *et al.* Multiple gene variants linked to Alzheimer’s-type clinical dementia via GWAS are also associated with non-Alzheimer’s neuropathologic entities. *Neurobiology of Disease* **174**, 105880 (2022).
81. Kaivola, K. *et al.* Genome-wide structural variant analysis identifies risk loci for non-Alzheimer’s dementias. *Cell Genomics* **3**, 100316 (2023).

82. Laureysen, C. *et al.* Hypothesis-based investigation of known AD risk variants reveals the genetic underpinnings of neuropathological lesions observed in Alzheimer's-type dementia. *Acta Neuropathol* **148**, 55 (2024).
83. Arai, T. *et al.* TDP-43 is a component of ubiquitin-positive tau-negative inclusions in frontotemporal lobar degeneration and amyotrophic lateral sclerosis. *Biochem Biophys Res Commun* **351**, 602–611 (2006).
84. Tartaglia, M. C. & Mackenzie, I. R. A. Recent Advances in Frontotemporal Dementia. *Can J Neurol Sci* **50**, 485–494 (2023).
85. Lee, J.-H. *et al.* Presenilin 1 maintains lysosomal Ca²⁺ homeostasis by regulating vATPase-mediated lysosome acidification. *Cell Rep* **12**, 1430–1444 (2015).
86. Marchant, J. S., Gunaratne, G. S., Cai, X., Slama, J. T. & Patel, S. NAADP-binding proteins find their identity. *Trends Biochem Sci* **47**, 235–249 (2022).
87. Gunaratne, G. S. *et al.* Convergent activation of two-pore channels mediated by the NAADP-binding proteins JPT2 and LSM12. *Sci Signal* **16**, eadg0485 (2023).
88. Gunaratne, G. S. *et al.* Essential requirement for JPT2 in NAADP-evoked Ca²⁺ signaling. *Sci Signal* **14**, eabd5605 (2021).
89. Gregori, M. *et al.* Lysosomal TPC2 channels disrupt Ca²⁺ entry and dopaminergic function in models of LRRK2-Parkinson's disease. *J Cell Biol* **224**, e202412055 (2025).
90. Hockey, L. N. *et al.* Dysregulation of lysosomal morphology by pathogenic LRRK2 is corrected by TPC2 inhibition. *J Cell Sci* **128**, 232–238 (2015).
91. Zhang, Y. *et al.* An RNA-Sequencing Transcriptome and Splicing Database of Glia, Neurons, and Vascular Cells of the Cerebral Cortex. *J. Neurosci.* **34**, 11929–11947 (2014).
92. Zhang, Y. *et al.* Purification and Characterization of Progenitor and Mature Human Astrocytes Reveals Transcriptional and Functional Differences with Mouse. *Neuron* **89**, 37–53 (2016).
93. Freeman, S. A. *et al.* Lipid-gated monovalent ion fluxes regulate endocytic traffic and support immune surveillance. *Science* **367**, 301–305 (2020).
94. Abdulla, S. *et al.* CZ CELLxGENE Discover: a single-cell data platform for scalable exploration, analysis and modeling of aggregated data. *Nucleic Acids Res* **53**, D886–D900 (2024).
95. Green, G. S. *et al.* Cellular dynamics across aged human brains uncover a multicellular cascade leading to Alzheimer's disease. *bioRxiv* 2023.03.07.531493 (2023) doi:10.1101/2023.03.07.531493.

96. Giulian, D. & Baker, T. Characterization of ameboid microglia isolated from developing mammalian brain. *J Neurosci* **6**, 2163–2178 (1986).
97. Aktories, P., Petry, P. & Kierdorf, K. Microglia in a Dish—Which Techniques Are on the Menu for Functional Studies? *Front. Cell. Neurosci.* **16**, (2022).
98. Llufrío, E. M., Wang, L., Naser, F. J. & Patti, G. J. Sorting cells alters their redox state and cellular metabolome. *Redox Biology* **16**, 381–387 (2018).
99. Mattei, D. *et al.* Enzymatic Dissociation Induces Transcriptional and Proteotype Bias in Brain Cell Populations. *International Journal of Molecular Sciences* **21**, 7944 (2020).
100. Blasi, E., Barluzzi, R., Bocchini, V., Mazzolla, R. & Bistoni, F. immortalization of murine microglial cells by a v-raf/v-myc carrying retrovirus. *J Neuroimmunol* **27**, 229–237 (1990).
101. Janabi, N., Peudenier, S., Héron, B., Ng, K. H. & Tardieu, M. Establishment of human microglial cell lines after transfection of primary cultures of embryonic microglial cells with the SV40 large T antigen. *Neurosci Lett* **195**, 105–108 (1995).
102. Nagamoto-Combs, K., Kulas, J. & Combs, C. K. A Novel Cell Line from Spontaneously Immortalized Murine Microglia. *J Neurosci Methods* **233**, 187–198 (2014).
103. Cheepsunthorn, P., Radov, L., Menzies, S., Reid, J. & Connor, J. R. Characterization of a novel brain-derived microglial cell line isolated from neonatal rat brain. *Glia* **35**, 53–62 (2001).
104. Horvath, R. J., Nutile-McMenemy, N., Alkaitis, M. S. & De Leo, J. A. Differential migration, LPS-induced cytokine, chemokine and NO expression in immortalized BV-2 and HAPI cell lines and primary microglial cultures. *J Neurochem* **107**, 557–569 (2008).
105. Nagai, A. *et al.* Generation and characterization of immortalized human microglial cell lines: expression of cytokines and chemokines. *Neurobiol Dis* **8**, 1057–1068 (2001).
106. Woolf, Z. *et al.* In vitro models of microglia: a comparative study. *Sci Rep* **15**, 15621 (2025).
107. Dello Russo, C. *et al.* The human microglial HMC3 cell line: where do we stand? A systematic literature review. *J Neuroinflammation* **15**, 259 (2018).
108. Kim, S. U. Immortalized human microglia cell and continuous cell line. (2002).
109. Rosario, A. M. *et al.* Microglia-specific targeting by novel capsid-modified AAV6 vectors. *Mol Ther Methods Clin Dev* **3**, 16026 (2016).

110. Okada, Y. *et al.* Development of microglia-targeting adeno-associated viral vectors as tools to study microglial behavior in vivo. *Commun Biol* **5**, 1–15 (2022).
111. Lin, R. *et al.* Directed evolution of adeno-associated virus for efficient gene delivery to microglia. *Nat Methods* **19**, 976–985 (2022).
112. Leone, C. *et al.* Characterization of human monocyte-derived microglia-like cells. *Glia* **54**, 183–192 (2006).
113. Muffat, J. *et al.* Efficient derivation of microglia-like cells from human pluripotent stem cells. *Nat Med* **22**, 1358–1367 (2016).
114. Tsuchiya, T. *et al.* Characterization of microglia induced from mouse embryonic stem cells and their migration into the brain parenchyma. *J Neuroimmunol* **160**, 210–218 (2005).
115. Abud, E. M. *et al.* iPSC-derived human microglia-like cells to study neurological diseases. *Neuron* **94**, 278–293.e9 (2017).
116. Brownjohn, P. W. *et al.* Functional Studies of Missense TREM2 Mutations in Human Stem Cell-Derived Microglia. *Stem Cell Reports* **10**, 1294–1307 (2018).
117. Dräger, N. M. *et al.* A CRISPRi/a platform in human iPSC-derived microglia uncovers regulators of disease states. *Nat Neurosci* **25**, 1149–1162 (2022).
118. Sargeant, T. J. & Fourier, C. Human monocyte-derived microglia-like cell models: A review of the benefits, limitations and recommendations. *Brain, Behavior, and Immunity* **107**, 98–109 (2023).
119. Qu, H. *et al.* Transcriptomic Profiling Reveals That HMGB1 Induces Macrophage Polarization Different from Classical M1. *Biomolecules* **12**, 779 (2022).
120. Mairuae, N., Connor, J. R. & Cheepsunthorn, P. Increased cellular iron levels affect matrix metalloproteinase expression and phagocytosis in activated microglia. *Neuroscience Letters* **500**, 36–40 (2011).
121. Pawate, S., Shen, Q., Fan, F. & Bhat, N. R. Redox regulation of glial inflammatory response to lipopolysaccharide and interferony. *Journal of Neuroscience Research* **77**, 540–551 (2004).
122. Jantaratnotai, N., Utaisincharoen, P., Piyachaturawat, P., Chongthammakun, S. & Sanvarinda, Y. Inhibitory effect of *Curcuma comosa* on NO production and cytokine expression in LPS-activated microglia. *Life Sciences* **78**, 571–577 (2006).
123. Lo, Y.-C. *et al.* Neuronal effects of 4-*t*-Butylcatechol: A model for catechol-containing antioxidants. *Toxicology and Applied Pharmacology* **228**, 247–255 (2008).

124. Hara, H. *et al.* Inhibitory effects of chalcone glycosides isolated from *Brassica rapa* L. 'hidabeni' and their synthetic derivatives on LPS-induced NO production in microglia. *Bioorganic & Medicinal Chemistry* **19**, 5559–5568 (2011).
125. Sheng, W. *et al.* Pro-inflammatory cytokines and lipopolysaccharide induce changes in cell morphology, and upregulation of ERK1/2, iNOS and sPLA2-IIA expression in astrocytes and microglia. *Journal of Neuroinflammation* **8**, 121 (2011).
126. Tocharus, J., Jamsuwan, S., Tocharus, C., Changtam, C. & Suksamrarn, A. Curcuminoid analogs inhibit nitric oxide production from LPS-activated microglial cells. *J Nat Med* **66**, 400–405 (2012).
127. Chuang, D. Y. *et al.* Magnolia polyphenols attenuate oxidative and inflammatory responses in neurons and microglial cells. *Journal of Neuroinflammation* **10**, 786 (2013).
128. Dallas, S. *et al.* Microglial activation decreases retention of the protease inhibitor saquinavir: implications for HIV treatment. *Journal of Neuroinflammation* **10**, 822 (2013).
129. Jantaratnotai, N., Utaisinchaoen, P., Sanvarinda, P., Thampithak, A. & Sanvarinda, Y. Phytoestrogens mediated anti-inflammatory effect through suppression of IRF-1 and pSTAT1 expressions in lipopolysaccharide-activated microglia. *International Immunopharmacology* **17**, 483–488 (2013).
130. Chamniansawat, S. & Chongthammakun, S. Inhibition of hippocampal estrogen synthesis by reactive microglia leads to down-regulation of synaptic protein expression. *NeuroToxicology* **46**, 25–34 (2015).
131. Hara, H. *et al.* Newly Synthesized 'Hidabeni' Chalcone Derivatives Potently Suppress LPS-Induced NO Production via Inhibition of STAT1, but Not NF- κ B, JNK, and p38, Pathways in Microglia. *Biological and Pharmaceutical Bulletin* **37**, 1042–1049 (2014).
132. McFarland, A. J. *et al.* Differences in statin associated neuroprotection corresponds with either decreased production of IL-1 β or TNF- α in an *in vitro* model of neuroinflammation-induced neurodegeneration. *Toxicology and Applied Pharmacology* **344**, 56–73 (2018).
133. Jantaratnotai, N., Thampithak, A., Utaisinchaoen, P., Pinthong, D. & Sanvarinda, P. Inhibition of LPS-Induced Microglial Activation by the Ethyl Acetate Extract of *Pueraria mirifica*. *International Journal of Environmental Research and Public Health* **19**, 12920 (2022).
134. Li, J. *et al.* Ginsenoside Rg1 Reduced Microglial Activation and Mitochondrial Dysfunction to Alleviate Depression-Like Behaviour Via the GAS5/EZH2/SOCS3/NRF2 Axis. *Mol Neurobiol* **59**, 2855–2873 (2022).

135. Hara, H., Manome, A. & Kamiya, T. Panobinostat, a Histone Deacetylase Inhibitor, Reduces LPS-Induced Expression of Inducible Nitric Oxide Synthase in Rat Immortalized Microglia HAPI Cells. *Biological and Pharmaceutical Bulletin* **47**, 1196–1203 (2024).
136. Giacomello, M., Pyakurel, A., Glytsou, C. & Scorrano, L. The cell biology of mitochondrial membrane dynamics. *Nat Rev Mol Cell Biol* **21**, 204–224 (2020).
137. Quintana-Cabrera, R. & Scorrano, L. Determinants and outcomes of mitochondrial dynamics. *Mol Cell* **83**, 857–876 (2023).
138. Ryu, K. W. *et al.* Cellular ATP demand creates metabolically distinct subpopulations of mitochondria. *Nature* **635**, 746–754 (2024).
139. Adebayo, M., Singh, S., Singh, A. P. & Dasgupta, S. Mitochondrial Fusion and Fission: The fine-tune balance for cellular homeostasis. *FASEB J* **35**, e21620 (2021).
140. Chen, W., Zhao, H. & Li, Y. Mitochondrial dynamics in health and disease: mechanisms and potential targets. *Sig Transduct Target Ther* **8**, 333 (2023).
141. Smirnova, E., Griparic, L., Shurland, D.-L. & van der Bliek, A. M. Dynamin-related Protein Drp1 Is Required for Mitochondrial Division in Mammalian Cells. *Mol Biol Cell* **12**, 2245–2256 (2001).
142. Wakabayashi, J. *et al.* The dynamin-related GTPase Drp1 is required for embryonic and brain development in mice. *J Cell Biol* **186**, 805–816 (2009).
143. Berthet, A. *et al.* Loss of Mitochondrial Fission Depletes Axonal Mitochondria in Midbrain Dopamine Neurons. *J Neurosci* **34**, 14304–14317 (2014).
144. Shields, L. Y. *et al.* Dynamin-related protein 1 is required for normal mitochondrial bioenergetic and synaptic function in CA1 hippocampal neurons. *Cell Death Dis* **6**, e1725 (2015).
145. Oettinghaus, B. *et al.* Synaptic dysfunction, memory deficits and hippocampal atrophy due to ablation of mitochondrial fission in adult forebrain neurons. *Cell Death Differ* **23**, 18–28 (2016).
146. Chen, Y., Culetto, E. & Legouis, R. The strange case of Drp1 in autophagy: Jekyll and Hyde? *BioEssays* **44**, 2100271 (2022).
147. Lemasters, J. J. Selective mitochondrial autophagy, or mitophagy, as a targeted defense against oxidative stress, mitochondrial dysfunction, and aging. *Rejuvenation Res* **8**, 3–5 (2005).
148. Deng, H., Dodson, M. W., Huang, H. & Guo, M. The Parkinson's disease genes pink1 and parkin promote mitochondrial fission and/or inhibit fusion in Drosophila. *Proc Natl Acad Sci U S A* **105**, 14503–14508 (2008).

149. Kageyama, Y. *et al.* Parkin-independent mitophagy requires Drp1 and maintains the integrity of mammalian heart and brain. *EMBO J* **33**, 2798–2813 (2014).
150. Oshima, Y. *et al.* Parkin-independent mitophagy via Drp1-mediated outer membrane severing and inner membrane ubiquitination. *J Cell Biol* **220**, e202006043 (2021).
151. König, T. *et al.* MIROs and DRP1 drive mitochondrial-derived vesicle biogenesis and promote quality control. *Nat Cell Biol* **23**, 1271–1286 (2021).
152. Divakaruni, S. S. *et al.* Long-term potentiation requires a rapid burst of dendritic mitochondrial fission during induction. *Neuron* **100**, 860-875.e7 (2018).
153. Itoh, K. *et al.* Brain-specific Drp1 regulates postsynaptic endocytosis and dendrite formation independently of mitochondrial division. *eLife* **8**, e44739.
154. Nolden, K. A. *et al.* Novel DNM1L variants impair mitochondrial dynamics through divergent mechanisms. *Life Sci Alliance* **5**, e202101284 (2022).
155. Waterham, H. R. *et al.* A lethal defect of mitochondrial and peroxisomal fission. *N Engl J Med* **356**, 1736–1741 (2007).
156. Yoon, G. *et al.* Lethal Disorder of Mitochondrial Fission Caused by Mutations in DNM1L. *J Pediatr* **171**, 313-316.e1–2 (2016).
157. Fahrner, J. A., Liu, R., Perry, M. S., Klein, J. & Chan, D. C. A Novel de novo Dominant Negative Mutation in DNM1L Impairs Mitochondrial Fission and Presents as Childhood Epileptic Encephalopathy. *Am J Med Genet A* **170**, 2002–2011 (2016).
158. Vanstone, J. R. *et al.* DNM1L-related mitochondrial fission defect presenting as refractory epilepsy. *Eur J Hum Genet* **24**, 1084–1088 (2016).
159. Gerber, S. *et al.* Mutations in DNM1L, as in OPA1, result in dominant optic atrophy despite opposite effects on mitochondrial fusion and fission. *Brain* **140**, 2586–2596 (2017).
160. Dong, W.-T. *et al.* Mitochondrial fission drives neuronal metabolic burden to promote stress susceptibility in male mice. *Nat Metab* **5**, 2220–2236 (2023).
161. Napoli, E. *et al.* Zdhc13-dependent Drp1 S-palmitoylation impacts brain bioenergetics, anxiety, coordination and motor skills. *Sci Rep* **7**, 12796 (2017).
162. Ikeda, A., Iijima, M. & Sesaki, H. Systemic phospho-defective and phospho-mimetic Drp1 mice exhibit normal growth and development with altered anxiety-like behavior. *iScience* **27**, 109874 (2024).

163. Chandra, R. *et al.* Drp1 mitochondrial fission in D1 neurons mediates behavioral and cellular plasticity during early cocaine abstinence. *Neuron* **96**, 1327-1341.e6 (2017).
164. Gu, X. *et al.* Drp1 mitochondrial fission in astrocyte modulates behavior and neuroinflammation during morphine addiction. *J Neuroinflammation* **22**, 108 (2025).
165. Kim, D. I. *et al.* A β -Induced Drp1 phosphorylation through Akt activation promotes excessive mitochondrial fission leading to neuronal apoptosis. *Biochim Biophys Acta* **1863**, 2820–2834 (2016).
166. Manczak, M., Calkins, M. J. & Reddy, P. H. Impaired mitochondrial dynamics and abnormal interaction of amyloid beta with mitochondrial protein Drp1 in neurons from patients with Alzheimer's disease: implications for neuronal damage. *Hum Mol Genet* **20**, 2495–2509 (2011).
167. Wang, X. *et al.* LRRK2 regulates mitochondrial dynamics and function through direct interaction with DLP1. *Hum Mol Genet* **21**, 1931–1944 (2012).
168. Cassidy-Stone, A. *et al.* Chemical inhibition of the mitochondrial division dynamin reveals its role in Bax/Bak-dependent mitochondrial outer membrane permeabilization. *Dev Cell* **14**, 193–204 (2008).
169. Liu, X. *et al.* Mdivi-1: a promising drug and its underlying mechanisms in the treatment of neurodegenerative diseases. *Histol Histopathol* **37**, 505–512 (2022).
170. Duan, C. *et al.* Mdivi-1 attenuates oxidative stress and exerts vascular protection in ischemic/hypoxic injury by a mechanism independent of Drp1 GTPase activity. *Redox Biol* **37**, 101706 (2020).
171. Yoon, Y., Krueger, E. W., Oswald, B. J. & McNiven, M. A. The Mitochondrial Protein hFis1 Regulates Mitochondrial Fission in Mammalian Cells through an Interaction with the Dynamin-Like Protein DLP1. *Mol Cell Biol* **23**, 5409–5420 (2003).
172. Gandre-Babbe, S. & van der Bliek, A. M. The Novel Tail-anchored Membrane Protein Mff Controls Mitochondrial and Peroxisomal Fission in Mammalian Cells. *MBoC* **19**, 2402–2412 (2008).
173. Nolden, K. A., Harwig, M. C. & Hill, R. B. Human Fis1 directly interacts with Drp1 in an evolutionarily conserved manner to promote mitochondrial fission. *J Biol Chem* **299**, 105380 (2023).
174. Kleele, T. *et al.* Distinct fission signatures predict mitochondrial degradation or biogenesis. *Nature* **593**, 435–439 (2021).

175. Wong, Y. C., Ysselstein, D. & Krainc, D. Mitochondria-lysosome contacts regulate mitochondrial fission via Rab7 GTP hydrolysis. *Nature* **554**, 382–386 (2018).
176. Friedman, J. R. *et al.* ER Tubules Mark Sites of Mitochondrial Division. *Science* **334**, 358–362 (2011).
177. Korobova, F., Ramabhadran, V. & Higgs, H. N. An Actin-Dependent Step in Mitochondrial Fission Mediated by the ER-Associated Formin INF2. *Science* **339**, 464–467 (2013).
178. Fröhlich, C. *et al.* Structural insights into oligomerization and mitochondrial remodelling of dynamin 1-like protein. *EMBO J* **32**, 1280–1292 (2013).
179. Kalia, R. *et al.* Structural Basis of Mitochondrial Receptor Binding and Constriction by DRP1. *Nature* **558**, 401–405 (2018).
180. Lee, J. E., Westrate, L. M., Wu, H., Page, C. & Voeltz, G. K. Multiple Dynamin family members collaborate to drive mitochondrial division. *Nature* **540**, 139–143 (2016).
181. Kamerkar, S. C., Kraus, F., Sharpe, A. J., Pucadyil, T. J. & Ryan, M. T. Dynamin-related protein 1 has membrane constricting and severing abilities sufficient for mitochondrial and peroxisomal fission. *Nat Commun* **9**, 5239 (2018).
182. Nakamura, K. *et al.* Direct Membrane Association Drives Mitochondrial Fission by the Parkinson Disease-associated Protein α -Synuclein \blacklozenge . *J Biol Chem* **286**, 20710–20726 (2011).
183. Guardia-Laguarta, C. *et al.* α -Synuclein Is Localized to Mitochondria-Associated ER Membranes. *J Neurosci* **34**, 249–259 (2014).
184. Roy, M., Ito, K., Iijima, M. & Sesaki, H. Parkin Suppresses Drp1-Independent Mitochondrial Division. *Biochem Biophys Res Commun* **475**, 283–288 (2016).
185. de Torre-Minguela, C., Gómez, A. I., Couillin, I. & Pelegrín, P. Gasdermins mediate cellular release of mitochondrial DNA during pyroptosis and apoptosis. *FASEB J* **35**, e21757 (2021).
186. Li, X. & Gould, S. J. The dynamin-like GTPase DLP1 is essential for peroxisome division and is recruited to peroxisomes in part by PEX11. *J Biol Chem* **278**, 17012–17020 (2003).
187. Koch, A. *et al.* Dynamin-like protein 1 is involved in peroxisomal fission. *J Biol Chem* **278**, 8597–8605 (2003).
188. Wong, Y. C., Peng, W. & Krainc, D. Lysosomal Regulation of Inter-mitochondrial Contact Fate and Motility in Charcot-Marie-Tooth Type 2. *Dev Cell* **50**, 339–354.e4 (2019).

189. Li, X. *et al.* Novel role of dynamin-related-protein 1 in dynamics of ER-lipid droplets in adipose tissue. *FASEB J* **34**, 8265–8282 (2020).
190. Adachi, Y. *et al.* Drp1 Tubulates the ER in a GTPase Independent Manner. *Mol Cell* **80**, 621-632.e6 (2020).
191. Duan, C. *et al.* Mitochondrial Drp1 recognizes and induces excessive mPTP opening after hypoxia through BAX-PiC and LRRK2-HK2. *Cell Death Dis* **12**, 1050 (2021).
192. Brown, H. J. *et al.* Imbalanced mitochondrial dynamics in human PD and α -synuclein mouse brains. *Neurobiol Dis* **212**, 106976 (2025).
193. Healy, D. G. *et al.* Phenotype, genotype, and worldwide genetic penetrance of LRRK2-associated Parkinson's disease: a case-control study. *Lancet Neurol* **7**, 583–590 (2008).
194. Santos, D., Esteves, A. R., Silva, D. F., Januário, C. & Cardoso, S. M. The Impact of Mitochondrial Fusion and Fission Modulation in Sporadic Parkinson's Disease. *Mol Neurobiol* **52**, 573–586 (2015).
195. Cui, M., Tang, X., Christian, W. V., Yoon, Y. & Tieu, K. Perturbations in Mitochondrial Dynamics Induced by Human Mutant PINK1 Can Be Rescued by the Mitochondrial Division Inhibitor mdivi-1. *J Biol Chem* **285**, 11740–11752 (2010).
196. Fan, R. Z., Guo, M., Luo, S., Cui, M. & Tieu, K. Exosome release and neuropathology induced by α -synuclein: new insights into protective mechanisms of Drp1 inhibition. *Acta Neuropathologica Communications* **7**, 184 (2019).
197. Rappold, P. M. *et al.* Drp1 inhibition attenuates neurotoxicity and dopamine release deficits in vivo. *Nat Commun* **5**, 5244 (2014).
198. Bido, S., Soria, F. N., Fan, R. Z., Bezard, E. & Tieu, K. Mitochondrial division inhibitor-1 is neuroprotective in the A53T- α -synuclein rat model of Parkinson's disease. *Sci Rep* **7**, 7495 (2017).
199. Zhang, X. *et al.* Drp1, a potential therapeutic target for Parkinson's disease, is involved in olfactory bulb pathological alteration in the Rotenone-induced rat model. *Toxicol Lett* **325**, 1–13 (2020).
200. Chen, N. *et al.* Drp1-mediated mitochondrial fission contributes to mitophagy in paraquat-induced neuronal cell damage. *Environ Pollut* **272**, 116413 (2021).
201. Chen, N. *et al.* LncRNA NR_030777 promotes mitophagy by targeting CDK1-related mitochondrial fission and ATG12 to attenuate paraquat-induced Parkinson's disease. *Environ Pollut* **349**, 123875 (2024).

202. Ma, J. *et al.* Inhibiting mitochondrial excessive fission alleviates the neuronal damage in Parkinson's disease via regulating PGC-1 α mediated mitochondrial biogenesis. *Exp Neurol* **391**, 115288 (2025).
203. Su, Y.-C. & Qi, X. Inhibition of excessive mitochondrial fission reduced aberrant autophagy and neuronal damage caused by LRRK2 G2019S mutation. *Hum Mol Genet* **22**, 4545–4561 (2013).
204. Qi, X., Qvit, N., Su, Y.-C. & Mochly-Rosen, D. A novel Drp1 inhibitor diminishes aberrant mitochondrial fission and neurotoxicity. *J Cell Sci* **126**, 789–802 (2013).
205. Filichia, E., Hoffer, B., Qi, X. & Luo, Y. Inhibition of Drp1 mitochondrial translocation provides neural protection in dopaminergic system in a Parkinson's disease model induced by MPTP. *Sci Rep* **6**, 32656 (2016).
206. Yu, W., Sun, Y., Guo, S. & Lu, B. The PINK1/Parkin pathway regulates mitochondrial dynamics and function in mammalian hippocampal and dopaminergic neurons. *Hum Mol Genet* **20**, 3227–3240 (2011).
207. Ma, P., Yun, J., Deng, H. & Guo, M. Atg1-mediated autophagy suppresses tissue degeneration in pink1/parkin mutants by promoting mitochondrial fission in *Drosophila*. *Mol Biol Cell* **29**, 3082–3092 (2018).
208. Ordonez, D. G., Lee, M. K. & Feany, M. B. α -synuclein induces mitochondrial dysfunction through spectrin and the actin cytoskeleton. *Neuron* **97**, 108-124.e6 (2018).
209. DeTure, M. A. & Dickson, D. W. The neuropathological diagnosis of Alzheimer's disease. *Mol Neurodegener* **14**, 32 (2019).
210. Wang, X. *et al.* Amyloid- β overproduction causes abnormal mitochondrial dynamics via differential modulation of mitochondrial fission/fusion proteins. *Proc Natl Acad Sci U S A* **105**, 19318–19323 (2008).
211. Cha, M.-Y. *et al.* Mitochondria-Specific Accumulation of Amyloid β Induces Mitochondrial Dysfunction Leading to Apoptotic Cell Death. *PLoS One* **7**, e34929 (2012).
212. Han, X.-J. *et al.* Amyloid β -42 induces neuronal apoptosis by targeting mitochondria. *Mol Med Rep* **16**, 4521–4528 (2017).
213. Golovynska, I., Chen, Q., Stepanov, Y. V., Lin, D. & Qu, J. Amyloid-induced mitochondrial network disruption in neurons monitored by STED super-resolution imaging. *Front Cell Dev Biol* **13**, 1610204 (2025).
214. Manczak, M. & Reddy, P. H. Abnormal interaction between the mitochondrial fission protein Drp1 and hyperphosphorylated tau in Alzheimer's disease neurons:

- implications for mitochondrial dysfunction and neuronal damage. *Hum Mol Genet* **21**, 2538–2547 (2012).
215. Gan, X. *et al.* Inhibition of ERK-DLP1 signaling and mitochondrial division alleviates mitochondrial dysfunction in Alzheimer's disease cybrid cell. *Biochim Biophys Acta* **1842**, 220–231 (2014).
216. Baek, S. H. *et al.* Inhibition of Drp1 Ameliorates Synaptic Depression, A β Deposition, and Cognitive Impairment in an Alzheimer's Disease Model. *J Neurosci* **37**, 5099–5110 (2017).
217. Wang, W. *et al.* Inhibition of mitochondrial fragmentation protects against Alzheimer's disease in rodent model. *Hum Mol Genet* **26**, 4118–4131 (2017).
218. Yuan, Y. *et al.* Activation of ERK–Drp1 signaling promotes hypoxia-induced A β accumulation by upregulating mitochondrial fission and BACE1 activity. *FEBS Open Bio* **11**, 2740–2755 (2021).
219. Joshi, A. U. *et al.* Inhibition of Drp1/Fis1 interaction slows progression of amyotrophic lateral sclerosis. *EMBO Mol Med* **10**, e8166 (2018).
220. Joshi, A. U. *et al.* Fragmented mitochondria released from microglia trigger A1 astrocytic response and propagate inflammatory neurodegeneration. *Nat Neurosci* **22**, 1635–1648 (2019).
221. Zhang, W. *et al.* A β -induced excessive mitochondrial fission drives type H blood vessels injury to aggravate bone loss in APP/PS1 mice with Alzheimer's diseases. *Aging Cell* **24**, e14374 (2025).
222. Pérez, M. J., Ponce, D. P., Osorio-Fuentealba, C., Behrens, M. I. & Quintanilla, R. A. Mitochondrial Bioenergetics Is Altered in Fibroblasts from Patients with Sporadic Alzheimer's Disease. *Front Neurosci* **11**, 553 (2017).
223. Wang, X., Su, B., Fujioka, H. & Zhu, X. Dynamin-Like Protein 1 Reduction Underlies Mitochondrial Morphology and Distribution Abnormalities in Fibroblasts from Sporadic Alzheimer's Disease Patients. *Am J Pathol* **173**, 470–482 (2008).
224. Wang, X. *et al.* Impaired Balance of Mitochondrial Fission and Fusion in Alzheimer's Disease. *J Neurosci* **29**, 9090–9103 (2009).
225. Martín-Maestro, P. *et al.* Slower Dynamics and Aged Mitochondria in Sporadic Alzheimer's Disease. *Oxid Med Cell Longev* **2017**, 9302761 (2017).
226. Morozov, Y. M., Datta, D., Paspalas, C. D. & Arnsten, A. F. T. Ultrastructural Evidence for Impaired Mitochondrial Fission in the Aged Rhesus Monkey Dorsolateral Prefrontal Cortex. *Neurobiol Aging* **51**, 9–18 (2017).

227. Zhang, H. *et al.* A novel fission-independent role of dynamin-related protein 1 in cardiac mitochondrial respiration. *Cardiovasc Res* **113**, 160–170 (2017).
228. Tyumentsev, M. A. *et al.* Mitochondrial Dysfunction as a Predictor and Driver of Alzheimer’s Disease-Like Pathology in OXYS Rats. *J Alzheimers Dis* **63**, 1075–1088 (2018).
229. Luo, G. *et al.* Defective Mitochondrial Dynamics Is an Early Event in Skeletal Muscle of an Amyotrophic Lateral Sclerosis Mouse Model. *PLoS One* **8**, e82112 (2013).
230. Altanbyek, V. *et al.* Imbalance of mitochondrial dynamics in Drosophila models of amyotrophic lateral sclerosis. *Biochem Biophys Res Commun* **481**, 259–264 (2016).
231. Wang, H. *et al.* ALS-associated mutation SOD1G93A leads to abnormal mitochondrial dynamics in osteocytes. *Bone* **106**, 126–138 (2018).
232. Petrozziello, T. *et al.* Targeting Tau Mitigates Mitochondrial Fragmentation and Oxidative Stress in Amyotrophic Lateral Sclerosis. *Mol Neurobiol* **59**, 683–702 (2022).
233. Nemtsova, Y., Steinert, B. & Wharton, K. “Compartment specific mitochondrial dysfunction in Drosophila knock-in model of ALS reversed by altered gene expression of OXPHOS subunits and pro-fission factor Drp1”. *Mol Cell Neurosci* **125**, 103834 (2023).
234. Wang, H., Lim, P. J., Karbowski, M. & Monteiro, M. J. Effects of overexpression of Huntingtin proteins on mitochondrial integrity. *Hum Mol Genet* **18**, 737–752 (2009).
235. Costa, V. *et al.* Mitochondrial fission and cristae disruption increase the response of cell models of Huntington’s disease to apoptotic stimuli. *EMBO Mol Med* **2**, 490–503 (2010).
236. Song, W. *et al.* MUTANT HUNTINGTIN BINDS THE MITOCHONDRIAL FISSION GTPASE DRP1 AND INCREASES ITS ENZYMATIC ACTIVITY. *Nat Med* **17**, 377–382 (2011).
237. Haun, F. *et al.* S-Nitrosylation of Dynamin-Related Protein 1 Mediates Mutant Huntingtin-Induced Mitochondrial Fragmentation and Neuronal Injury in Huntington’s Disease. *Antioxid Redox Signal* **19**, 1173–1184 (2013).
238. Guo, X. *et al.* Inhibition of mitochondrial fragmentation diminishes Huntington’s disease-associated neurodegeneration. *J Clin Invest* **123**, 5371–5388 (2013).
239. Manczak, M. & Reddy, P. H. Mitochondrial division inhibitor 1 protects against mutant huntingtin-induced abnormal mitochondrial dynamics and neuronal damage in Huntington’s disease. *Hum Mol Genet* **24**, 7308–7325 (2015).

240. Roe, A. J. & Qi, X. Drp1 phosphorylation by MAPK1 causes mitochondrial dysfunction in cell culture model of Huntington's disease. *Biochem Biophys Res Commun* **496**, 706–711 (2018).
241. Zhao, Y., Sun, X. & Qi, X. Inhibition of Drp1 hyperactivation reduces neuropathology and behavioral deficits in zQ175 knock-in mouse model of Huntington's disease. *Biochem Biophys Res Commun* **507**, 319–323 (2018).
242. Zhao, Y. *et al.* ATAD3A oligomerization causes neurodegeneration by coupling mitochondrial fragmentation and bioenergetics defects. *Nat Commun* **10**, 1371 (2019).
243. Cherubini, M., Lopez-Molina, L. & Gines, S. Mitochondrial fission in Huntington's disease mouse striatum disrupts ER-mitochondria contacts leading to disturbances in Ca²⁺ efflux and Reactive Oxygen Species (ROS) homeostasis. *Neurobiol Dis* **136**, 104741 (2020).
244. Gharaba, S., Sprecher, U., Baransi, A., Muchtar, N. & Weil, M. Characterization of fission and fusion mitochondrial dynamics in HD fibroblasts according to patient's severity status. *Neurobiol Dis* **201**, 106667 (2024).
245. Choi, S. Y. *et al.* Prevention of mitochondrial impairment by inhibition of protein phosphatase 1 activity in amyotrophic lateral sclerosis. *Cell Death Dis* **11**, 888 (2020).
246. Kijima, K. *et al.* Mitochondrial GTPase mitofusin 2 mutation in Charcot-Marie-Tooth neuropathy type 2A. *Hum Genet* **116**, 23–27 (2005).
247. Züchner, S. *et al.* Mutations in the mitochondrial GTPase mitofusin 2 cause Charcot-Marie-Tooth neuropathy type 2A. *Nat Genet* **36**, 449–451 (2004).
248. Detmer, S. A. & Chan, D. C. Complementation between mouse Mfn1 and Mfn2 protects mitochondrial fusion defects caused by CMT2A disease mutations. *J Cell Biol* **176**, 405–414 (2007).
249. Dang, X. *et al.* Mitochondrial Phenotypes in Genetically Diverse Neurodegenerative Diseases and Their Response to Mitofusin Activation. *Cells* **11**, 1053 (2022).
250. Noack, R. *et al.* Charcot-Marie-Tooth disease CMT4A: GDAP1 increases cellular glutathione and the mitochondrial membrane potential. *Hum Mol Genet* **21**, 150–162 (2012).
251. Martin, A. M., Maradei, S. J. & Velasco, H. M. Charcot Marie Tooth disease (CMT4A) due to GDAP1 mutation. *Colomb Med (Cali)* **46**, 194–198 (2015).
252. Vivar, C. & Avila, J. D. GDAP1-Related Charcot-Marie-Tooth Disease: Additional Evidence for the c.692C>T Variant as a Pathogenic Mutation (P3.4-045). *Neurology* **92**, P3.4-045 (2019).

253. Alexander, C. *et al.* OPA1, encoding a dynamin-related GTPase, is mutated in autosomal dominant optic atrophy linked to chromosome 3q28. *Nat Genet* **26**, 211–215 (2000).
254. Thiselton, D. L. *et al.* A comprehensive survey of mutations in the OPA1 gene in patients with autosomal dominant optic atrophy. *Invest Ophthalmol Vis Sci* **43**, 1715–1724 (2002).
255. Lenaers, G. *et al.* Dominant optic atrophy. *Orphanet J Rare Dis* **7**, 46 (2012).
256. Davies, V. J. *et al.* Opa1 deficiency in a mouse model of autosomal dominant optic atrophy impairs mitochondrial morphology, optic nerve structure and visual function. *Hum Mol Genet* **16**, 1307–1318 (2007).
257. Lin, Y. *et al.* Targeting DRP1 with Mdivi-1 to correct mitochondrial abnormalities in ADOA+ syndrome. *JCI Insight* **9**, e180582 (2024).
258. Mallat, A. *et al.* Discovery and characterization of selective small molecule inhibitors of the mammalian mitochondrial division dynamin, DRP1. *Biochem Biophys Res Commun* **499**, 556–562 (2018).
259. Wu, D. *et al.* Identification of novel dynamin-related protein 1 (Drp1) GTPase inhibitors: Therapeutic potential of Drpitor1 and Drpitor1a in cancer and cardiac ischemia-reperfusion injury. *FASEB J* **34**, 1447–1464 (2020).
260. Rosdah, A. A. *et al.* A novel small molecule inhibitor of human Drp1. *Sci Rep* **12**, 21531 (2022).
261. Furuya, T. *et al.* Discovery of Potent Allosteric DRP1 Inhibitors by Disrupting Protein–Protein Interaction with MiD49. *ACS Med Chem Lett* **14**, 1095–1099 (2023).
262. Hekal, H. A., Salem, M. M. & El Salam, H. A. A. Inhibition of DRP-1 mitochondrial mitophagy and fission by novel α -aminophosphonates bearing pyridine: synthesis, biological evaluations, and computer-aided design. *BMC Chemistry* **18**, 174 (2024).
263. Bordt, E. A. *et al.* The Putative Drp1 Inhibitor mdivi-1 Is a Reversible Mitochondrial Complex I Inhibitor that Modulates Reactive Oxygen Species. *Dev Cell* **40**, 583–594.e6 (2017).
264. Numadate, A., Mita, Y., Matsumoto, Y., Fujii, S. & Hashimoto, Y. Development of 2-thioxoquinazoline-4-one derivatives as dual and selective inhibitors of dynamin-related protein 1 (Drp1) and puromycin-sensitive aminopeptidase (PSA). *Chem Pharm Bull (Tokyo)* **62**, 979–988 (2014).
265. Ruiz, A., Alberdi, E. & Matute, C. Mitochondrial Division Inhibitor 1 (mdivi-1) Protects Neurons against Excitotoxicity through the Modulation of Mitochondrial

- Function and Intracellular Ca²⁺ Signaling. *Frontiers in Molecular Neuroscience* **11**, (2018).
266. Wang, W.-H. *et al.* Multiomics Reveals Induction of Neuroblastoma SK-N-BE(2)C Cell Death by Mitochondrial Division Inhibitor 1 through Multiple Effects. *J Proteome Res* **23**, 301–315 (2024).
267. Marx, N., Ritter, N., Disse, P., Seebohm, G. & Busch, K. B. Detailed analysis of Mdivi-1 effects on complex I and respiratory supercomplex assembly. *Sci Rep* **14**, 19673 (2024).
268. Koch, B. *et al.* A Metabolic Checkpoint for the Yeast-to-Hyphae Developmental Switch Regulated by Endogenous Nitric Oxide Signaling. *Cell Reports* **25**, 2244-2258.e7 (2018).
269. Bordt, E. A., Zhang, N., Waddell, J. & Polster, B. M. The Non-Specific Drp1 Inhibitor Mdivi-1 Has Modest Biochemical Antioxidant Activity. *Antioxidants (Basel)* **11**, 450 (2022).
270. Ruiz, A. *et al.* Mitochondrial division inhibitor 1 disrupts oligodendrocyte Ca²⁺ homeostasis and mitochondrial function. *Glia* **68**, 1743–1756 (2020).
271. Preau, S. *et al.* Endotoxemia Engages the RhoA Kinase Pathway to Impair Cardiac Function By Altering Cytoskeleton, Mitochondrial Fission, and Autophagy. *Antioxid Redox Signal* **24**, 529–542 (2016).
272. Aishwarya, R. *et al.* Pleiotropic effects of mdivi-1 in altering mitochondrial dynamics, respiration, and autophagy in cardiomyocytes. *Redox Biol* **36**, 101660 (2020).
273. Murata, D., Arai, K., Iijima, M. & Sesaki, H. Mitochondrial division, fusion and degradation. *J Biochem* **167**, 233–241 (2020).
274. Malpartida, A. B., Williamson, M., Narendra, D. P., Wade-Martins, R. & Ryan, B. J. Mitochondrial Dysfunction and Mitophagy in Parkinson’s Disease: From Mechanism to Therapy. *Trends Biochem Sci* **46**, 329–343 (2021).
275. Fivenson, E. M. *et al.* Mitophagy in neurodegeneration and aging. *Neurochem Int* **109**, 202–209 (2017).
276. Fang, E. F. *et al.* Mitophagy inhibits amyloid- β and tau pathology and reverses cognitive deficits in models of Alzheimer’s disease. *Nat Neurosci* **22**, 401–412 (2019).
277. Quirós, P. M. *et al.* Multi-omics analysis identifies ATF4 as a key regulator of the mitochondrial stress response in mammals. *J Cell Biol* **216**, 2027–2045 (2017).

278. Bilen, M., Benhammouda, S., Slack, R. S. & Germain, M. The integrated stress response as a key pathway downstream of mitochondrial dysfunction. *Current Opinion in Physiology* **27**, 100555 (2022).
279. Vasudevan, D. *et al.* Translational induction of ATF4 during integrated stress response requires noncanonical initiation factors eIF2D and DENR. *Nat Commun* **11**, 4677 (2020).
280. Neill, G. & Masson, G. R. A stay of execution: ATF4 regulation and potential outcomes for the integrated stress response. *Front Mol Neurosci* **16**, 1112253 (2023).
281. Restelli, L. M. *et al.* Neuronal Mitochondrial Dysfunction Activates the Integrated Stress Response to Induce Fibroblast Growth Factor 21. *Cell Rep* **24**, 1407–1414 (2018).
282. Chakrabarty, Y., Yang, Z., Chen, H. & Chan, D. C. The HRI branch of the integrated stress response selectively triggers mitophagy. *Mol Cell* **84**, 1090-1100.e6 (2024).
283. Singh, P. K. *et al.* Kinome screening identifies integrated stress response kinase EIF2AK1/HRI as a negative regulator of PINK1 mitophagy signaling. *Sci Adv* **11**, eadn2528 (2025).
284. Sasaki, K. *et al.* Mitochondrial translation inhibition triggers ATF4 activation, leading to integrated stress response but not to mitochondrial unfolded protein response. *Biosci Rep* **40**, BSR20201289 (2020).
285. Sabouny, R. *et al.* The Keap1-Nrf2 Stress Response Pathway Promotes Mitochondrial Hyperfusion Through Degradation of the Mitochondrial Fission Protein Drp1. *Antioxid Redox Signal* **27**, 1447–1459 (2017).
286. Ahn, S. I., Choi, S. K., Kim, M. J., Wie, J. & You, J. S. Mdivi-1: Effective but complex mitochondrial fission inhibitor. *Biochem Biophys Res Commun* **710**, 149886 (2024).
287. De Vos, K. J., Allan, V. J., Grierson, A. J. & Sheetz, M. P. Mitochondrial function and actin regulate dynamin-related protein 1-dependent mitochondrial fission. *Curr Biol* **15**, 678–683 (2005).
288. Pivovarova, N. B. *et al.* Excitotoxic Calcium Overload in a Subpopulation of Mitochondria Triggers Delayed Death in Hippocampal Neurons. *J Neurosci* **24**, 5611–5622 (2004).
289. Kushnareva, Y., Andreyev, A. Y., Kuwana, T. & Newmeyer, D. D. Bax Activation Initiates the Assembly of a Multimeric Catalyst that Facilitates Bax Pore Formation in Mitochondrial Outer Membranes. *PLoS Biol* **10**, e1001394 (2012).

290. So, E. C., Hsing, C.-H., Liang, C.-H. & Wu, S.-N. The actions of mdivi-1, an inhibitor of mitochondrial fission, on rapidly activating delayed-rectifier K⁺ current and membrane potential in HL-1 murine atrial cardiomyocytes. *Eur J Pharmacol* **683**, 1–9 (2012).
291. Qian, W. *et al.* Novel combination of mitochondrial division inhibitor 1 (mdivi-1) and platinum agents produces synergistic pro-apoptotic effect in drug resistant tumor cells. *Oncotarget* **5**, 4180–4194 (2014).
292. Wang, J. *et al.* A novel strategy for targeted killing of tumor cells: Induction of multipolar acentrosomal mitotic spindles with a quinazolinone derivative mdivi-1. *Mol Oncol* **9**, 488–502 (2015).
293. Fang, C.-T., Kuo, H.-H., Yuan, C.-J., Yao, J.-S. & Yih, L.-H. Mdivi-1 induces spindle abnormalities and augments taxol cytotoxicity in MDA-MB-231 cells. *Cell Death Discov* **7**, 118 (2021).
294. Lucantoni, F., Dussmann, H. & Prehn, J. H. M. Metabolic Targeting of Breast Cancer Cells With the 2-Deoxy-D-Glucose and the Mitochondrial Bioenergetics Inhibitor MDIVI-1. *Front Cell Dev Biol* **6**, 113 (2018).
295. Dai, W. *et al.* Mitochondrial division inhibitor (mdivi-1) decreases oxidative metabolism in cancer. *Br J Cancer* **122**, 1288–1297 (2020).
296. Ahmed, A. *et al.* The drp-1-mediated mitochondrial fission inhibitor mdivi-1 impacts the function of ion channels and pathways underpinning vascular smooth muscle tone. *Biochemical Pharmacology* **203**, 115205 (2022).
297. Ahmed, A. *et al.* Dynamin-independent CaV1.2 and KCa1.1 channels regulation and vascular tone modulation by the mitochondrial fission inhibitors dynasore and dyngo-4a. *European Journal of Pharmacology* **951**, 175786 (2023).
298. Silva-Pavez, E. *et al.* Mitochondrial division inhibitor (mdivi-1) induces extracellular matrix (ECM)-detachment of viable breast cancer cells by a DRP1-independent mechanism. *Sci Rep* **14**, 14178 (2024).
299. Hoshino, A. *et al.* The ATP/ADP translocase drives mitophagy independent of nucleotide exchange. *Nature* **575**, 375–379 (2019).
300. Andersson, B. S. *et al.* Ph-positive chronic myeloid leukemia with near-haploid conversion in vivo and establishment of a continuously growing cell line with similar cytogenetic pattern. *Cancer Genetics and Cytogenetics* **24**, 335–343 (1987).
301. Kotecki, M., Reddy, P. S. & Cochran, B. H. Isolation and characterization of a near-haploid human cell line. *Exp Cell Res* **252**, 273–280 (1999).
302. Carette, J. E. *et al.* Ebola virus entry requires the cholesterol transporter Niemann-Pick C1. *Nature* **477**, 340–343 (2011).

303. Carette, J. E. *et al.* Haploid genetic screens in human cells identify host factors used by pathogens. *Science* **326**, 1231–1235 (2009).
304. Essletzbichler, P. *et al.* Megabase-scale deletion using CRISPR/Cas9 to generate a fully haploid human cell line. *Genome Res* **24**, 2059–2065 (2014).
305. Lackner, D. H. *et al.* A generic strategy for CRISPR-Cas9-mediated gene tagging. *Nat Commun* **6**, 10237 (2015).
306. Horii, T. & Hatada, I. Genome Editing Using Mammalian Haploid Cells. *Int J Mol Sci* **16**, 23604–23614 (2015).
307. Beigl, T. B., Kjosås, I., Seljeseth, E., Glomnes, N. & Aksnes, H. Efficient and crucial quality control of HAP1 cell ploidy status. *Biol Open* **9**, bio057174 (2020).
308. Banerjee, R., Sotero-Caio, C. G., Fu, B. & Yang, F. Chromosomal instability (CIN) in HAP1 cell lines revealed by multiplex fluorescence in situ hybridisation (M-FISH). *Mol Cytogenet* **15**, 46 (2022).
309. Simkin, D. *et al.* Homozygous might be hemizygous: CRISPR/Cas9 editing in iPSCs results in detrimental on-target defects that escape standard quality controls. *Stem Cell Reports* **17**, 993–1008 (2022).
310. Law, W. D., Warren, R. L. & McCallion, A. S. Establishment of an eHAP1 Human Haploid Cell Line Hybrid Reference Genome Assembled from Short and Long Reads. *Genomics* **112**, 2379–2384 (2020).
311. Goh, C. G. *et al.* TDP1 splice-site mutation causes HAP1 cell hypersensitivity to topoisomerase I inhibition. *Nucleic Acids Res* **53**, gkae1163 (2024).
312. Smith, P. K. *et al.* Measurement of protein using bicinchoninic acid. *Anal Biochem* **150**, 76–85 (1985).
313. Wu, M. *et al.* Multiparameter metabolic analysis reveals a close link between attenuated mitochondrial bioenergetic function and enhanced glycolysis dependency in human tumor cells. *Am J Physiol Cell Physiol* **292**, C125-136 (2007).
314. Gerencser, A. A. *et al.* Quantitative Microplate-Based Respirometry with Correction for Oxygen Diffusion. *Anal Chem* **81**, 6868–6878 (2009).
315. Wang, K., Li, M. & Hakonarson, H. ANNOVAR: functional annotation of genetic variants from high-throughput sequencing data. *Nucleic Acids Res* **38**, e164 (2010).
316. Dranka, B. P. *et al.* Assessing bioenergetic function in response to oxidative stress by metabolic profiling. *Free Radic Biol Med* **51**, 1621–1635 (2011).

317. Jaber, S. M., Yadava, N. & Polster, B. M. Mapping Mitochondrial Respiratory Chain Deficiencies by Respirometry: Beyond the Mito Stress Test. *Exp Neurol* **328**, 113282 (2020).
318. García-Rúa, V. *et al.* Endolysosomal two-pore channels regulate autophagy in cardiomyocytes. *J Physiol* **594**, 3061–3077 (2016).
319. Pereira, G. J. S. *et al.* Glutamate induces autophagy via the two-pore channels in neural cells. *Oncotarget* **8**, 12730–12740 (2016).
320. Pryde, K. R., Taanman, J. W. & Schapira, A. H. A LON-ClpP Proteolytic Axis Degrades Complex I to Extinguish ROS Production in Depolarized Mitochondria. *Cell Rep* **17**, 2522–2531 (2016).
321. Höglinger, G. U. *et al.* Dysfunction of mitochondrial complex I and the proteasome: interactions between two biochemical deficits in a cellular model of Parkinson's disease. *J Neurochem* **86**, 1297–1307 (2003).
322. Rath, S. *et al.* MitoCarta3.0: an updated mitochondrial proteome now with sub-organelle localization and pathway annotations. *Nucleic Acids Res* **49**, D1541–D1547 (2020).
323. Neeve, V. C. M. *et al.* Clinical and functional characterisation of the combined respiratory chain defect in two sisters due to autosomal recessive mutations in MTFMT. *Mitochondrion* **13**, 743–748 (2013).
324. Mustaly-Kalimi, S. *et al.* Protein mishandling and impaired lysosomal proteolysis generated through calcium dysregulation in Alzheimer's disease. *Proceedings of the National Academy of Sciences* **119**, e2211999119 (2022).
325. Pitt, S. J., Lam, A. K. M., Rietdorf, K., Galione, A. & Sitsapesan, R. Reconstituted Human TPC1 Is a Proton-Permeable Ion Channel and Is Activated by NAADP or Ca²⁺. *Sci Signal* **7**, ra46 (2014).
326. Cao, W. *et al.* The Role of PGK1 in Promoting Ischemia/Reperfusion Injury-Induced Microglial M1 Polarization and Inflammation by Regulating Glycolysis. *Neuromol Med* **25**, 301–311 (2023).
327. Li, Y., Li, J., Yu, Q., Ji, L. & Peng, B. METTL14 regulates microglia/macrophage polarization and NLRP3 inflammasome activation after ischemic stroke by the KAT3B-STING axis. *Neurobiology of Disease* **185**, 106253 (2023).
328. Shen, G. *et al.* Knockdown of repulsive guidance molecule a promotes polarization of microglia into an anti-inflammatory phenotype after oxygen-glucose deprivation-reoxygenation *in vitro*. *Neurochemistry International* **170**, 105546 (2023).

329. Zhu, Q. *et al.* Lycopene Alleviates Chronic Stress-Induced Hippocampal Microglial Pyroptosis by Inhibiting the Cathepsin B/NLRP3 Signaling Pathway. *J. Agric. Food Chem.* **71**, 20034–20046 (2023).
330. Albalawi, F. E. *et al.* Immunomodulatory effects of Kaempferol on microglial and Macrophage cells during the progression of diabetic retinopathy. *International Immunopharmacology* **133**, 112021 (2024).
331. Gao, Z. *et al.* Melatonin alleviates chronic stress-induced hippocampal microglia pyroptosis and subsequent depression-like behaviors by inhibiting Cathepsin B/NLRP3 signaling pathway in rats. *Transl Psychiatry* **14**, 1–14 (2024).
332. Peng, L. *et al.* Indole-3-carbinol (I3C) reduces apoptosis and improves neurological function after cerebral ischemia–reperfusion injury by modulating microglia inflammation. *Sci Rep* **14**, 3145 (2024).
333. Wei, Z., Fang, R., Wang, Y. & Dong, J. Maternal exposure to di-(2-ethylhexyl) phthalate impaired the social interaction via activating microglia in male pups. *Ecotoxicology and Environmental Safety* **272**, 116069 (2024).
334. Wang, L. *et al.* microRNA-125b-5p alleviated CCI-induced neuropathic pain and modulated neuroinflammation via targeting SOX11. *Synapse* **78**, e22306 (2024).
335. Shukitt-Hale, B. *et al.* Intermittent Versus Continuous Wild Blueberry Feeding Alters Inflammation and Behavior in Aged Male Rats. *J Med Food* **28**, 639–646 (2025).
336. Haag, S. M. & Murthy, A. Murine Monocyte and Macrophage Culture. *Bio Protoc* **11**, e3928 (2021).
337. Tanabe, H. *et al.* Cell Line Individualization by Str Multiplex System in the Cell Bank Found Cross-Contamination Between Ecv304 and Ej-1/T24. *Tissue Culture Research Communications* **18**, 329–338 (1999).
338. Bryan, N. S. & Grisham, M. B. Methods to Detect Nitric Oxide and its Metabolites in Biological Samples. *Free Radic Biol Med* **43**, 645–657 (2007).
339. Griess, P. Vorläufige Notiz über die Einwirkung von salpetriger Säure auf Amidinitro- und Aminitrophenylsäure. *Justus Liebigs Annalen der Chemie* **106**, 123–125 (1858).
340. Almeida, J. L. *et al.* Interlaboratory study to validate a STR profiling method for intraspecies identification of mouse cell lines. *PLoS One* **14**, e0218412 (2019).
341. Almeida, J. L., Hill, C. R. & Cole, K. D. Mouse cell line authentication. *Cytotechnology* **66**, 133–147 (2014).

342. Thampithak, A. *et al.* Transcriptional regulation of iNOS and COX-2 by a novel compound from *Curcuma comosa* in lipopolysaccharide-induced microglial activation. *Neuroscience Letters* **462**, 171–175 (2009).
343. Chénais, B., Morjani, H. & Drapier, J.-C. Impact of endogenous nitric oxide on microglial cell energy metabolism and labile iron pool. *J Neurochem* **81**, 615–623 (2002).
344. Roy, E. R. *et al.* Concerted type I interferon signaling in microglia and neural cells promotes memory impairment associated with amyloid β plaques. *Immunity* **55**, 879–894.e6 (2022).
345. Talavera-López, C., Capuccini, B., Mitter, R., Lin, J. & Langhorne, J. Transcriptomes of microglia in experimental cerebral malaria in mice in the presence and absence of Type I Interferon signaling. *BMC Res Notes* **11**, 913 (2018).
346. Koneru, R. *et al.* Reversing interferon-alpha neurotoxicity in a HIV-associated neurocognitive disorder mouse model. *AIDS* **32**, 1403–1411 (2018).
347. Yoshimoto, N., Nakamura, Y., Hisaoka-Nakashima, K. & Morioka, N. Mitochondrial dysfunction and type I interferon signaling induce anxiodepressive-like behaviors in mice with neuropathic pain. *Exp Neurol* **367**, 114470 (2023).
348. Banati, R. B. *et al.* Mitochondria in activated microglia in vitro. *J Neurocytol* **33**, 535–541 (2004).
349. Park, J. *et al.* Mitochondrial dynamics modulate the expression of pro-inflammatory mediators in microglial cells. *J Neurochem* **127**, 221–232 (2013).
350. Katoh, M. *et al.* Polymorphic regulation of mitochondrial fission and fusion modifies phenotypes of microglia in neuroinflammation. *Sci Rep* **7**, 4942 (2017).
351. Verma, I. M., Stevenson, J. K., Schwarz, E. M., Van Antwerp, D. & Miyamoto, S. Rel/NF-kappa B/I kappa B family: intimate tales of association and dissociation. *Genes Dev* **9**, 2723–2735 (1995).
352. Ballabriga, J., Pozas, E., Planas, A. M. & Ferrer, I. bFGF and FGFR-3 immunoreactivity in the rat brain following systemic kainic acid administration at convulsant doses: localization of bFGF and FGFR-3 in reactive astrocytes, and FGFR-3 in reactive microglia. *Brain Research* **752**, 315–318 (1997).
353. Rehman, R. *et al.* The FGFR inhibitor Rogaratinib reduces microglia reactivity and synaptic loss in TBI. *Front Immunol* **15**, 1443940 (2024).
354. Rajendran, R. *et al.* The small molecule fibroblast growth factor receptor inhibitor ingratinib exerts anti-inflammatory effects and remyelination in a model of multiple sclerosis. *Br J Pharmacol* **180**, 2989–3007 (2023).

355. Narayana, J. & Horton, W. A. FGFR3 biology and skeletal disease. *Connect Tissue Res* **56**, 427–433 (2015).
356. Kouhara, H. *et al.* A lipid-anchored Grb2-binding protein that links FGF-receptor activation to the Ras/MAPK signaling pathway. *Cell* **89**, 693–702 (1997).
357. Guagnano, V. *et al.* FGFR genetic alterations predict for sensitivity to NVP-BGJ398, a selective pan-FGFR inhibitor. *Cancer Discov* **2**, 1118–1133 (2012).
358. Nair, S. *et al.* Lipopolysaccharide-induced alteration of mitochondrial morphology induces a metabolic shift in microglia modulating the inflammatory response in vitro and in vivo. *Glia* **67**, 1047–1061 (2019).
359. Montilla, A. *et al.* Role of Mitochondrial Dynamics in Microglial Activation and Metabolic Switch. *ImmunoHorizons* **5**, 615–626 (2021).
360. Hong, C. *et al.* Protective Effects of Mdivi-1 on Cognition Disturbance Following Sepsis in Mice via Alleviating Microglia Activation and Polarization. *CNS Neurosci Ther* **31**, e70149 (2025).
361. Liu, X. *et al.* Mdivi-1 Modulates Macrophage/Microglial Polarization in Mice with EAE via the Inhibition of the TLR2/4-GSK3 β -NF- κ B Inflammatory Signaling Axis. *Mol Neurobiol* **59**, 1–16 (2022).
362. Song, C., Zhang, K., Luo, C., Zhao, X. & Xu, B. Inhibiting the NF- κ B/DRP1 Axis Affords Neuroprotection after Spinal Cord Injury via Inhibiting Polarization of Pro-Inflammatory Microglia. *Front Biosci (Landmark Ed)* **29**, 307 (2024).
363. KATO, M. FGFR inhibitors: Effects on cancer cells, tumor microenvironment and whole-body homeostasis (Review). *Int J Mol Med* **38**, 3–15 (2016).
364. Cookson, M. R. The evolution of neurodegeneration. *Curr Biol* **22**, R753–R761 (2012).
365. Landeck, N. *et al.* Two C-terminal sequence variations determine differential neurotoxicity between human and mouse α -synuclein. *Molecular Neurodegeneration* **15**, 49 (2020).
366. Chen, Z. *et al.* Human-lineage-specific genomic elements are associated with neurodegenerative disease and APOE transcript usage. *Nat Commun* **12**, 2076 (2021).
367. Mestas, J. & Hughes, C. C. W. Of mice and not men: differences between mouse and human immunology. *J Immunol* **172**, 2731–2738 (2004).
368. Seok, J. *et al.* Genomic responses in mouse models poorly mimic human inflammatory diseases. *Proc Natl Acad Sci U S A* **110**, 3507–3512 (2013).

369. Takao, K. & Miyakawa, T. Genomic responses in mouse models greatly mimic human inflammatory diseases. *Proc Natl Acad Sci U S A* **112**, 1167–1172 (2015).
370. Guo, Z. *et al.* miRNA-939 regulates human inducible nitric oxide synthase posttranscriptional gene expression in human hepatocytes. *Proc Natl Acad Sci U S A* **109**, 5826–5831 (2012).
371. Hoos, M. D. *et al.* The impact of human and mouse differences in NOS2 gene expression on the brain's redox and immune environment. *Mol Neurodegener* **9**, 50 (2014).
372. Pradhan, P. *et al.* Distinct metabolic responses to heme in inflammatory human and mouse macrophages - Role of nitric oxide. *Redox Biol* **73**, 103191 (2024).
373. Piers, T. M. *et al.* A locked immunometabolic switch underlies TREM2 R47H loss of function in human iPSC-derived microglia. *FASEB J* **34**, 2436–2450 (2020).
374. Kontinen, H. *et al.* PSEN1 Δ E9, APP^{swe}, and APOE4 Confer Disparate Phenotypes in Human iPSC-Derived Microglia. *Stem Cell Reports* **13**, 669–683 (2019).
375. Solomon, S. *et al.* Heterozygous expression of the Alzheimer's disease-protective PLC γ 2 P522R variant enhances A β clearance while preserving synapses. *Cell Mol Life Sci* **79**, 453 (2022).
376. Sabogal-Guáqueta, A. M. *et al.* Species-specific metabolic reprogramming in human and mouse microglia during inflammatory pathway induction. *Nat Commun* **14**, 6454 (2023).
377. Ryan, K. J. *et al.* A human microglia-like cellular model for assessing the effects of neurodegenerative disease gene variants. *Science Translational Medicine* **9**, eaa17635 (2017).
378. Ohgidani, M. *et al.* Direct induction of ramified microglia-like cells from human monocytes: Dynamic microglial dysfunction in Nasu-Hakola disease. *Sci Rep* **4**, 4957 (2014).
379. Ohgidani, M., Kato, T. A. & Kanba, S. Introducing directly induced microglia-like (iMG) cells from fresh human monocytes: a novel translational research tool for psychiatric disorders. *Front Cell Neurosci* **9**, 184 (2015).
380. Sellgren, C. M. *et al.* Patient-specific models of microglia-mediated engulfment of synapses and neural progenitors. *Mol Psychiatry* **22**, 170–177 (2017).
381. Clere-Jehl, R. *et al.* Septic Shock Alters Mitochondrial Respiration of Lymphoid Cell-Lines and Human Peripheral Blood Mononuclear Cells: The Role of Plasma. *Shock* **51**, 97–104 (2019).

382. Warren, M., Subramani, K., Schwartz, R. & Raju, R. Mitochondrial dysfunction in rat splenocytes following hemorrhagic shock. *Biochim Biophys Acta* **1863**, 2526–2533 (2017).
383. Yadava, N., Houchens, T., Potluri, P. & Scheffler, I. E. Development and characterization of a conditional mitochondrial complex I assembly system. *J Biol Chem* **279**, 12406–12413 (2004).
384. Luger, A.-L. *et al.* Doxycycline Impairs Mitochondrial Function and Protects Human Glioma Cells from Hypoxia-Induced Cell Death: Implications of Using Tet-Inducible Systems. *Int J Mol Sci* **19**, 1504 (2018).